Fall 2014

An assessment of urbanization impact in China by using WRF-Chem and configuration optimization

Man Yu
University of Iowa

AN ASSESSMENT OF URBANIZATION IMPACT IN CHINA BY USING WRF-CHEM AND CONFIGURATION OPTIMIZATION

by

Man Yu

A thesis submitted in partial fulfillment
of the requirements for the Doctor of Philosophy degree
in Chemical and Biochemical Engineering
in the Graduate College of
The University of Iowa

May 2014

Thesis Supervisor: Professor Gregory R. Carmichael

Graduate College
The University of Iowa
Iowa City, Iowa

CERTIFICATE OF APPROVAL

PH.D. THESIS

This is to certify that the Ph.D. thesis of

Man Yu

has been approved by the Examining Committee
for the thesis requirement for the Doctor of Philosophy
degree in Chemical and Biochemical Engineering at the May 2014 graduation.

Thesis Committee: _____
Gregory R. Carmichael, Thesis Supervisor

_____
Charles O. Stanier

_____
Eric E. Nuxoll

_____
Scott Spak

_____
Thomas Peters

To My Family and Friends

ACKNOWLEDGMENTS

Ph.D is really a long way to go and I am about to accomplish it now. This has been the most wonderful 5 years for me. First I want to thank my advisor, Prof. Carmichael, for taking me in when I just finished my bachelor degree. He encouraged me every time and guided me to the right direction. I want thank Dr. Charles Stanier, Dr Eric Nuxoll and Dr. Thomas Peters for teaching me the interesting courses. Also I want to thank Dr. Scott Spak for helping with new data. Also thank CGRER and people inside it for providing me with the most pleasant working environment, special thanks to Jane Frank and Jeremie Moen for their support during the past 5 years.

I'd like to give my special thanks to Dr. Yafang Cheng for teaching me modeling and most importantly how to think critically. And I really missed the days we hang out together. Also I want to thank Dr. Aditsuda Jamroensan, Dr. Pallavi Marrapu, Dr. Pablo Saide, Dr. Chao Wei, Dr. Sinan Sousan, Dr. Jaemeen Baek and Dr. Sarika Kulkarni for their generous help and precious friendship. I also want to expend my thanks to Meng Gao, Ashish Singh Lingyun Du and Cancan Dong for all the encouragement during my painful thesis writing.

Special thanks to my family, especially to my mother, my father, and mother-in-law for their generous help. Without them I couldn't accomplish what I have now. Finally thank my husband for his love and unconditional support.

ABSTRACT

Urbanization is an inevitable process for every developing and developed country. In China this process accelerated after the reform and open-door policies initialed in 1980s. Urbanization can bring tremendous influences on air quality and in turn adverse health effects. Therefore it is of importance to access and evaluate urbanization process. In this Thesis, we focus on three major impacts in China: land-cover change (from nature land type to urban land type), anthropogenic heat emission (due to human activity), and pollutant emission increase (mainly from industry, power, transportation and residential). The model tool used in this paper is called WRF-Chem (the fully coupled Weather Research and Forecast Model with Chemistry Module). After designing and performing three different sensitivity runs, it turns out that all of these three impacts from urbanization tend to worsen air quality conditions in Beijing, especially for ozone and PM2.5 concentrations. The first impact from land-cover change in Chapter 2 increases temperature by 2.4 ℃ for Beijing and ozone by 20 ppb. Adding human heat release (the second impact) also increases surface temperature by 0.8 ℃ at daytime and 1.2 ℃ at nighttime (Chapter 4). Consequently, model outputs a more polluted scenario in Beijing, with 18 ppb more ozone during nocturnal time. When exploring the third impact from emission change, we found out that the government's mitigation regulations on emissions in Beijing has in effect. Around Beijing area, the emissions for CO and SO_2 remains the same level from 2006 to 2010, while other cities inside North China Plain are experiencing rapid growths in anthropogenic emissions. Results show a slightly increase in surface temperature and ozone concentrations. Meanwhile, the concentration of particulate matters tends to increase near surface and decrease in the upper atmosphere. For future study, it is highly recommended to include these impacts into model configurations. Additional sensitivity runs were conducted to optimize forecast computing in China, concerning both spatial and vertical resolutions. This sensitivity

studies represented 4 different grid resolutions and three different vertical meshes. Regards to the analysis with available observation data, a resolution of 9 km and 27 vertical layers is determined to be the best option for future efficient and accurate forecasts in China. For horizontal aspects, both 81-km and 27-km resolutions are not able to capture pollutant distributions and no significant discrepancy is found out between 9-km and 3-km case. In vertical resolution sensitivity runs, we use 9 layers, 27 layers, and 54 layers mesh with same top and bottom staggers. Analysis reveals totally different vertical profile between 9 layers and 27 layers cases and similar profile between 27 layers and 54 layers. Therefore, we recommend spatial settings with 9-km resolution and a vertical mesh with 27 layers. Finally, the updated 3-d model, involving three urbanization impacts and using recommended resolution settings is used to support a field campaign in summer 2013 for North China Plain. Some preliminary results show a confidence using our model, by capturing both meteorological and chemical trends in Beijing.

TABLE OF CONTENTS

LIST OF TABLES

LIST OF FIGURES

CHAPTER 1 GENERAL INTRODUCTION

1.1 Motivation and Importance of Work

Urbanization is an inevitable and rapid process coming along with economic development and population boost in China (Li et al., 2012). In Beijing, the built-up area increased from 184 km^2 in 1973 to 1210 km^2 in 2005 (Mu et al., 2007). Figure 1.1 below is the spatial plots for urban fraction over the two biggest cities (Beijing and Shanghai) in China. According to the comparison between 1992 and 2004, urban land expanded over 10~20 times. And this is a universal phenomenon for most cities in China (Chen et al., 2007).

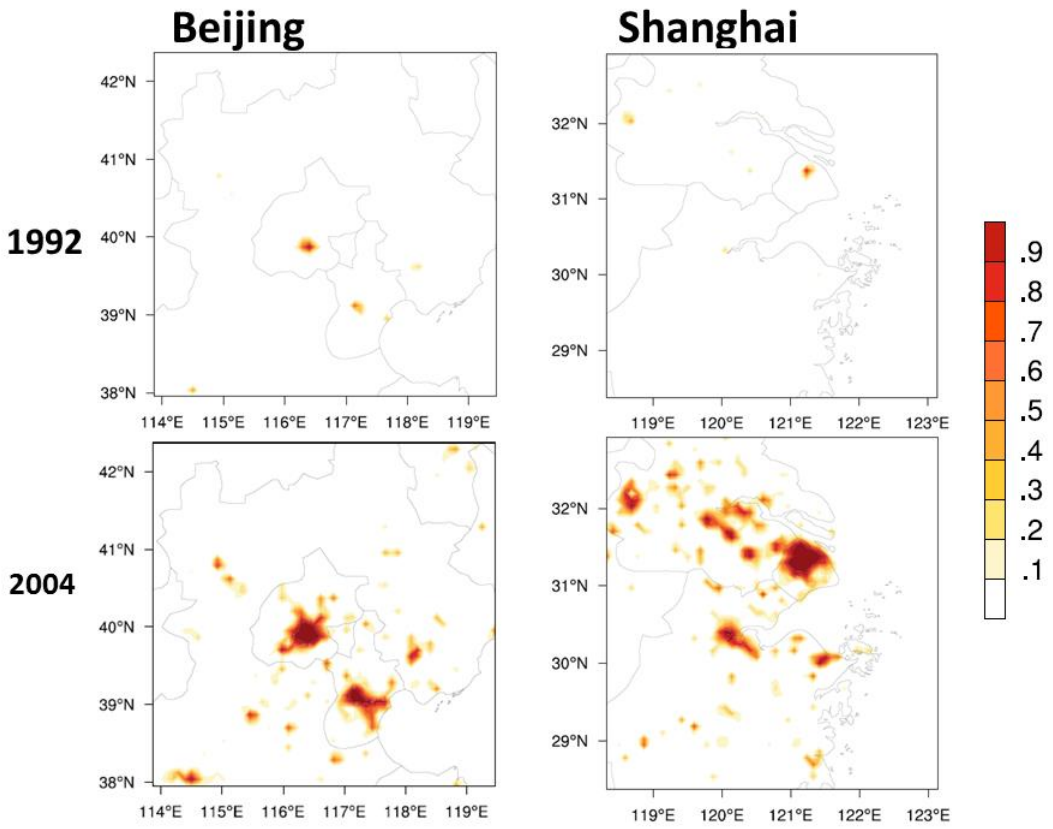

Figure 1.1 Urban and Built-on land cover fraction (range 0~1) for Beijing and Shanghai in 1992 and 2004

Besides land type changes, urban population is anticipated to increase at a rate of 2.3 % per year in developing countries (United Nations, 2004). The overall proportion of the urban population in China increased from only 20 % in the 1980s to 45 % in 2010 (Van De Poel et al., 2012). According to the sixth national census (2010) in China, for Beijing alone, there are more than 20 million people living within this city cluster. In Figure 1.2, the total urban population for developing regions continues to increase and will exceed 4 billion by the year 2030.

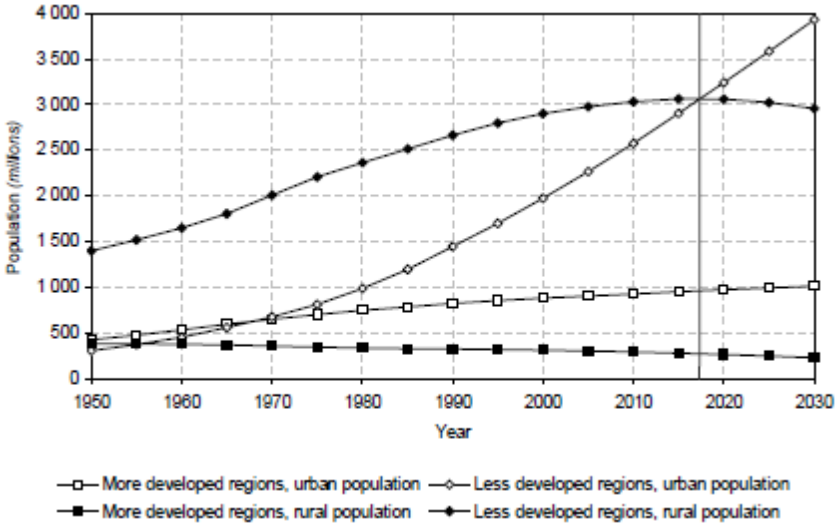

(United Nations, 2004)

Figure 1.2 Urban and rural population of more developed regions and less developed regions: 1950-2030

Both urban land and urban population boost put pressure on air quality for cities in China. In the past several years, air pollution, mostly photochemical smog and widespread haze, have developed into severe scenarios in China (Zhao et al., 2013 and

Tao et al., 2014). The maximum hourly PM2.5 exceeded 680 $\mu g/m^3$ in the Greater Beijing Area (Wang et al., 2014). Researches have demonstrated various illnesses associated with air pollutants. Buka et al. (2006) found out that carbon monoxide reduces oxygen delivery to body organs and tissues. According to Bascom et al. (1996), current ambient levels of PM10 are associated with increases in daily cardiorespiratory mortality and total mortality. And ambient ozone is associated with mortality and respiratory illnesses (Bell et al., 2004). However, there is no threshold concentration on health for particulate matters and ozone (Brunekreef et al., 2002).

There is a need for better understanding of the relationship between urbanization and air quality in China. In this study, we employ the fully coupled Weather Research and Forecast Model with Chemistry Module (WRF-Chem) to evaluate how urbanization interacts with air quality and model sensitivities to each impact from urbanization. Specifically, three major impacts from urbanization are investigated in this study. The first one is from land-cover change, evaluating grid type change from nature to urban and its associating physical parameters, including albedo and surface roughness. Second impact is from additional heat release from human activities. And the third impact is from anthropogenic emission. To better predict pollutant levels in China and prevent long exposure for human health, optimal configurations are also recommended for improving model fidelity.

Chapter 2 focuses on the development of implanting new land-cover data into WRF-Chem and pollutant sensitivity to land-cover change. In this chapter, we simulated urban expansion from 1992 to 2004 in China and pollutant sensitivities. This chapter is based on the results published in Yu et al. (2012).

In Chapter 3, we analyze a special land-surface forcing on ozone and other chemical species in Beijing. Two cases (one is pre-industrialization and one is current) were used in this chapter. It focused on industrialization impact and interactions with different local circulations.

Chapter 4 presents our study on the second impact from urbanization. In this chapter, a new reliable heat emission model was developed and tested for China. After incorporating this emission stream into WRF-Chem, sensitivity tests were designed in the Greater Beijing area. This chapter is based on the results published in Yu et al. (2014a).

Chapter 5 assesses the third impact, anthropogenic emission change. In this study, we employed emissions from 2006 and 2010 and tried to quantify model sensitivities. Also a brief description on impact from emission regulation is included in this chapter.

Chapter 6 investigates resolution impacts for forecast by using WRF-Chem. Both spatial and vertical impacts were taken into considerations. Based on sensitivity runs in this chapter, optimal domain configurations are recommended. This chapter is based on the results published in Yu et al. (2014b).

Chapter 7 describes our contributions and performances in CAREBEIJING2013 Field Campaign. In summer 2013, we provided groups in the project with every day forecast on both meteorology and pollutant levels. Some preliminary results are also represented in this chapter.

1.2 WRF-Chem Backgroud

For air quality modeling, there are two different types, offline and online. The commonly used approach, called "offline", requires initially running a meteorological model independently and use its output to drive the chemical transport model. WRF-Chem used in this study is "online" model (Grell et al., 2005). It can compute one step of meteorology then one step of chemical model. Therefore it is able to include two-way feedbacks. More information about WRF-Chem can be found at http://ruc.noaa.gov/wrf/WG11/. WRF-Chem has been proved to be a reliable tool in simulating air quality in China (Li et al., 2011; Jiang et al., 2012; Tie et al., 2013).

The differences between "on-line" and "off-line" model is shown in Figure 1.3. For off-line models, they compute the weather model separately, then utilize its output to

drive the chemical transport model. The feedbacks between meteorology and chemistry are shut-off completely. Unlike it, the WRF-Chem is able to include this feedback step by step. It runs one-step of meteorology, one-step of chemistry, and so on. Many previous studies have proven that WRF-Chem is the better option, especially for regional modeling (Grell et al., 2005) (Jiang et al., 2012).

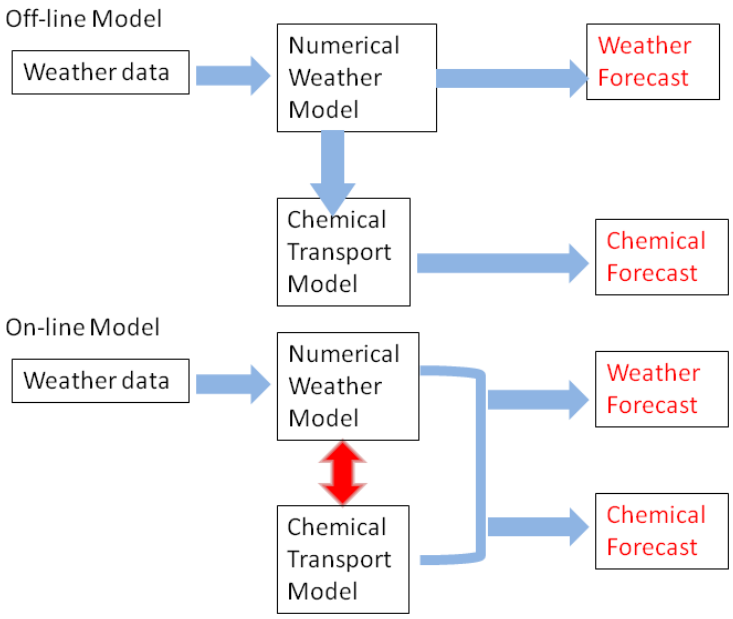

Figure 1.3 Flow chat for off-line and on-line air quality models

1.3 Biogenic and Anthropogenic Emissions

The Model of Emissions of Gases and Aerosols from Nature (MEGAN) Version 2.04 (the latest one) (Guenther, 2006) was used for the biogenic emissions. The MEGAN is an on-line calculation of biomass emissions by using Leaf Area Index (LAI) and percentage of each Plant Functional Type (PFT) for each model grid, as well as meteorological variables, like temperature, pressure and solar radiation obtained from

model simulations. The first part of inputs, LAI and PFT data, according to Guenther (2006), is data for the year 2003.

In this study, the anthropogenic emission data was prepared by Qiang Zhang and David Streets from Argonne National Laboratory. Data was collected during INTEX-B project (2006) of the National Aeronautics and Space Administration (NASA). It includes emissions of SO2, NOx, CO, VOC, PM10, PM2.5, BC and OC by sector (power, industry, residential and transportation) and six speciated VOCs by sector files. Now it can be downloaded from CGRER website: http://cgrer.uiowa.edu/projects/emmison-data.

1.4 Initial Chemical State and Lateral Boundary Conditions

Inside WRF-Chem model, there is a need to update the chemical boundary conditions for air quality modeling. After running real.exe to generate the wrfinput files, we modified the values on boundaries to incorporate potential mass and pollutants exchange between modeled domains and their surroundings, most importantly the intrusions from stratosphere to troposphere. The Model for Ozone and Related chemical Tracers, version 4 (MOZART-4) is used in this study as the initial chemical state and the lateral boundary conditions (Emmons et al., 2010). MOZART-4 is an offline global chemical transport model, including online calculations of a number of processes, like dry deposition and emissions of VOCs. Outputs from online downloads is every 6 hour. Since our case is three two-way nesting domains, only the first (largest) domain adopted the MOZART-4 chemical initial and lateral boundary conditions. For the possible upper troposphere/stratospheric intrusions concern, using MOZART-4 data has taken it into consideration. The download website is http://www.acd.ucar.edu/wrf-chem/mozart.shtml.

CHAPTER 2 SENSITIVITY OF PREDICTED POLLUTANT LEVELS TO LAND COVER CHANGE IN CHINA

2.1 Abstract

Urbanization in China accompanies economic development and population growth. Changes in land use leads to changes in both meteorological and chemical fields. In this study, the impact of land use change in Jing-Jin-Ji (JJJ, indicating Beijing-Tianjin-Hebei) and Yangtze River Delta (YRD) areas on meteorology and ozone concentrations are studied using the WRF-Chem model. Land use change is represented two different land cover data sets: USGS and MODIS. Monthly-average simulations show that urbanization causes an increase in 2-m temperature by maximum 2.4 ℃ and 3.2 ℃ in these two areas, respectively. Wind speed simulations suggest a decrease (average 1.2 m/s) in daytime for YRD and in nighttime for JJJ. Dew point differences show a dry effect over both areas, with maximum -3 ℃, in JJJ and -2.4 ℃ in YRD. Planetary Boundary Layer (PBL) height increases by 400 m (maximum in JJJ) and 600m (maximum in YRD) for daytime, and nighttime increases are less than 100m. Daytime ozone concentrations in JJJ increase by 20 ppb due to urbanization, while in YRD the difference is around 5 ppb. Compared to observations, mean errors in urban areas was improved when using updated land use information by 14.2% and 35.6%, and in suburban areas by 5.8% and 10.7%. Updating land use data set in air quality is important in application to regions with rapid urbanization such as China. The effects due to land use can be as large as those due to 20% in emissions.

2.2 Introduction

China is currently undergoing rapid urbanization (Li et al., 2012), especially for the Yangtze River Delta (Gu et al., 2011) and Jing-Jin-Ji (Beijing-Tianjin-Hebei) region. The overall proportion of the urban population in China increased from only 20% in the 1980s to 45% in 2010 (Van De Poel et al., 2012). One of the major effects from urbanization is changes in land use, typically from vegetated surfaces to imperious built surfaces. Land-cover properties play an important role in environmental simulations, as they help determine the surface soil moisture, albedo, and roughness length, which, in turn, influence the surface heat budget (Crawford et al., 2001). Urbanization and its related consequences contribute to changes in summertime ozone-related mortality across the metropolitan areas (Knowlton et al., 2004). Hence, it is important to study and evaluate the impact of urbanization in these two regions on air quality predictions.

There have been several previous studies on the impact of urbanization on air quality modeling, especially for ozone concentration. Cirerolo et al. (2007) simulated the future (year 2050) urbanization in NYC, while holding emissions constant and found that episode-average O3 levels increased by 1-5 ppb. Wang et al. (2009) simulated urbanization impacts over two coastal regions in China, including YRD area, by changing land-cover maps from early 1990s to 2001. The averaged daytime and nighttime increase in temperature for March 2010 was 0.6 ℃ and 1.4 ℃ for YRD area and the surface ozone level was enhanced by 4.7% for nighttime and 2.9% for daytime. Another study by Jiang et al. (2008) found that the impact of urbanization in Houston, Texas for 2050 showed an average 2 ℃ increases in near-surface temperature and 6.2 ppb increase in ozone concentration.

The above studies illustrate that land use change associated with urbanization can have significant impacts on meteorological parameters and pollution concentrations. In this paper, the impact of land use change on pollution levels is studied by using the fully coupled Weather Research and Forecast Model with Chemistry Module (WRF-Chem).

More detailed descriptions of WRF-Chem can be found in (Grell et al., 2005) and at http://ruc.noaa.gov/wrf/WG11/.

In this study we use a version of WRF-Chem that includes direct, semi-direct and indirect feedbacks to study the impact of land use change on pollutant concentrations in two fast growing regions in China, i.e., the Yangtze River Delta and Jing-Jin-Ji (Beijing-Tianjin-Hebei) regions. In modeling air quality in rapidly developing areas there is the need for models to update the land use data sets. Widely used community models such as WRF-Chem come with a default land use data set based on the U.S. Geological Survey (USGS) data, collected by the Advanced Very High Resolution Radiometer (AVHRR) during April 1992 to March 1993 at 1-km spatial resolution (Loveland et al., 2000). In this study we modify the WRF-Chem model to allow updates in land use data sets and demonstrate the method using land use data obtained from the MODerate resolution Imaging Spectroradiometer (MODIS) during mid-2000. We analyze results using USGS and MODIS land-use to evaluate the sensitivity of modeled meteorological and chemical fields to urbanization in these two regions since 1990s.

2.3 Description of study areas and observation data

2.3.1Jing-Jin-Ji Area

The Jing-Jin-Ji Area (JJJ) covering Beijing, Tianjin and part of the Hebei Province, is the political and financial center of northern China. More than 40 million people live within this area and contribute ~10% of the total Gross Domestic Product (GDP) of China, with major contributions for electronic, machinery, and metallurgical industries. Inside JJJ, there is a five-city cluster, including Beijing and Tianjin. For Beijing alone, the built-up area increased from 183.84 km2 in 1973 to 1209.97 km2 in 2005 (Mu et al., 2007). Figure 1.1(left panel) shows the urban-fraction in JJJ area from

USGS and MODIS land-cover data sets, respectively. The differences between MODIS and USGS land-cover data sets (Figure 2.1.a) are significant over the two time periods.

The Campaign of Air Quality Research in Beijing (CAREBeijing), initiated by the Beijing Municipal Environmental Protection Bureau (Beijing EPB) and Peking University (PKU), obtained observations of gaseous pollutant concentrations between August and mid-September, 2006. There were two observation sites in the Beijing area. One was located in Yufang (YF, 116.31°E, 39.51°N), which is an open spot in a suburban area, 50 km to the south of the Beijing urban center. The other one was on the campus of Peking University (PKU, 116.31°E, 39.99°N) located next to the Forth-Ring main road of Beijing and surrounded by urban area. In order to match the available observations in Beijing, the simulation period for this region was from 0000 UTC 01 August to 0000 UTC 15 September 2006, which belongs to the rainy season(from Jun to September) (Sun et al., 2007).

2.3.2 Yangtze River Delta Area

The Yangtze River Delta (YRD) area is located in the middle-east coastline of China and contains several large cities, including Hangzhou, Suzhou and Shanghai, the financial center and the largest city in China. Figure 2.1.b illustrates that land use in the YRD area has changed significantly since the 1990s. Large amounts of cropland and forests inside this region (about 45% of the total area) have been converted to human-dominated uses, especially for the suburban areas of Shanghai, Hangzhou and other cities.

In order to improve the air quality and to measure regional ozone and PM concentrations during 2010 EXPO, the Shanghai Meteorological Bureau, along with Shanghai Regional Meteorological Center and Shanghai Center for Urban Environmental Meteorology, launched a new set of observation stations both inside and outside Shanghai area. Hourly observations of ozone concentrations are posted on the website:

http://222.66.83.20:808/forecast/index.asp, since September 2009. The locations selected for this study are a base location with little change in urban fraction, Jin Shan (JS, 121.30°E, 30.7°N), and an urban location, XuJiaHui (XJH, 121.45°E, 31.16°N). To monitor and profile pollutant distributions during EXPO 2010, the simulation period for YRD from 0000 UTC 01 May to 0000 UTC 31 May 2010 was chosen for analysis. For May 2010, YRD was under the extension of spring drought in the Huaihe River watershed (Shi et al., 2012) and monthly total precipitation over Shanghai was smaller than 10mm. To compare the effect of season on the importance of land use change, simulations for August were also conducted for the YRD region.

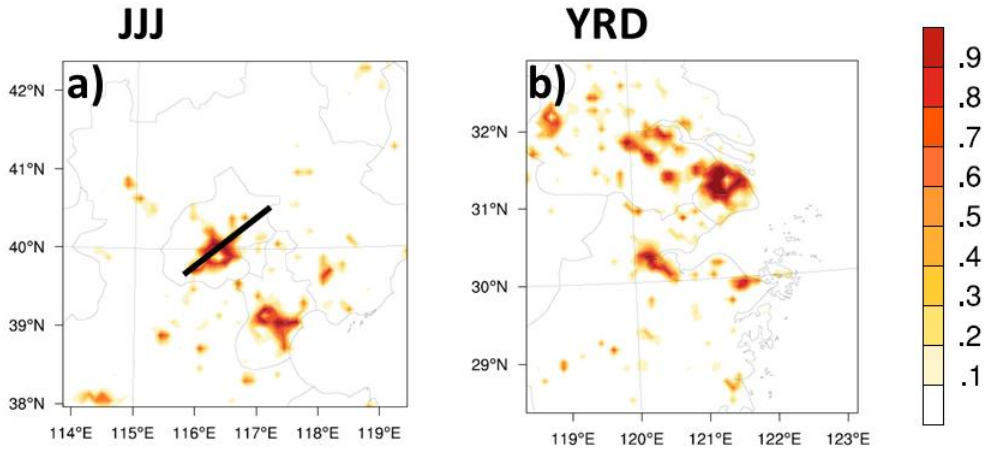

Figure 2.1 Urban fraction differences over Jing-Jin-Ji (JJJ, Beijing-Tianjin-Hebei) and Yangtze River Delta (YRD) areas between USGS and MODIS land-use datasets. The heavy black line indicates the cross-section position for vertical plots in section 2.5.2.4.

2.4 Methodology

2.4.1Mapping MODIS land-use into USGS classification

In order to study the impact of changes in land cover on predicted pollution levels, it is necessary to link the MODIS data set to WRF-Chem. This was been done by mapping the MODIS data set into the USGS classification, which can be directly invoked by WRF-Chem. The USGS land-cover data includes 24 classes of land. However, beginning with WRF Version 3.1, the Noah Land Surface Model was coupled into WRF, and this allows the usage of the MODIS land-cover data set. The land-use and land-cover types in the modified-MODIS data has 20 classes, defined by the International Geosphere-Biosphere Programme (IGBP), and includes 11 classes of natural vegetation cover broken down by plant type, 3 classes of non-vegetated lands and 3 classes of developed and mosaic lands (Friedl et al., 2002), plus three classes of tundra. In order to update the land-cover data in WRF-Chem, we built a mapping bridge between the 24-class USGS and the 20-class MODIS land cover data sets.

Table 2.1 summarizes the mapping scheme between these two classifications. Most of the IGBP classes have a direct mapping to their USGS equivalent, which we call a 'one-step mapping'. For instance, the class No.14 in MODIS named 'Cropland/Nature Vegetation Mosaic' is equal to the class No.4 in USGS, called 'Cropland/Grassland'. The definition of 'Cropland/Nature Vegetation Mosaic' in MODIS is 'Lands with a mosaic of croplands, forests, shrubland, and grasslands in which no one component comprises more than 60% of the landscape' (Strahler et al., 1999), which is equivalent to the description of class 'Cropland/Grassland' in USGS. However, some MODIS classes have to be split, in order to fit into the USGS scheme, which we call a 'multiple-step mapping'. First, for each individual cell, the original relative ratio among these specified USGS classes is checked. If the ratio exists, it is applied to the MODIS data. Otherwise, a new value is calculated, taking its geographic location, surrounding land-cover units, and local climate

into consideration. For example, 'No.11 Permanent Wetlands' in MODIS needed to be divided into two classes in USGS, No.17 Herbaceous Wetland and No.18 Wooden Wetland. For some districts, new herbaceous wetlands or wooden wetlands were formed after 1992, due to climate change or other human activities. Therefore, no existing ratio is available in the USGS land-cover data. Xu et al. (2010) pointed out that the dominant ecosystem on the East China Sea Shelf (ECSS) is herbaceous wetland during the past 3000 years, while on the South China Sea Shelf (SCSS) the wooden wetland is the primary type. For this case, the geographic location is a requirement to estimate the ratio.

2.4.2 WRF-Chem configuration

WRF-Chem Version 3.1 was employed to investigate the impact of urbanization for both JJJ and YRD areas. Simulations were performed using three-nested domains. In the JJY simulated area, three nested domains were defined as shown in Figure 2.2. The largest domain covered most of East Asia, including China, Japan and part of Southeast Asia with a grid resolution 81 km. The second domain focused on the Northeast part of China at a grid resolution 27 km. The finest domain centered at Beijing, contained the entire JJY area, with a resolution of 9 km. The numbers of horizontal grids were 81X57, 49X49, and 55X55, respectively. Similarly, the YRD modeled area was also constructed by three nested domains (Figure 2.2). The coarse domain was the same as the JJJ's largest domain, but with different second and finest domain settings. Domain 2 contained the central-east part of China at 27 km resolution, and domain 3 centered over Shanghai, with grid size of 9 km covering the whole YRD area. The horizontal grid numbers were 81 X 57, 52 X 49, and 55 X 58. All model domains had the default 28 vertical layers and the model top was set at 10 hPa. The eta values on the bottom 10 full levels were: 1.00, 0.993, 0.983, 0.97, 0.954, 0.934, 0.909, 0.88, 0.83, 0.779. The physical schemes used in this study include Purdue Lin microphysics scheme (Lin et al., 1983), Rapid Radiative Transfer Model (RRTM) longwave radiation(Mlawer et al., 1997), Goddard shortwave

scheme(Kim et al., 2011), Monin-Obukhov surface layer scheme with the Yonsei University(YSU) scheme (Hong et al., 2006) and the Noah Land Surface Model(Chen et al., 2001). For the urban surface scheme, the Urban Canopy Model (UCM) (Chen et al., 2011) was chosen in this study. The Carbon Bond (CBMZ) chemical mechanism and MOSAIC using 4 sectional aerosol bins (Fast et al, 2006) were used. National Center for Environmental Protection (NCEP) 1° by 1° reanalysis data (http://dss.ucar.edu/datasets/ds083.2/) for every 6 hours was used as meteorological initial and boundary conditions. For anthropogenic and biogenic emissions, the Intercontinental Chemical Transport Experiment Phase B (INTEX-B) by NASA (Zhang et al., 2009) and the Model of Emissions of Gases and Aerosols from Nature (MEGAN) Version 2.04 (the latest one) (Guenther et al., 2006) were used in both domains. The Model for Ozone and Related chemical Tracers, version 4 (MOZART-4) is used in this study for the initial chemical state and the lateral boundary conditions (Emmons et al., 2010).

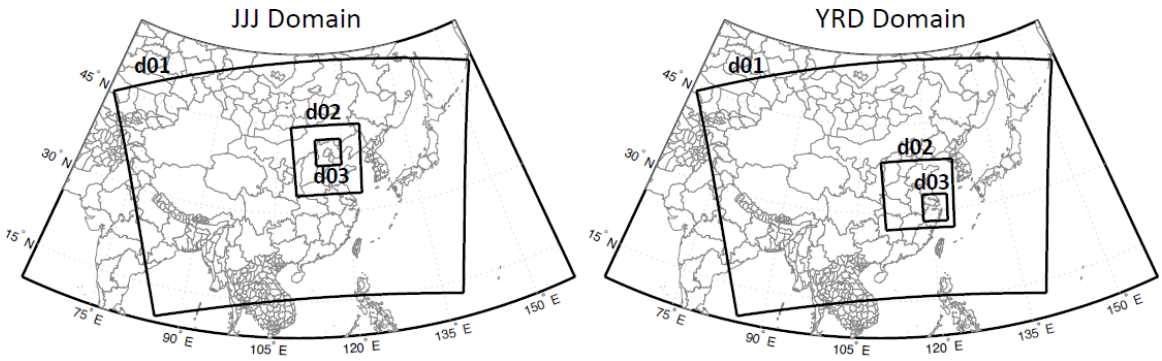

Figure 2.2 WRF-Chem domain settings for Jing-Jin-Ji (JJJ) and Yangtze River Delta (YRD) areas.

2.4.3 Verification

WRF-Chem as stated above, couples the meteorology and chemistry. Since feedbacks between meteorological and chemical variables are included, differences in predicted meteorological variables using different land-cover data sets can be caused in part by chemical feedbacks, induced by the urbanization impacts. Therefore, a test case is needed to evaluate that the land cover mapping was implemented correctly.

In this test case, three comparison runs in WRF without the chemical part were conducted from 0000 UTC 01 May to 0000 UTC 31 May 2010 in the YRD area. They were: a) using original USGS data, b) using original MODIS data and c) using the method described above to convert original MODIS data into USGS 24-categorie format. For a) and b) runs, the regular recommended three step routine in the WRF Pre-Processing System were used: geogrid, ungrid and metgrid, with different land-cover data resources. Regarding to c) run, after running geogrid.exe with both USGS and MODIS land-cover, two sets of intermediate files are generated, with a slight disparity in the variable, 'LANDUSEF'. By mapping the 'LANDUSEF' in MODIS into USGS format (Table 2.1) and replacing the 'LANDUSEF' in USGS with it, the whole updated process is completed. This is followed by the two steps, ungrid and metgrid.

Table 2.1 Mapping Scheme from MODIS to USGS

No. MODIS		No. USGS
1.	Evergreen Needleleaf Forest	14. Evergreen Needleleaf
2.	Evergreen Broadleaf Forest	13. Evergreen Broadleaf
3.	Deciduous Needleleaf Forest	12. Deciduous Needleleaf Forest
4.	Deciduous Broadleaf Forest	11. Deciduous Broadleaf Forest
5.	Mixed Forests	15. Mixed Forest
6.	Closed Shrublands	8. Shrubland
7.	Open Shrublands	8. Shrubland + 9. Mixed Shrubland/Grassland
8.	Woody Savannas	10. Savanna
9.	Savannas	10. Savanna
10.	Grasslands	7. Grassland
11.	Permanent Wetlands	17. Herbaceous Wetland+ 18. Wooden Wetland
12.	Croplands	2. Dryland +3. Irrigated +4. Mixed Dryland/Irrigated Cropland and Pasture
13.	Urban and Built-up	1. Urban and Built-up Land
14.	Cropland/Natural Vegetation Mosaic	4. Cropland/Grassland
15.	Snow and Ice	24. Snow or Ice
16.	Barren or Sparsely Vegetated	19. Barren or Sparsely Vegetated
17.	Water	16. Water Bodies
18.	Wooded Tundra	21. Wooded Tundra
19.	Mixed Tundra	22. Mixed Tundra
20.	Barren Tundra	23. Bare Ground Tundra

To evaluate the impact of urbanization among these three runs, results were analyzed at the grid cell (Longitude 121.34° E, Latitude 31.10°N), which has the largest urban-fraction shift between the two land-cover data sets and completely changed from "Cropland" into "Urban and Built-up land". As Figure 2.3 illustrates, run b) and c) produce similar results over this location, which show that the mapping is implemented correctly. Run a) compared to c) results in a lower temperature by 8.9%, higher wind speeds by 16% and lower PBL height by 60%, which is in line with the results from Yucel et al., (2006). These results demonstrate the impact of urbanization on the meteorology distributions.

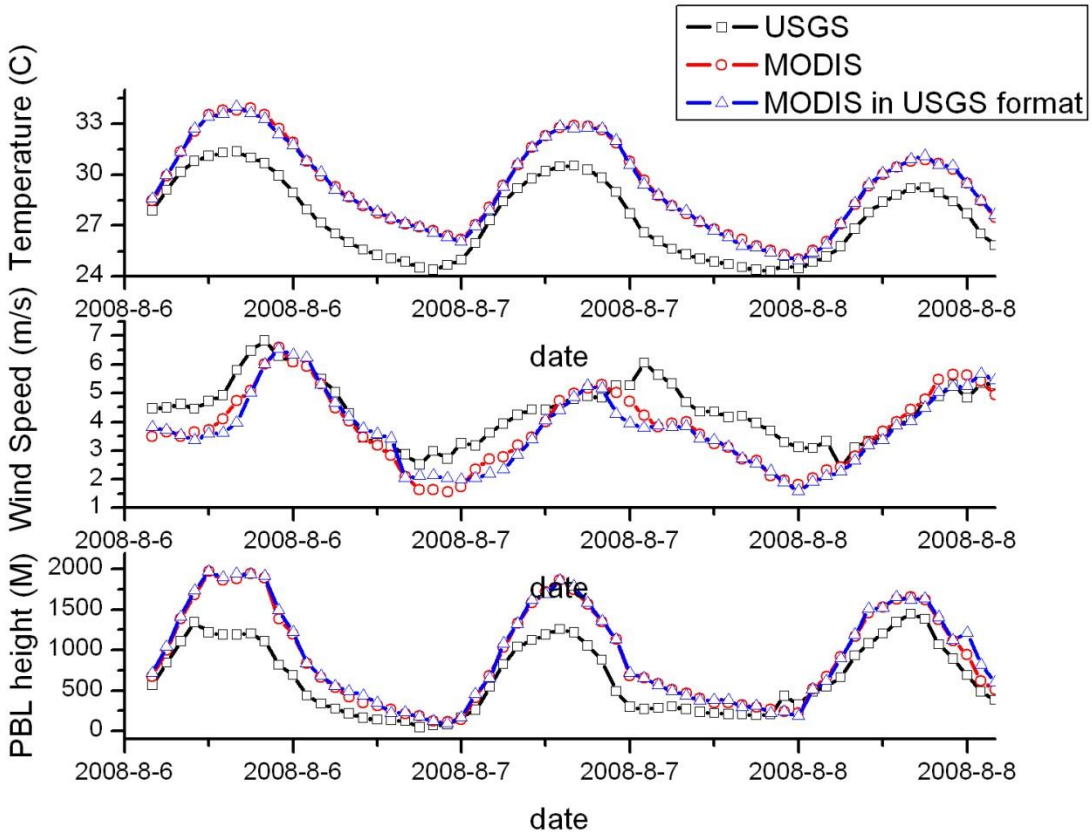

Figure2.3 Comparisons between three different runs (USGS, MODIS, MODIS in USGS format) in test case for meteorological variables: Temperature at 2-m, Wind speed at 10-m and PBL height on the maximum point

2.5 Results and Discussion

For both study areas, WRF-Chem was used to simulate two cases: a) USGS, using the default land-cover data in WRF-Chem, and b) MODIS, mapping MODIS data into USGS format. In order to match the time-periods when observation available in the individual areas, the model simulation was conducted from 0000 UTC 01 August to 0000 UTC 15 September 2006 for the JJJ area and 0000 UTC 01 May to 0000 UTC 3 May 2010 for the YRD area. Only difference plots between USGS and MODIS is shown in this paper.

2.5.1 Spatial Influence of land-cover on meteorology

2.5.1.12-m Temperature

The 2-m temperature (T-2) is affected directly from land-cover change, resulting from its dependence on soil parameters, such as heat capacity and leaf index. Figure 2.4 shows the spatial 2-m Temperature difference between MODIS and USGS runs at 1400 China Standard Time (CST) and 0200 CST for JJJ and YRD, respectively. Some similarities are shared between these plots. First, for most areas where the urban-fraction in both data sets remained the same, MODIS and USGS produce similar results in temperature, usually with differences smaller than 0.5℃. These changes are mainly caused by changes in convective and diffusive heat fluxes, from areas with large urban fraction changes. Second, in both JJJ and YRD, the biggest positive differences occur around big cities where urbanization was large, most obviously in Beijing, Tianjin, Shanghai, Ningbo and Hangzhou (indicated as red circles). The spatial patterns in T-2 are, individually, similar to the spatial plots of urban-fraction change (Figure 2.1). However, there are several dissimilarities between the two study areas. One is that YRD manifested a bigger corresponding increase in temperature with urbanization, with a maximum of 3.2 ℃ change, while for JJJ the maximum temperature changed only by about 1.8 ℃. One of the possible causes is the vertical moisture distributions, especially for the bottom layer of atmosphere. As mentioned before, May 2010 was a drought month for YRD. Temperature differences are consistent with the sensible heat flux increases from land surface to atmosphere. While for JJJ, the increase in latent heat flux was the main driver for the increase of temperature. For nighttime, the monthly-average difference in JJJ was as high as 2.4℃, which is higher than YRD (1.8℃).

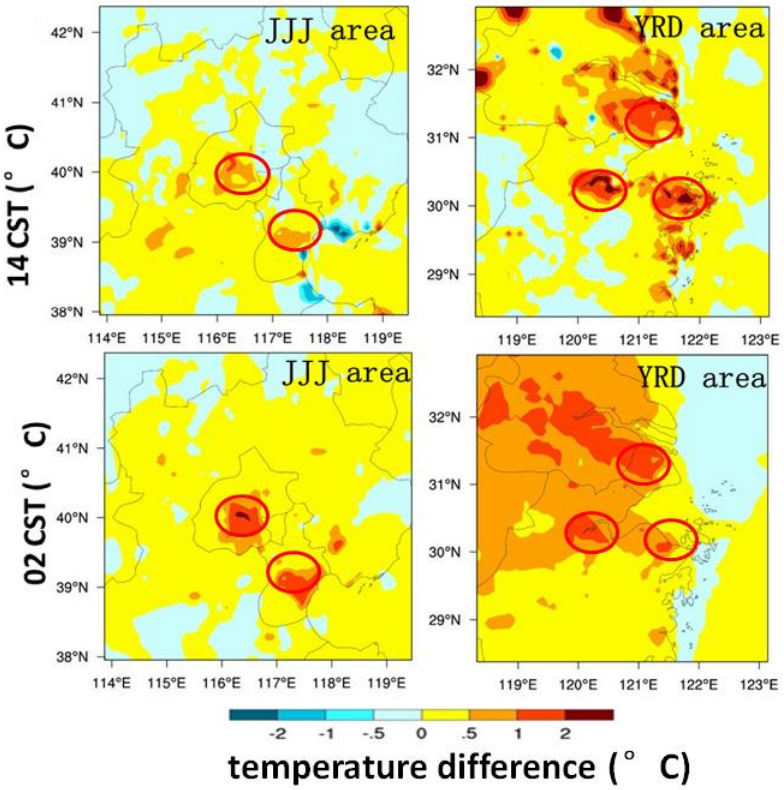

Figure 2.4 Monthly-average spatial distribution for 1400 and 0200 CST for 2-m temperature differences in JJJ and YRD. The red circles indicate large cities, such as Beijing and Tianjin in JJJ and Shanghai, Hangzhou and Ningbo in the YRD area.

2.5.1.2 Surface Wind Speed

Changes in albedo, surface roughness and other physical parameters also impact wind speed and mass transport in the atmosphere. One of the major influences from urbanization is an increase in land roughness. With more wind friction, there should be a decrease in 10-m wind speed. Figure 2.5 shows this decrease at 1400 and 0200 CST for both areas. For daytime, monthly-averaged changes in wind-speed in YRD are associated with the pattern of urbanization, with a maximum decrease of 1.2 m/s in Shanghai,

Hangzhou and Ningbo. Around Beijing in JJJ, the average decrease is around 0.2 m/s, while other cities, Tianjin and Tangshan, show a difference of more than 0.4 m/s. For nighttime, wind speed decreases are more obvious in JJJ (1.0 m/s) than YRD (less than 0.2 m/s). This reveals that urbanization has a stronger impact during daytime in YRD, but at nighttime in JJJ. Compared to Figure 2.5, wind speed decrease is closely related to the 2-m temperature increase. Differences between these two regions are due to the different periods simulated and to their locations. YRD area is located on the eastern coastline of China, mainly influenced by land and sea breeze circulations, while JJJ is an inland, where wind speed and direction are heavily influenced by the surrounding topography.

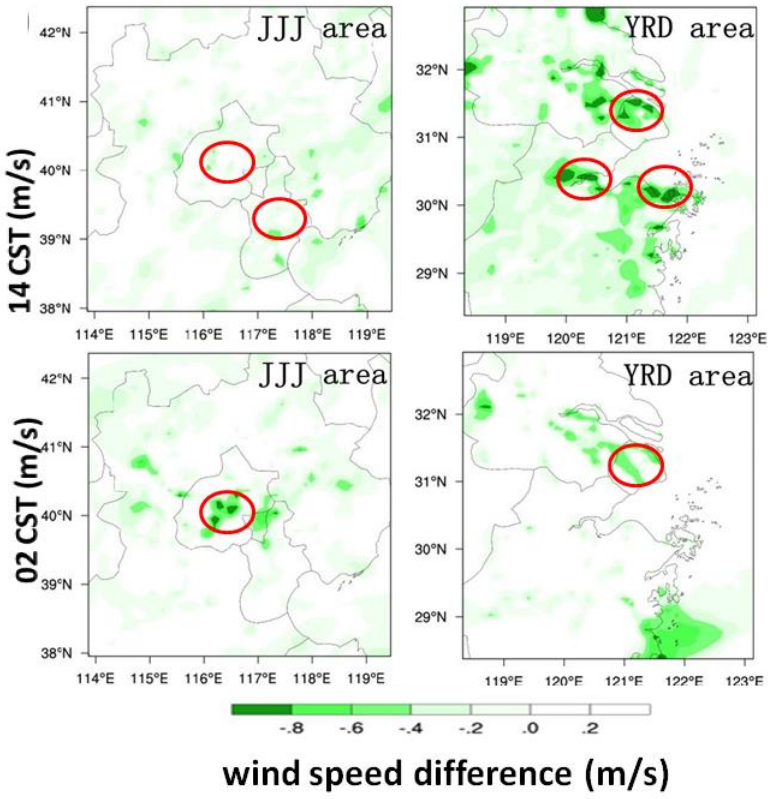

Figure 2.5 Monthly-average spatial distribution for 1400 and 0200 CST for wind speed differences in JJJ and YRD. The red circles indicate large cities, such as Beijing and Tianjin in JJJ and Shanghai, Hangzhou and Ningbo in the YRD area.

2.5.1.3 Surface Dew Point

Within the land-surface and PBL schemes, spatial and vertical moisture distribution is another key variable dependent on land cover. Moisture not only plays an important role in mass and energy transfer between land surface and lower atmospheric layers, but it is also involved in chemical formation and destruction processes, such as the photochemical oxidant cycle and wet deposition, which are influenced by relative humidity and clouds. In this study, we choose 2-m dew point as an indicator for moisture and vapor fields. Hu et al. (2010) pointed out the choice of land surface and PBL scheme can bring a warm/dry bias into WRF simulations. Figure 2.6 shows the spatial plots for monthly-averaged dew point differences at 1400 and 0200 CST for JJJ and YRD, respectively. The opposite sign of temperature and dew point difference corresponds with the warm/dry state (Hu et al., 2010). During daytime, the maximum difference for JJJ is over -3℃ for the mega-cities, like Beijing and Tianjin. While for YRD the maximum difference is about -1.6 ℃ for Shanghai and -2.4 ℃ for Hangzhou. For both areas the shapes of negative dew point differences correspond with the urban-fraction change plot. Nighttime differences are relatively small for YRD, but reach a maximum of -1.3 ℃ for JJJ. The larger differences in JJJ reflect the wet season.

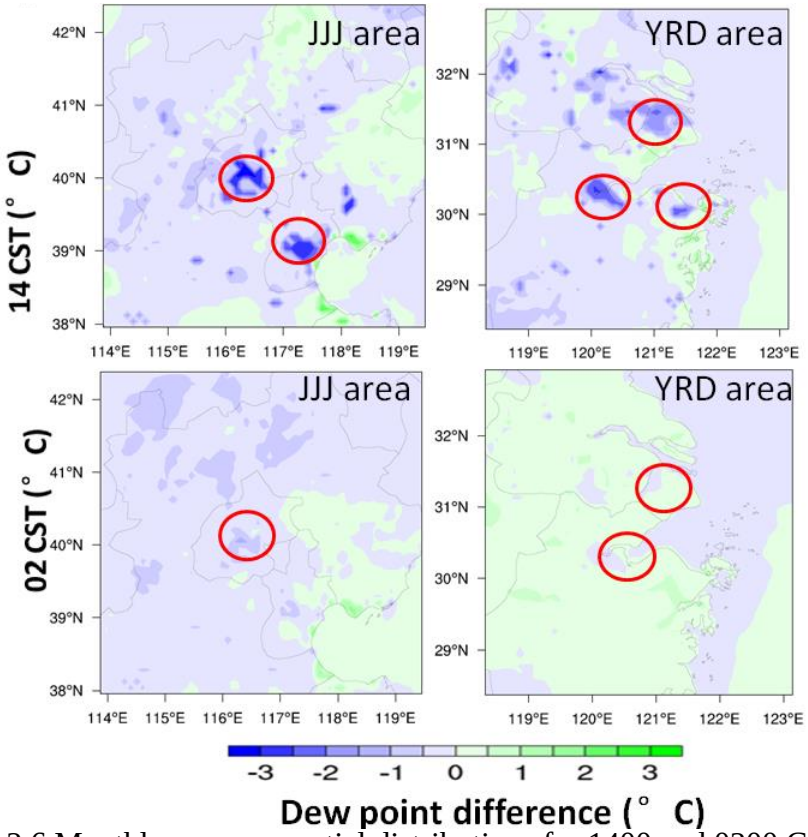

Figure 2.6 Monthly-average spatial distributions for 1400 and 0200 CST for 2-m dew point differences in JJJ and YRD. The red circles indicate large cities, such as Beijing and Tianjin in JJJ and Shanghai, Hangzhou and Ningbo in the YRD area.

2.5.1.4 Planetary Boundary Layer Height

Planetary Boundary Layer height is another crucial variable that controls pollutant transport and surface concentrations. The spatial plots of monthly PBL height difference in both JJJ and YRD for daytime and nighttime, after updating the new land-cover data are shown in Figure 2.7. For mega-cities like Beijing and Shanghai, due to surface temperature changes, the maximum differences at 1400 CST are as high as 400 m and 600 m. Besides positive values over urban areas, negative values, especially for JJJ, occur over suburban and rural areas. For nighttime, the average changes in PBL heights are

around 100 m for both areas. Overall, both JJJ and YRD show similar diurnal pattern in PBL height change, with maximum value around noon and minimum value at night.

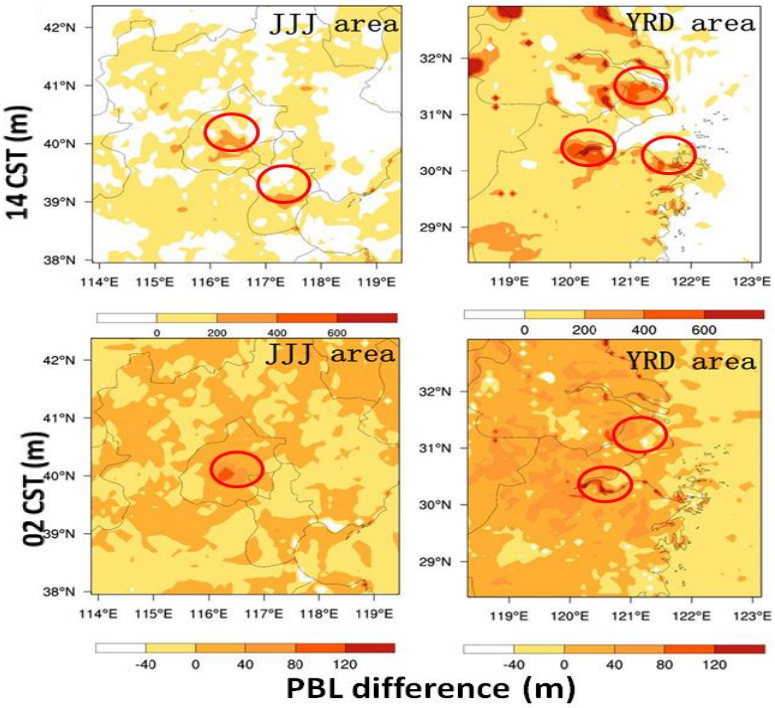

Figure 2.7 Monthly-average spatial distribution for 1400 and 0200 CST for PBL height differences in JJJ and YRD. The red circles indicate large cities, such as Beijing and Tianjin in JJJ and Shanghai, Hangzhou and Ningbo in the YRD area.

2.5.2 Influence of Land-use Change on Pollutant Distributions

2.5.2.1 CO Spatial Concentration

CO is chosen as an indicator for primary pollutant transport. Figure 2.8.a shows the spatial plots for monthly-averaged surface CO concentration difference over JJJ and YRD areas at 1400 CST and 0200 CST. During daytime, the decrease in wind-speed limits the horizontal convection and transport, resulting in an accumulation of CO on urban surfaces of Beijing and Shanghai. The maximum difference is over 60 ppb (or

7.8%) for both areas. Outside of the urban areas, the daytime CO values are lower due to enhanced vertical mixing and increase in photochemical destruction due to temperature increase. During nighttime, negative difference centers form in urban areas due to increasing mixing.

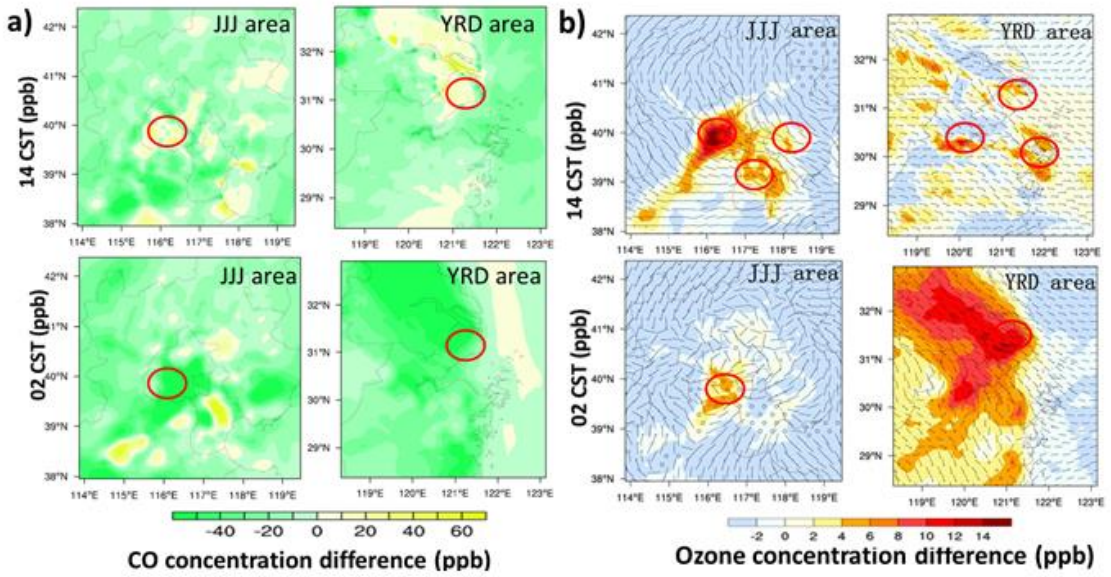

Figure 2.8 Spatial distributions of 1400 and 0200 CST difference between MODIS and USGS for a (CO) and b (Ozone) over JJJ and YRD areas. The red circles indicate big cities, like Beijing, Tianjin in JJJ and Shanghai, Hangzhou and Ningbo in the YRD area.

2.5.2.2 Ozone Spatial Concentration

The impact of the changes in temperature, wind speed, dew point and PBL height due to urbanization on ozone was also investigated. It is anticipated that a temperature increase will accelerate ozone production by raising reaction rates, wind speed decrease will lead to less transport and an accumulation of pollutants, and increases in PBL heights will dilute the concentrations inside PBL, which in urban areas should increase ozone production efficiencies. Figure 2.8.b shows the 1400 CST and 0200 CST difference in ozone (MODIS-USGS) over both areas. The net impact of urbanization is to increase

ozone levels in the urban area. Some large increases are shown in Beijing, a 20 ppb 20% increase during the daytime. The effects of land use change can be as large as those due to 20% increase in emissions. For nighttime in Beijing, ozone concentrations also increased, normally by less than 3 ppb. Compared to JJJ, YRD shows a somewhat different situation, with increases in daytime ozone concentrations over a wider area, but with lower peak values. The higher PBL heights reduced the peak daytime ozone distributions and the lower wind speeds decreased the dry deposition velocities of ozone. During nighttime, ozone differences were significantly enhanced over the region due to the higher PBL heights and lower NOx concentrations. Meanwhile, more ozone from urban areas is transported to downwind areas, where ozone destruction rates are decreased due to lower nitrogen oxides concentrations. Regions with lower ozone differences also occur in areas with little urban fraction change. Overall, the spatial plots of ozone differences in both JJJ and YRD areas are highly related to urban fraction change plots (Figure 2.1.a and Figure 2.1.b) over Beijing, Shanghai, Hangzhou and other cities.

2.5.2.3 Ozone Concentration for Maximum Points

For each study domain, a location was selected based on maximum urban-fraction change. The max points in JJJ and YRD areas, are (Longitude 116.29° E, Latitude 40.07°N) and (Longitude 121.34° E, Latitude 31.10°N), respectively. For the JJJ max point, the urban fraction change was 0.98, which means 98% of the original land cover had turned into urban area from 1992 to mid-2000. Similarly, the max point in YRD had an urban fraction change of 0.89.

Figure 2.9.a shows ozone concentrations using the USGS and MODIS land cover datasets at the two selected max points over the whole simulated period. Overall, the MODIS case produces higher ozone values during both daytime and nighttime. For the JJJ max point, the largest differences occur at noon, with a value of 20 ppb around 2 PM.

Nighttime differences between these two cases are in the range of 5-10 ppb. The diurnal cycle is determined by the diurnal pattern of temperature increase and the diurnal pollutant emission patterns. The plot of max point in YRD shows that during daytime ozone concentrations between USGS and MODIS are close to each other, while for nighttime, the MODIS ozone values are 20 ppb higher.

Cumulative frequency plots for both max points are shown in Figure 2.9.b. In JJJ, the upper 25% of the ozone concentrations in the USGS case are higher than 75 ppb and in the MODIS case they are higher than 80 ppb. For YRD, the upper 25% in concentration difference between USGS and MODIS are more than 10 ppb. Furthermore for JJJ nearly the entire distribution is shifted to higher values for the MODIS case, while for YRD, above 50 ppb, the distributions are similar. This also can be explained by the different diurnal pattern for the ozone differences in the two regions. In the daytime when high value occurs, ozone simulations by MODIS and USGS are close to each other in YRD, while in JJJ, the peak value differences are enhanced.

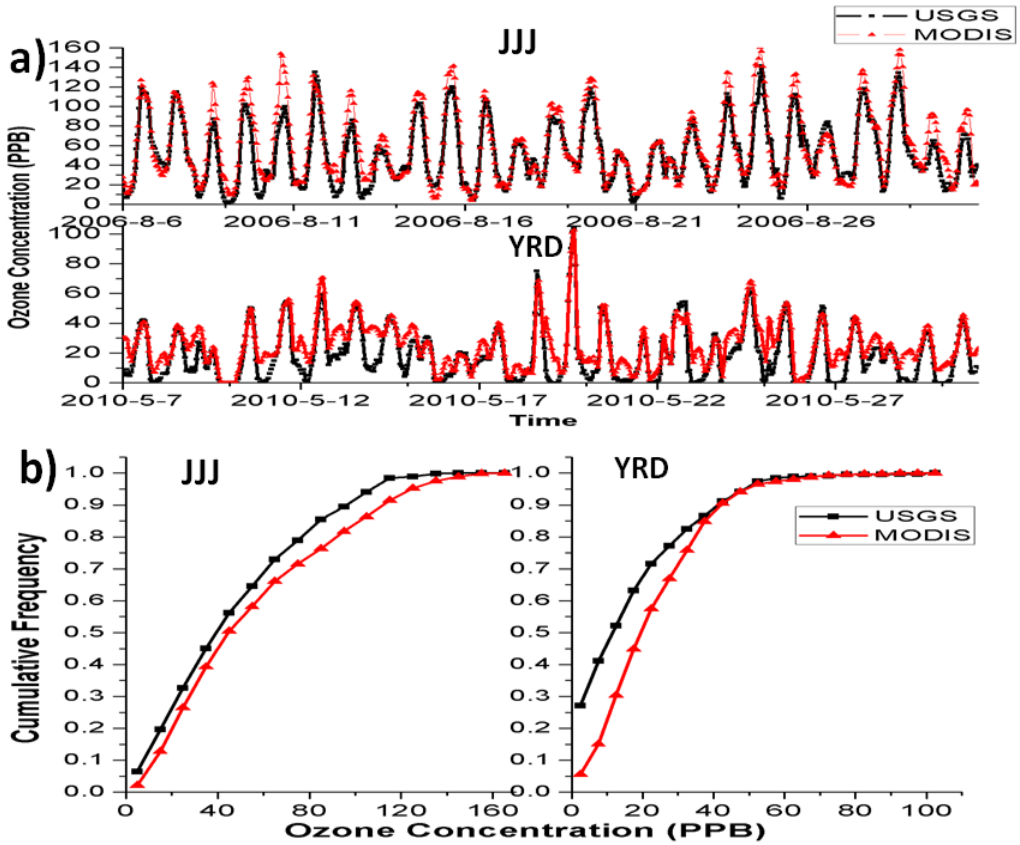

Figure 2.9. For Max points a) full-time ozone concentration plots in USGS and MODIS. b) Cumulative frequency plots in USGS and.

2.5.2.4 Vertical Profile of Ozone Concentration

In order to investigate changes in vertical winds and ozone transport due to urbanization, a cross section, between (39.5° N, 115.5° E) and (40.8 °N, 117.6° N), shown as the black line in Figure 2.1, was selected in the JJJ area. Along this cross-section the urban fraction in MODIS changes from left to right: from 0 % to nearly 100%, then decreases to 0% again (Figure 2.10). Over the urban area, higher surface temperatures result in stronger updrafts and downdrafts. The effect of these changes in atmospheric conditions on pollution transport is shown in Figure 2.11.a and 2.11.b, for daytime and nighttime, respectively. CO is an indicator of regional transport of a primary pollutant. Figure 8.a.a and 8.a.b show the vertical plot of daytime CO concentrations

overlaid with vertical wind in the USGS and MODIS cases, respectively, and 2.11.c is the difference between them. For the USGS case there is, weaker vertical transport and the CO emissions are more localized within the urban boundary layer. In the MODIS plot, CO has been transported and well-mixed within 1km above surface. The differences between them (Figure 2.11.c) show a large decrease in CO over the urban center. To the east, the positive values are due to the vertical redistribution and strong downdrafts.

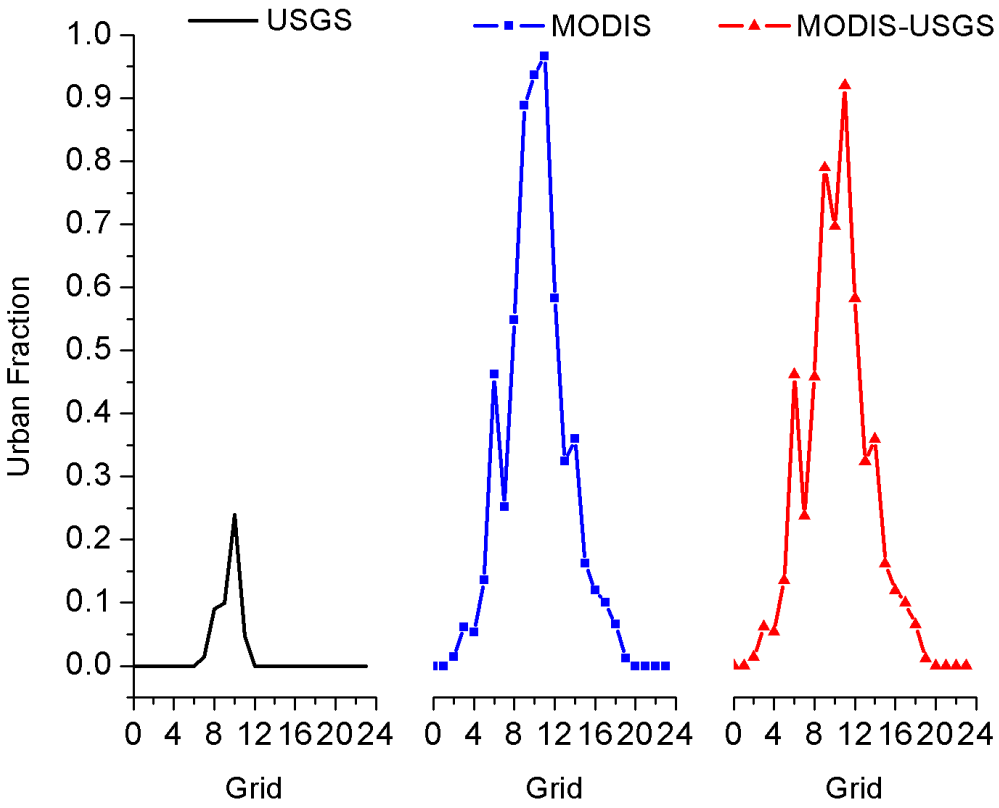

Figure 10 Urban Fraction plots on cross section line for USGS, MODIS, and the difference between them.

For ozone distributions, Figure 2.11.a, d, e and f, show a similar distribution opposite to CO. Higher surface temperatures and higher mixing layer heights result in the MODIS case bring a large increase in ozone concentrations over the urban areas and to

the west. During the nighttime, ozone values over the urban center are due to stronger updrafts over the urban center. To the east, a converging center due to circulation re-structure, transports more ozone from adjacent areas and forms a high value center.

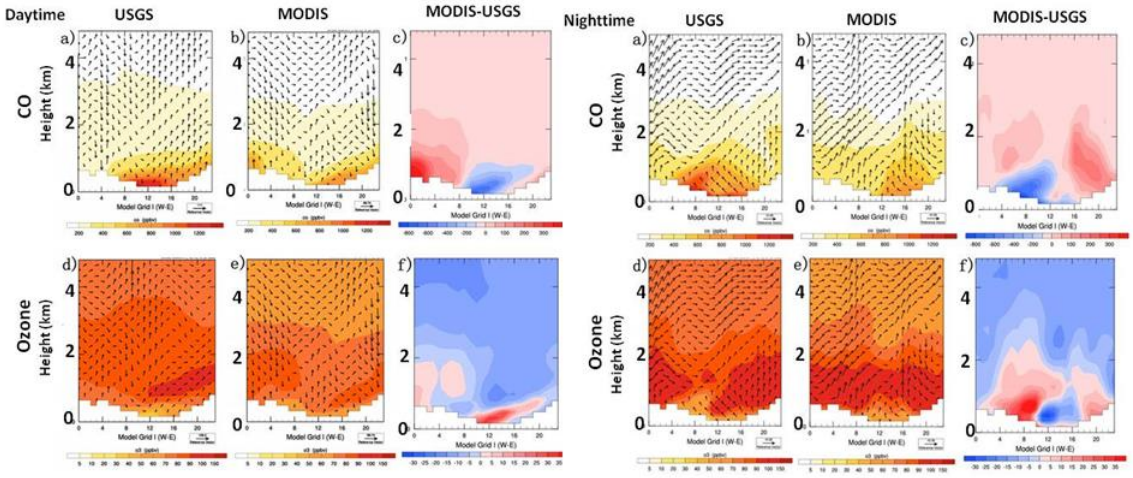

Figure 11 Daytime and nighttime vertical plots from point (39.5° N, 115.5° E) to point (40.8 °N, 117.6° N) (shown as the black line in Figure 1c) by USGS, MODIS, and difference (MODIS-USGS) : a)-c) CO , d)-f) O3

2.5.3 Comparison between Dry and Wet Seasons

To study the effect of season on air quality modeling, an additional simulation was conducted in YRD for August 2010. With an average cumulative rainfall for the whole simulated month of 230mm, August was a relative-wet month for YRD. The maximum increase in 2-m Temperature for each local time drops from 3.2 ℃ in May to 1.8 ℃in August for 1400 CST and from 1.8 ℃ in May to 1.0℃ in August for 0200 CST, respectively. According to the warm/dry, or cool/wet bias in simulation within the PBL scheme (Hu et al., 2010), these negative centers for dew point at the urban areas, with maximum at -2.4 ℃ and -1 ℃ for each local time, indicate an enhanced intensity relative to the May case. With a smaller increase in surface temperature and a weaker vertical

mixing, the PBL height difference for 1400 CST drops from 600 m to 400 m. Although higher surface temperature in the daytime leads to higher ozone concentrations, other factors, like PBL height and wet deposition, influence the ozone difference between MODIS and USGS case for YRD. Compared to May, the dry case, the differences in ozone concentration in August case are smaller, especially for nighttime.

2.5.4 Improved Predictions by Updating the Land-use by Comparing with Observations

For both JJJ and YRD, two locations were selected to compare with observations; one site with little urbanization chosen as the base point, and the other site that has changed from farm-land or other non-urban types to urban area.

At the base point (Figure 2.12.b and d), USGS and MODIS outputs are close to each other with differences smaller than 5%, while for the urbanized locations (Figure 2.12.a and c), MODIS land-cover gives higher estimates, with maximum differences of ~20 ppb. When compared with observations, MODIS outperformed USGS, reducing both Mean Bias and Mean Error and increasing correlations (Table 2.2). For urban points, PKU and XJH, the Mean Error improved by 14.2% (from 9.74 ppb to 8.36 ppb) and 35.6% (from 10.97 ppb to 7.07 ppb). For the base points, compared to the urban points, MODIS produced some improvement, 5.8% for YF and 10.7% for JS. When compared with JJJ, YRD reacted more significantly than JJJ, suggesting a larger impact on dry seasons over wet seasons.

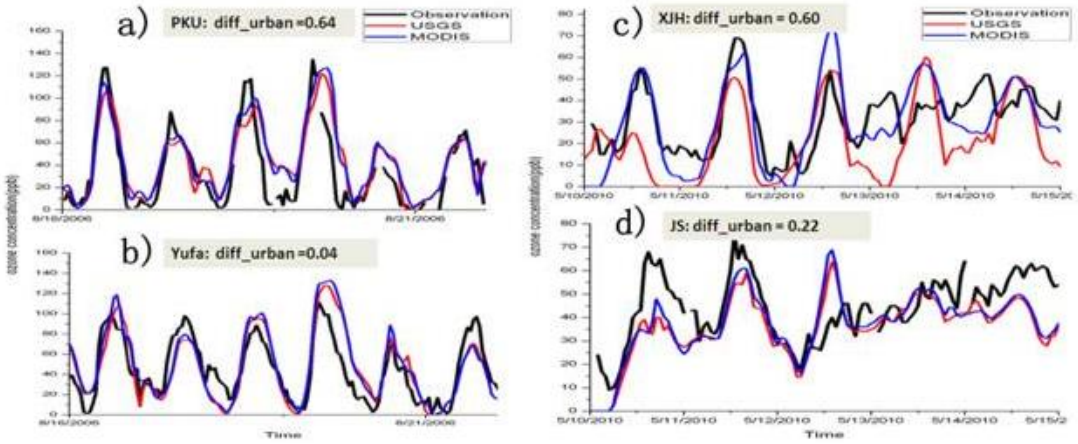

Figure 2.12 Comparisons between observation and simulations with USGS and MODIS land-use data at four locations: a) PKU, b) YF, c) XJH and d) JS

Table 2.2Mean bias, mean error and correlation comparisons for ozone simulations in USGS and MODIS at four selected locations.

	PKU			XJH		
	Mean Bias (ppb)	Mean Error (ppb)	Correlation	Mean Bias (ppb)	Mean Error (ppb)	Correlation
USGS	-0.63	9.74	0.94	-8.34	10.97	0.84
MODIS	0.66	8.36	0.97	-2.20	7.07	0.83
	JF			JS		
	Mean Bias (ppb)	Mean Error (ppb)	Correlation	Mean Bias (ppb)	Mean Error (ppb)	Correlation
USGS	-2.24	15.50	0.80	-12.63	12.20	0.89
MODIS	1.18	14.60	0.81	-9.79	10.80	0.83

2.6 Conclusions

In this study, sensitivity in both meteorology and chemistry to change in land use due to urbanization were evaluated. After updating the land cover data, 2-m temperature increased in JJJ and YRD, with maximum values of 3.2 ℃and 2.4 ℃. Wind speeds decreased with a different diurnal pattern for two areas. For JJJ, the biggest reductions occurred during nighttime (1 m/s), while for YRD they occurred during daytime (1.2m/s). Negative dew point changes in urban areas indicated a dryer situation for both areas. The maximum change in dew point in JJJ (wet seasons) was over -3 ℃ and in YRD (dry

seasons) -2.4 ℃. PBL heights also increased during daytime by 400 m (JJJ) and 600 m (YRD) and nighttime by 120 m (JJJ) and 110 m (YRD).

This study showed that, with the same emission inventory, updating the land use (after urbanization) produced higher ozone values for both areas, with the maximum over 20 ppb in JJJ and 14 ppb in YRD. Analysis of a vertical cross section over demonstrated that the effects of urbanization resulted in stronger upward and downward drifts, which in turn change pollution distribution over a wide region.

When compared with the available observations in both areas, MODIS gave a better performance of ozone concentration. For urban points, it reduced the mean error in JJJ by 14.2% (from 9.74 ppb to 8.36 ppb) and 35.6% (from 10.97 ppb to 7.07 ppb). For base points, where urbanization is minor, it also improved the simulation by 5.8% (JJJ) and 10.7% (YRD).

The MODIS data set used in this study was obtained in mid-2000s and already brought in a considerable change in WRF-Chem simulations, regarding both meteorological and chemical fields. Therefore, for simulation in late-2000s or the next decade more recent MODIS land cover product is needed to further update the land cover data set. The original MODIS land cover product, available yearly, contains 17 classes, which is a subset of the modified-MODIS data set used in this paper. There might be a limitation for further updating. We will further discuss this topic in next paper.

In addition to the effects discussed here, urbanization also results in an increase in anthropogenic heat flux. This additional input of energy will further exacerbate of the effects discussed here. This is a topic of our ongoing studies.

2.7 Collaborators and Funding Sources

This paper was supported in part by NSF grant CHE-1049140 and NASA grant NNX11AI52G.

The CAREBeijing 2006 campaign was supported by the Beijing Council of Science and Technology (HB200504-6, HB200504-2).

CHAPTER 3 LAND-USE CHANGE BETWEEN MID-2000S AND BEFORE-INDUSTRIALIZATION IN BEIJING

3.1 Abstract

This study quantifies the maximum impacts from land-cover change on air quality modeling in China. Since it is a follow-up study, we adopt the exact same domain settings in Chapter 2, except land-cover data. Two parallel test runs are conducted using pre-industrialization land-cover and current land-cover data. Preliminary results show a significant improvement in 2-m temperature and high ozone episodes. Also different patterns of latent and sensible heat flux are simulated on urban cells. The maximum temperature increase is around 2 ℃ in Beijing area. With a deeper PBL and more precipitation (28.8%) on urban cells, the simulations of surface ozone indicate a maximum increase about 20 ppb is expected in Beijing.

3.2 Introduction

In chapter 2, the land-cover change between 1992 and 2004 in Beijing area had been fully tested. Previous study has shown us how much impacts can be brought into model by certain land-cover change. And this drove us to find out the potential or total impacts from land-cover change. Therefore in this chapter a follow-up sensitivity test on the total impact of land-cover change is studied. We developed the pre-industrialization land-cover scenario with no urban land and then compared it with the current urbanization situation.

There are some previous studies investigating urban heat islands. Hidalgo et al. (2008a) observed the urban-breeze circulation in France and found a warmer city center due to negligible evaporation and strong sensible heat flux. And PBL heights were expected to increase by 300 meters (Hidalgo et al. 2008b). Another study by Makar et al.

(2010) demonstrated that the regional ozone concentration is highly dependent on local circulations. Ryu et al. (2013) designed and tested land-surface impacts on ozone concentrations in Seoul and discovered that more ozone (13 ppb) is simulated in the urban area. However, fewer studies were performed in China area, where the rapidest urbanization occurs. In this paper, we are devoting to calculate the quantitative of maximum change and impacts from land-cover change.

3.3 Methodology

In this study, WRF-Chem (the fully coupled Weather Research and Forecast Model with Chemistry Module) is used as the simulation tool. We use the same domain settings as in section 2.4.2 for Beijing area. For more information, please refer to Yu et al. (2012) and Yu et al. (2014). In order to investigate the absolute impact from land-cover change, two similar tests are conducted with different land-cover data. One is using the MODIS data (retrieved by the methodology in section 2.4.1) and the other one is replacing those urban grids with its surrounding nature land. To distinguish two runs, we call the MODIS case reflecting current land-cover situation, the urban case and call the pre-industrialization case the cropland case. As shown in Figure 3.1 below, seven major land-cover types exist around Beijing area. They are Urban, Cropland, Water Body, Mixed Forest, Grassland, Barren land and Shrubland. Based on MODIS data from 2004, urban and built-on grids are replaced with its surrounding nature land type, in this case, mostly into cropland type. Besides this change, all of other surface characters and emission scenarios remain the same.

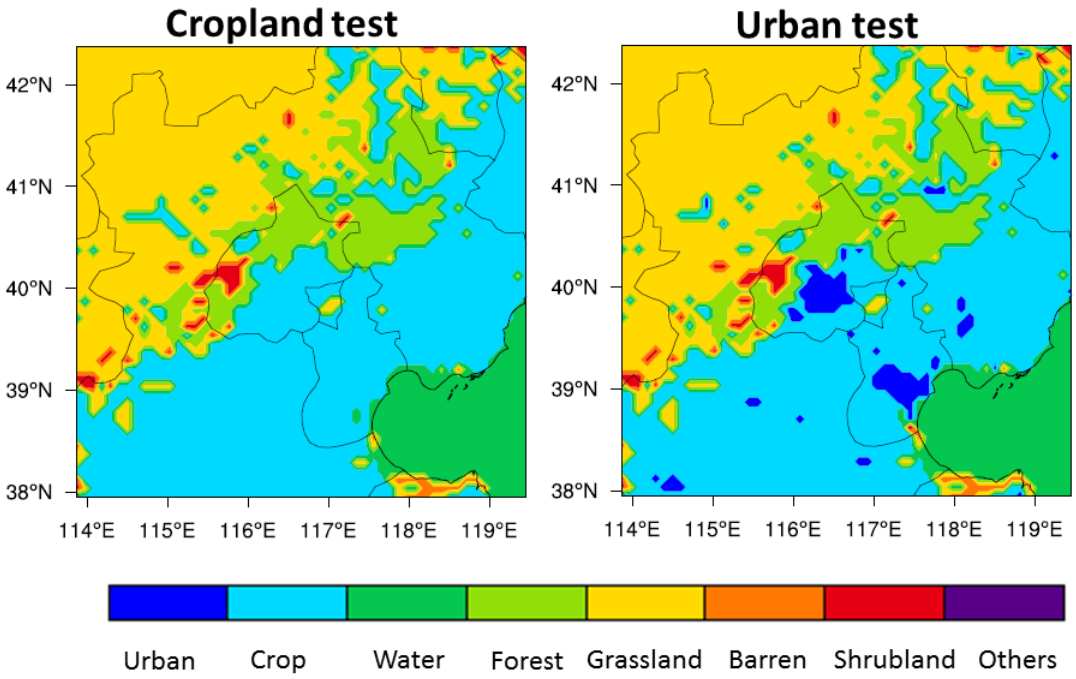

Figure 3.1 Dominant land types in cropland case and urban case in smallest domain

3.4 Results and Discussion

Two different runs (cropland case and urban case) were conducted from 0000 UTC 01 August to 0000 UTC 31 August 2006. Some preliminary results are shown as followed.

3.4.1 Data Validation with Observations

Observation data is available on two sites, (PKU (116.31 °E, 39.99 °N) and Yufang (116.31 °E, 39.51 °N)) from CAREBeijing 2006 field campaign. Since Yufang is the rural site in both cases, the simulations on it are highly similar. For this reason, the comparison on Yufang is not shown here. In this study, we focus on the changes on urban site to disclosure the total impact. Figure 3.2 is the statistical plots between observation and model results on PKU site. From the scatter plot, cropland case tends to underestimate 2-m temperature. The mean bias deduces from -2.82 ℃ to -0.42 ℃ by using current land-cover data. The improvement in ozone simulations is relatively

smaller in nocturnal scenarios. Both cases are likely to yield a higher ozone concentration at night, mainly due to insufficient emissions. However, urban case is able to better capture the high ozone episodes. The averaged peak time increase is as large as 10 ppb.

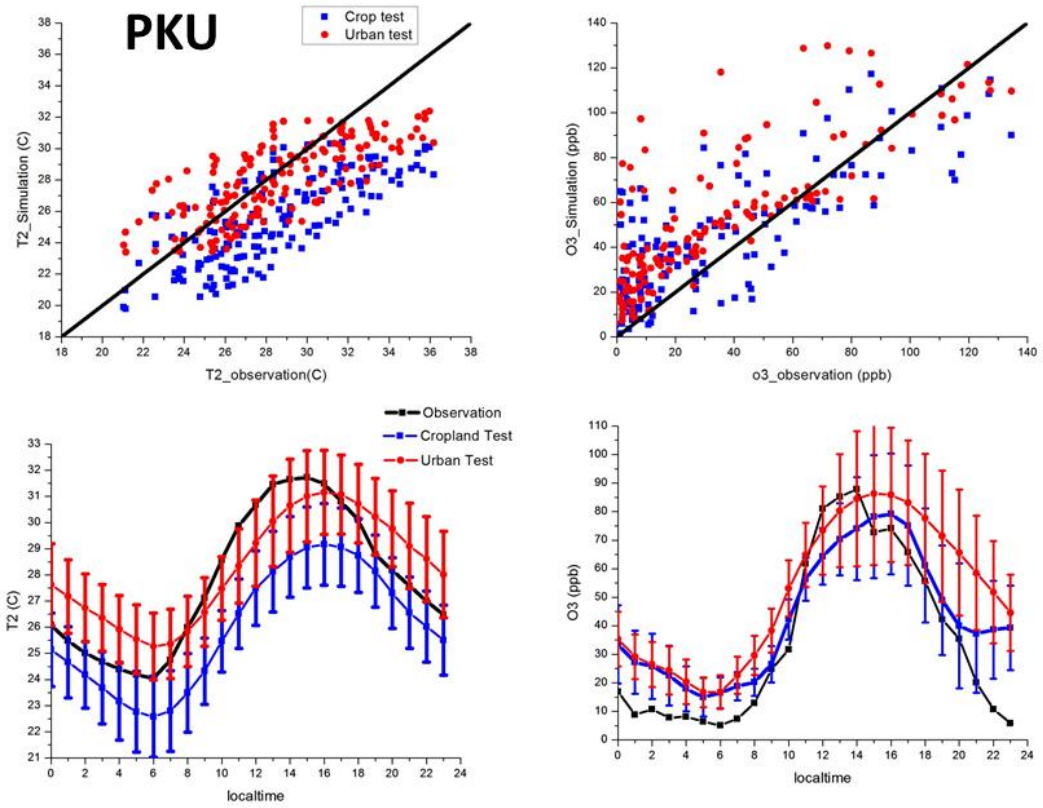

Figure 3.2 Comparison between observations and simulations on PKU site

3.4.2 Vertical Influences on Urban Cells

The heterogeneity from surface (like paved and nature) together with heat release results in the urban heat island. The differences in temperature distribution further drive the formation of urban-breeze circulations. One modification within the surface energy balance is the heat flux redistribution. Figure 3.3 shows the averaged flux for sensible and

latent heat from urban surface. The major part of net radiation is converted into sensible heat in the urban case and into latent heat in the cropland case. The maximum value for sensible heat flux is around 250 W/m^2 on 2 PM local time, while the maximum of latent heat flux appears at noon, highly correlated to solar radiations. Using paved surface in model introduces a very limited latent heat flux in urban cells. The maxima are less than 30 W/m^2, while using nature land-cover promises a continuous moisture flow from surface (the maxima over 300 W/m^2). This result is consistent with the previous study in urban circulations (Ryu et al., 2013). Vertical advection and re-distribution of heat flux is a key factor in representing urban circulations. Another series of meteorological variables are extracted on urban cells for 10 AM, 1 PM and 4PM respectively (shown in Figure 3.4). The solid line is from cropland case and dotted line is urban case. Vertical pressures reveal an insignificant sensitivity to surface land-cover and diurnal changes (Figure 3.4.b). For both temperature and water vapor above PBL, the difference is relatively smaller. With regards to temperature simulations within the PBL, urban case gives higher value. The largest enhancement occurs at the surface (about 2 ℃) and it decreases rapidly with height. Water vapor in cropland case is much higher than that in urban case. Also the surface moisture maintains high values from the morning to the afternoon and a significant increase in moisture fields is also spotted around 0.8 km. This results from continuous vapor flow from surface evaporation and plant transpiration. Meanwhile in urban case, the moisture decreases by 0.001 kg*kg-1 (~10 %) from morning to afternoon on surface and increases in the upper atmosphere. Different shapes for 10 AM, 1 PM and 4 PM demonstrates an intense vertical transportation up to 1.6 km above ground level. Besides these, when comparing the vertical profiles, urban case reveals stronger vertical updrafts and deeper PBL heights. Figure 3.5 below is vertical profiles for temperature, pressure and relative humidity beyond PBL on urban cells. It is consistent with our findings in Figure 3.4. The differences between urban and cropland cases mainly exist within

PBL heights. Urban case tends to provide a dryer situation from the bottom to the top of atmosphere. Meanwhile a deeper PBL is expected in urban case.

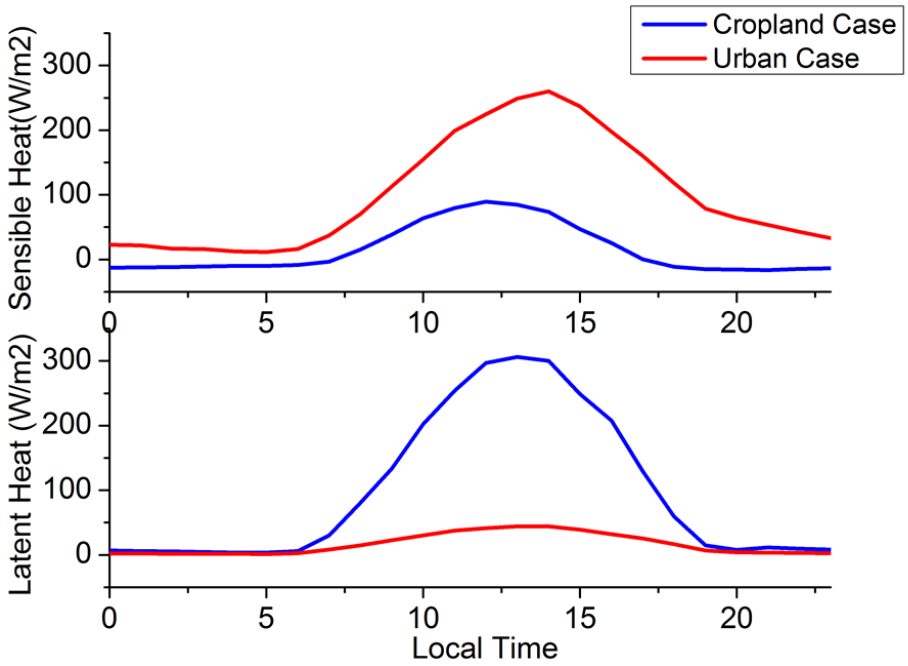

Figure 3.3 Sensible and latent heat distributions on surface in cropland and urban cases.

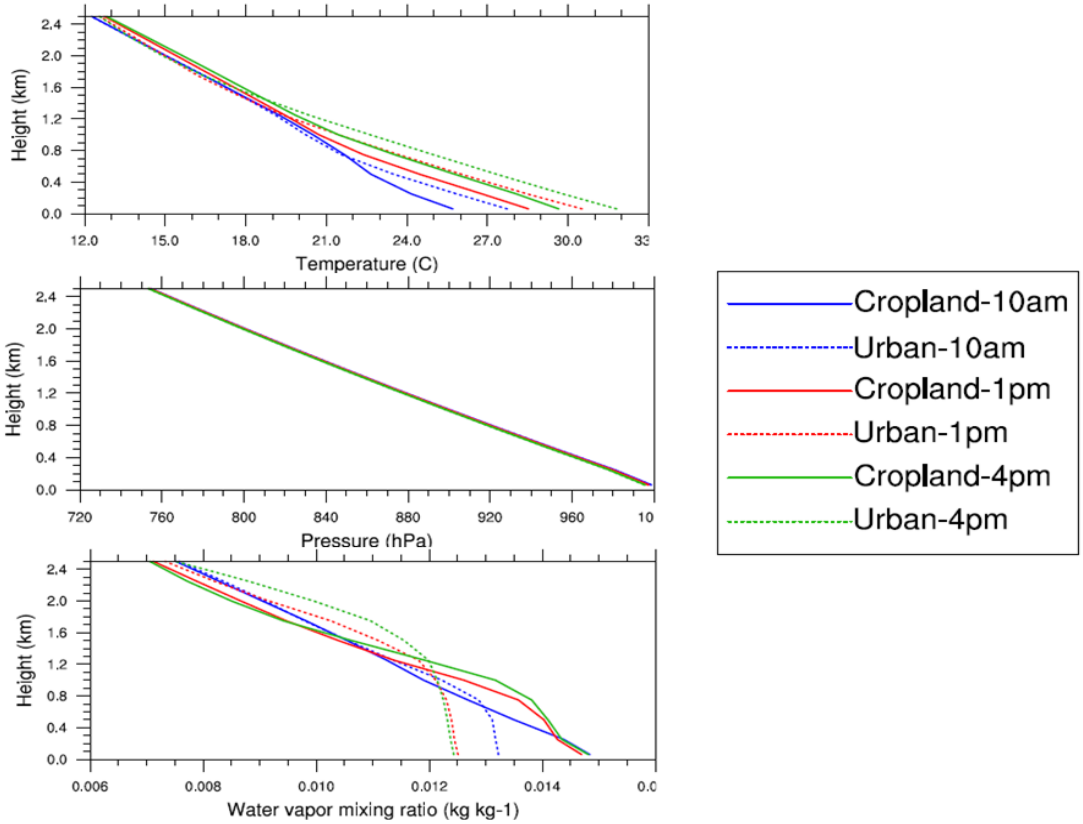

Figure 3.4 Vertical profiles for temperature, pressure and water vapor within PBL in cropland and urban cases

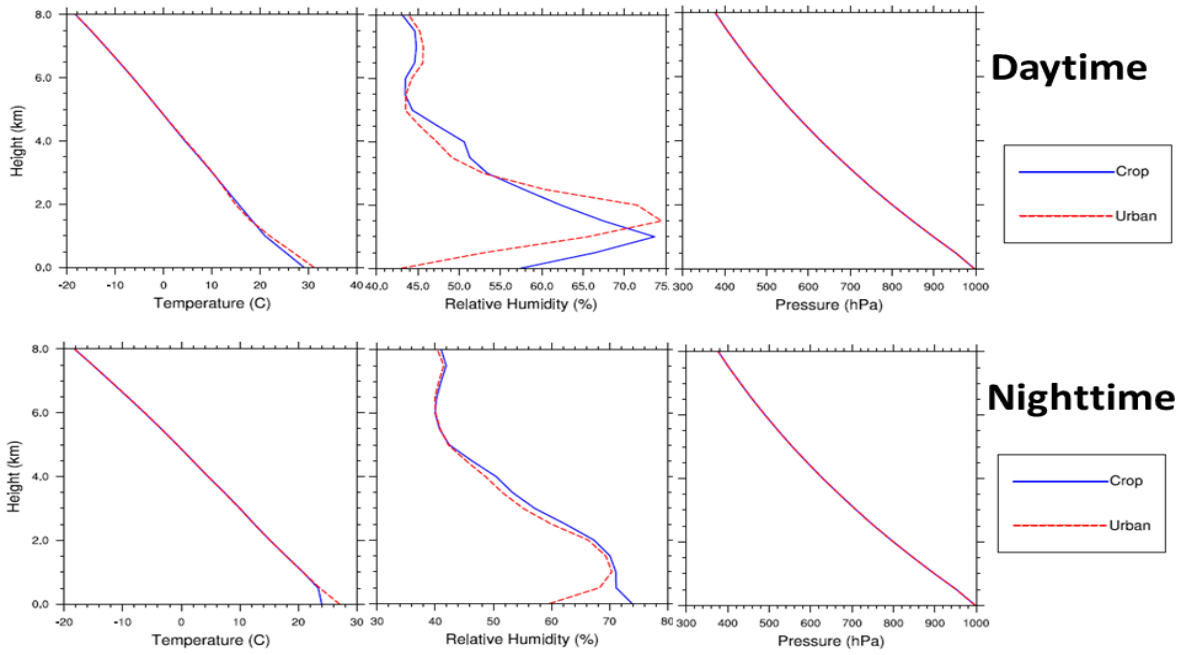

Figure 3.5 Daytime and nighttime vertical profiles for temperature, pressure and relative humidity from surface to 8 km above ground.

3.4.3 Spatial Influences in 3rd Domain

Figure 3.6 shows the monthly-averaged spatial difference plots in 3rd domain for 2-m temperature, PBL height, precipitation, vapor, ozone and NOx concentrations. The arrows represent the wind direction. With more anthropogenic heat emissions and less vapor inside Beijing, the urban case produces higher surface temperatures. The maximum temperature difference is 1.6 ℃ in Beijing and 1 ℃ in Tianjin. Also in the difference plots, wind difference around cities indicates a converged pattern, which is part of the urban-breeze circulation during daytime. Because of this reinforced updrafts driven from temperature gradients, the PBL extended in urban case by as large as 600 meters. Intense convection and moisture re-distribution brings in more rainfalls (28.8% or 160 mm) in urban case. As we discussed before in Chapter 4.3.2, a dryer surface is expected in Beijing area. Several factors contribute to this drought on urban cells. More vapor is transported into upper layers and also more precipitation in Beijing could further decrease surface humidity. Despite of extended PBL heights, surface ozone simulations in urban case still show a significant enhancement on urban cells. The increase is more than 20 ppb. Comparing with ozone enhancement in chapter 2.5.2, this finding reveals another 6 ppb increase.

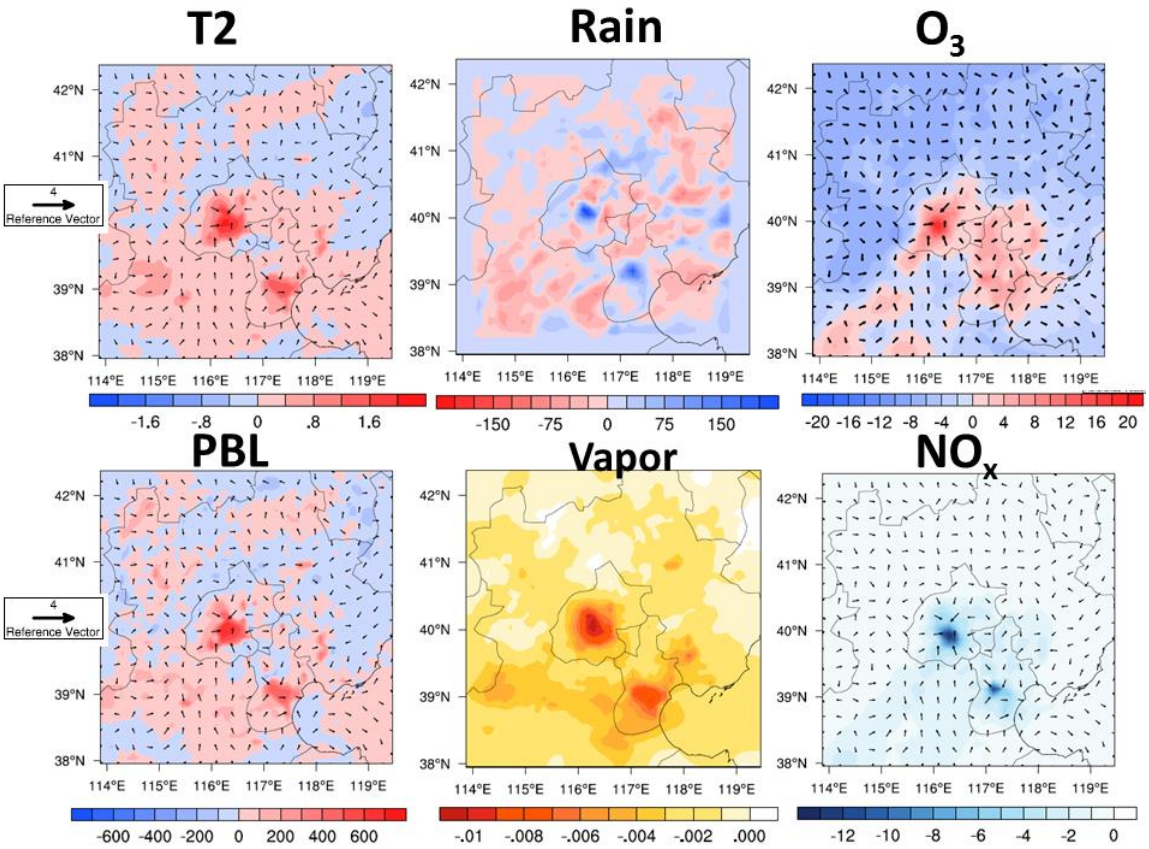

Figure 3.6 Monthly-averaged spatial difference plots in 3rd domain for 2-m temperature, PBL height, precipitation, vapor, ozone and NOx concentrations

3.5 Conclusions

Based on the study in Chapter 2, we analyze another land-cover impact in Beijing area. In this chapter, two different land-cover data are used. One is from MODIS and the other one is reflecting the pre-industrialization scenario.

Significant improvements are found out on PKU site, with mean error decreases by 2.4 ℃ for surface temperature simulations. Urban case is also capable to improve model's reliability during high ozone episodes. Further analysis in vertical distributions helps to understand vertical dilution and transportation for chemical species. Cropland case tends to convert net radiation into latent heat flux, while urban case focuses on sensible heat. A warm and dryer surface is simulated in urban

case, which is consistent with our findings in Chapter 2. For ozone concentration, despite of the dilution effects from extended PBL, changing land-cover seems to worsen the air quality on surface. The maximum increase is as large as 20 ppb, a further 6 ppb increase compared to Chapter 2.

CHAPTER4SENSITIVITY OF PREDICTED POLLUTANT LEVELS TO ANTHROPOGENIC HEAT EMISSIONS IN BEIJING

4.1 Abstract

A new parameterization method for anthropogenic heat (AH) parameterization (called NewLUCY) is developed in the WRF-Chem model, which estimates hourly heat fluxes with a single-peak diurnal variation pattern and utilizes updated urban built-up land use data. The impacts of accounting for anthropogenic heat (AH) fluxes on the meteorology and air quality of the Greater Beijing area are studied using this upgraded WRF-Chem model system. Including AH is shown to increase the surface temperature by 0.8 ℃in daytime and 1.2 ℃ at nighttime. The Planetary Boundary Layer (PBL)heights are also increased, with a maximum enhancement exceeding 320 m during daytime and 160m at night. Spatial and vertical distributions of the simulated pollutants are also impacted by the AH. Surface ozone concentrations increase in the urban areas (4ppb for daytime and 18 ppb for nighttime) when AH is included in the analyses. Moreover, the impacts of AH are not limited to the urban centers, but extend regionally. For example, the simulated PM2.5 concentrations increase in the rural areas as well, due to a decrease in rural precipitation rates when AH is included. In general, incorporations of AH increase the accuracy of the predictions to observations. At the Peking University site (PKU), the mean error (ME) of the 2-m temperature prediction is reduced from 1.55 ℃ to 0.61 ℃. The predictions of the high ozone episodes are also improved.

4.2 Introduction

Driven by economic and population growth in China, rapid urbanization has been ongoing ever since 1980s when reform and open-door policies were initialed. The built-up area in Beijing increased from 184 km^2 in 1973 to 1210 km^2 in 2005 (Mu et al., 2007). According to the sixth national census in China (2010) and Van de Poel et al. (2012), the percentage of urban population has increased from 20% in 1980 to nearly 50% in 2010. Yan et al. (2012) found that rates of hypertension and inflammation have also increased with urbanization. Hence, it is important to understand how urbanization impacts local meteorology and air quality. Based on this understanding better mitigation strategies can be developed.

Urbanization impacts the atmospheric environment in many ways. These include increases in pollution emissions from intensification of transport and economic activities, and changes in surface albedo. Another impact is associated with changes in sensible heat due to intense human energy demand in urban environments. In most air quality modeling applications, the surface sensible heat flux is calculated via

$$Q_H = F_{veg}*Q_{veg}+F_{urb}*Q_{Hurb} \quad (1)$$

Where QH is the total sensible heat flux from the surface to the lowest atmosphere layer, F_{veg} is the fractional coverage of vegetation, Q_{Hveg} is the sensible heat flux from vegetation cover, F_{urb} is the fractional coverage of urban and the built environments, and Q_{Hurb} is the sensible heat flux from the urban cover.

Urbanization results in land-cover change from vegetative to urban (built-up and paved) surfaces, which modify the values of F_{veg} and F_{urb} in equation 1. Land-cover changes lead to surface temperature increase, Planetary Boundary Layer (PBL) height increase and an enhancement in surface ozone concentration, which has been discussed in details in previous studies (Yu et al., 2012). A second impact is the additional heat release due to human activity, a major contributor to the Urban Heat Island (UHI) (Taha, 1997).With anthropogenic heat (AH) emissions, Q_{Hurb} will be enhanced.

AH only contributes about 0.3% of the total energy emitted by the atmosphere and ocean circulation (Zhang et al., 2013), but it can directly alter the surface energy balance and chemical production and destruction rates. Several previous studies have focused on urban AH emissions. For instance, Fan et al. (2005) showed that the AH release in Philadelphia, US can increase the nighttime temperature by 2-3 ℃ for winter and change the structure of the nocturnal PBL. Moriwaki et al. (2008) did a similar analysis in Tokyo Japan and found the daily maximum AH emissions in August exceeded 25 W/m^2. The annual mean AH emission for Greater London, were estimated by Lamarino et al. (2012) to be10.9 W/m^2 for the period 2005 to 2008. With AH emissions, Ryu et al. (2013) simulated a stronger urban-breeze circulation in megacity and a higher ozone concentration (averaged 3.8 ppb) over the urban area. There have been few studies on AH emissions in China. He et al. (2007) incorporated AH into PBL model for Nanjing 2002 and found a temperature increase (0.5~1 ℃) at night. Feng et al. (2012) estimated a 0.35 ℃ difference by adding a fixed AH emission to Beijing area. However, most of the previous studies only focused on the influence of AH on the meteorological fields, but our study will estimate also the impacts on local air quality. Instead of using limited local emission data, a methodology to develop AH emission is also needed for China cities.

In this paper, we focus on (1) how to estimate the AH emissions in China, (2) implementing of the improved AH flux parameterization into WRF-Chem model, and (3) evaluating its impact on meteorology and air quality. Beijing, the capitol of China and the financial center for Northern China, has a population of about 19 million (the sixth national census in China, 2010). The urban built-up area has expanded for over 10 times in the past 30 years. Ozone, PM10, PM2.5 has been proved primary pollutants in Beijing (Duan et al., 2008; Wu et al., 2011; Gao et al., 2012) and air quality is associated with inflammation, hemostasis and many other kinds of illness in Beijing (Zhang et al., 2013). Our upgraded WRF-Chem model system with the new AH parameterization is applied for the Greater Beijing area to demonstrate the impact of the additional heat source on the

air quality and meteorology of the region. These impacts are evaluated in addition to the impacts from land use change we reported in Yu et al. (2012).

4.3 Description of Study Area, Tools and Data

The study area is the Greater Beijing Area. The study domains and configurations have been described in Yu et al. (2012).Three nested domains, with resolution of 81 km, 27 km, and 9 km respectively, were employed (Figure 4.1). The largest domain covers East Asia, including the whole China. The smallest domain was centered over Beijing, and also included its surrounding large cities. WRF-Chem V 3.1.1(Grell et al., 2005) has been proved to be a reliable tool in simulating air quality from city-scale to meso-scale in China (Tie et al., 2013; Jiang et al., 2012; Li et al., 2011). In this study a configuration that includes direct and indirect feedbacks was used. The model top was set as 10 hPa with 28 vertical layers. The Single Layer Urban Canopy Model (SLUCM) (Kusaka et al., 2001), using default urban parameters, was chosen as the urban surface scheme. The Carbon Bond (CBMZ) chemical mechanism and MOSAIC using 4 sectional aerosol bins (Fast et al, 2006) were used. We used the Intercontinental Chemical Transport Experiment Phase B (INTEX-B) (Zhang et al., 2009) as anthropogenic emissions and the Model of Emissions of Gases and Aerosols from Nature (MEGAN) Version 2.04(Guenther et al., 2006) for biogenic emissions. Land-cover data is from MODerate resolution Imaging Spectro radiometer (MODIS) (Yu et al., 2012). Further details regarding the model configuration can be found at Yu et al. (2012).

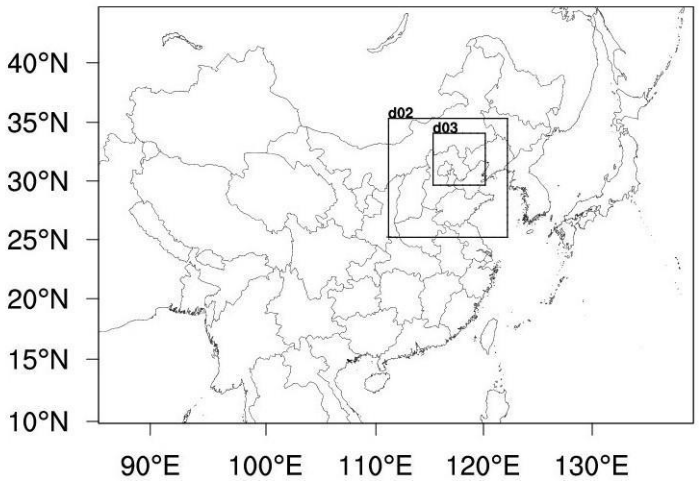

Figure 4.1 three nested domain settings for the Greater Beijing

Observation data was from the Campaign of Air Quality Research in Beijing (CAREBeijing) 2006. It was initiated by the Beijing Municipal Environmental Protection Bureau (Beijing EPB) and Peking University (PKU).In this study data in August 2006 from CAREBeijing campaign (Wiedensohler et al., 2009) at the urban site located in Peking University (PKU, (116.31°E, 39.99°N)) was used to evaluate the model results.

4.4 Methodology for Estimating AH Fluxes

Within the WRF-Chem model, there are currently two different ways of including AH. One is using the urban scheme SLUCM (Single Layer Urban Canopy Model) with the option for AH (Chen et al., 2011). With this method, the AH for each grid is determined by two factors: a fixed temporal diurnal pattern and the urban fraction value on each grid. This uniform diurnal pattern has two peaks, in the morning and afternoon (Chen et al., 2011). Based on Single Layer Urban Canopy Model, this method is called SLUCM. The second method is to input self-generated anthropogenic emissions into WRF-Chem. For the second method, we adopted LUCY (Large scale Urban Consumption of energY model) (Version 3.1) as our AH emission model. This is a global AH emission model developed by Sue Grimmond, King's College London UK and the

outputs vary with time of day, time of year and the location (Allen et al., 2011). LUCY produces a temporal diurnal pattern, with one peak value in the afternoon to reflect the major contribution from office buildings. Recent studies had confirmed that limited variations from LT (Local Time) 0700 to LT 1800 and also the percentages of traffic section (only around 10% to 15%) developed the diurnal pattern for mega cities into one peak shape (Ichinose et al., 1999; Offerle et al., 2005; Narumi et al., 2009).

4.4.1 Sensitivity Cases for AH Emissions

Three test runs were conducted in the Greater Beijing area from 0000 UTC 01 August to 0000 UTC 31 August 2006. These were simulations with no AH emissions and runs using the two different methods.

Figure 4.2.a &4.2.b show the spatial plots of the maximum AH release (at 1400 local Time (LT)) for SLUCM (a) and LUCY (b). For the SLUCM module, the maximum value is 50 W/m^2 in the city centers of Beijing, with decreasing gradients towards the suburban and rural areas. LUCY gave higher peak values (more than 90 W/m^2). However the heat distribution for LUCY is spatially limited to only the largest city centers.

Figure 4.2.f gives the AH heat fluxes at the PKU location for the two different methods and base run. The LUCY method produces slightly higher estimates with a single peak (around 250 W/m2), while the SLUCM produces a double peak. This AH changes the upward sensible heat fluxes (HFX), a crucial parameter for energy and momentum exchange in the lower atmosphere and also a major contributor for urban-breeze circulation. After adding the AH into WRF-Chem, there is an enhancement in HFX as large as 40 W/m^2 for SLUCM and 45W/m2 for LUCY case (Figure4.2.d). The average 2-m temperatures increase by 0.5 ℃ in the SLUCM case and 0.4 ℃in the LUCY case (Figure 4.2.e) with the addition of AH.

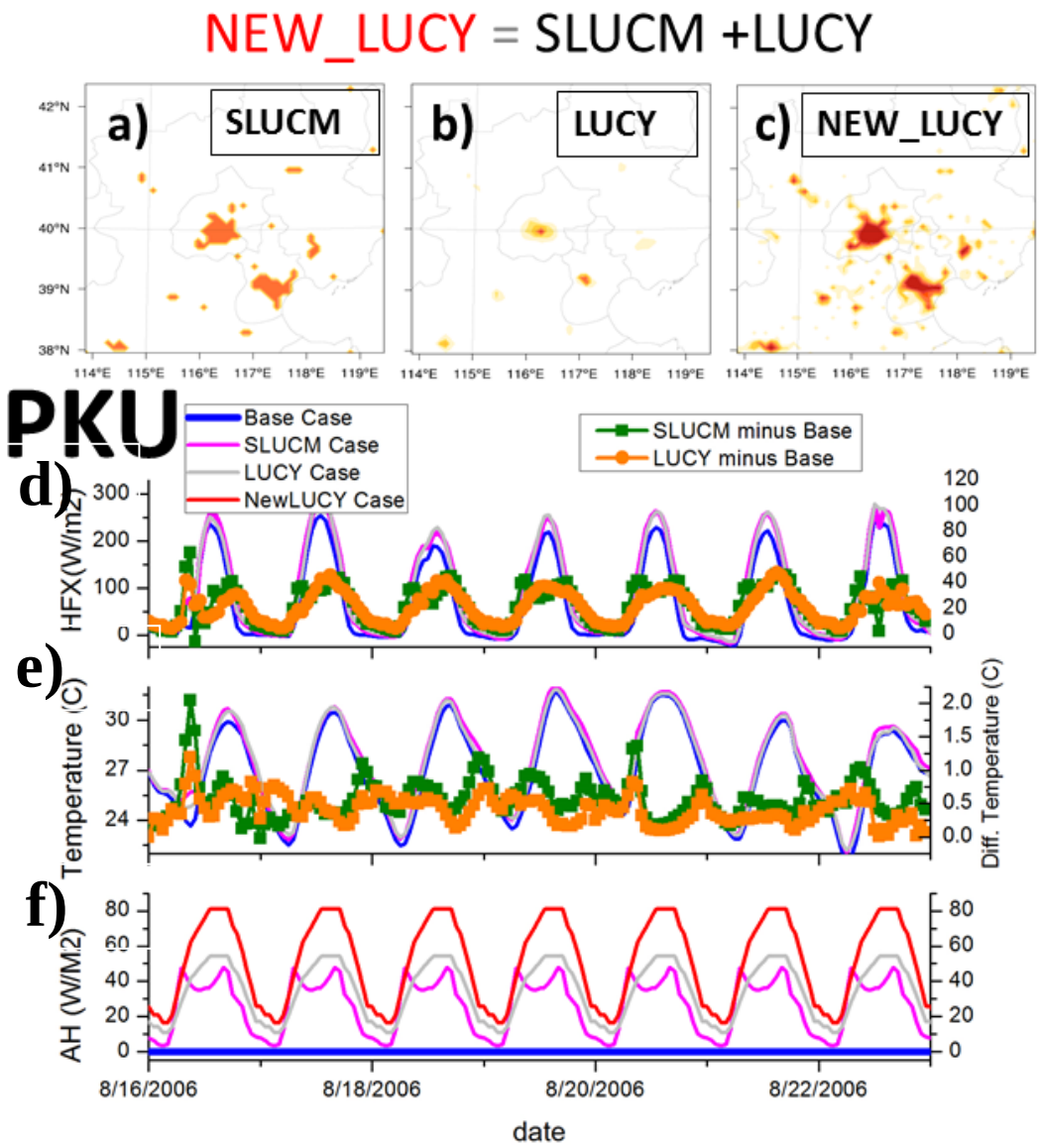

Figure 4.2 Spatial plots for the maximum AH release: a) SLUCM b) LUCY and c) NewLUCY cases. Temporary plots on PKU site for d) HFX and difference, e) Temperature and difference, and f) AH.

4.4.2 NewLUCY Parameterization

The differences in the spatial distributions of the heat fluxes are important. A key issue in any urban heat estimate is to ensure that the urbanized land use used in the model is reflective of the time period analyzed. This is particularly true in places like China that

are developing rapidly. To illustrate, the PKU site was a suburban location into the 1990s. However, with rapid urbanization in Beijing, it has been completely changed into urban surface (96.2% urban fraction) in the mid-2000s. The default data sets used in LUCY including urban fraction, population census and power consumption statistics for China are reflective of earlier time periods. Hence LUCY underestimates the AH emission at PKU by giving a value of only 50 W/m^2, while estimating other old-town grids over 90 W/m^2.

SLUCM and LUCY have their own advantages and dis-advantages in estimating AH flux (Table 4.1). A new estimate of AH, called NewLUCY was developed by combining the advantages of both SLUCM and LUCY, including more realistic urban shape from SLUCM, more reliable peak values from LUCY and one-peak diurnal pattern from LUCY. For every single hour, an AH value was assigned on each grid according to its new urban fraction (MODIS data, mid-2000s) and the maximum AH from LUCY on that specific hour. The generated AH estimates from NewLUCY are shown in Figure 2.c) for the greater Beijing area. The spatial pattern now reflects updated urban development and peak values. Figure 2f reveals more clearly the differences between the various models, including the timings of the peaks, and enhanced fluxes with peak values of nearly 90 W/m^2at PKU.

Table 4.1 Advantage and disadvantage for SLUCM and LUCY

	SLUCM	LUCY
Advantage	Updated urban shape and center	Reliable peak values for every hour
		AH gradient from City center
		One-peak diurnal pattern (major contributions from buildings)
Dis-advantage	Uniform peak values	Outdated urban data
	Two-peak diurnal pattern	Shift between city center and AH center
	No gradients in urban areas	

4.5 Results and Discussions

The impacts of AH inputs based on the NEW_LUCY hourly emissions are compared to the no AH simulations and the results are discussed below.

4.5.1 Spatial Impacts from AH

4.5.1.1 Local Meteorology Changes

Figure 4.3a-b shows monthly-averaged difference plots (with AH minus without AH) of 2-m temperature and winds at 1400 and 0200 Local Time (LT), respectively. The arrows inside Figure 4.3 represent the wind velocity and direction differences. For city centers like Beijing and Tianjin, adding AH leads to an increase in both daytime and nighttime temperature, generating an enhanced Urban Heat Island. The nighttime maximum increase (1.2 ℃) is larger than that in the daytime (0.8 ℃), forming a weakened diurnal variation of 2-m temperature.

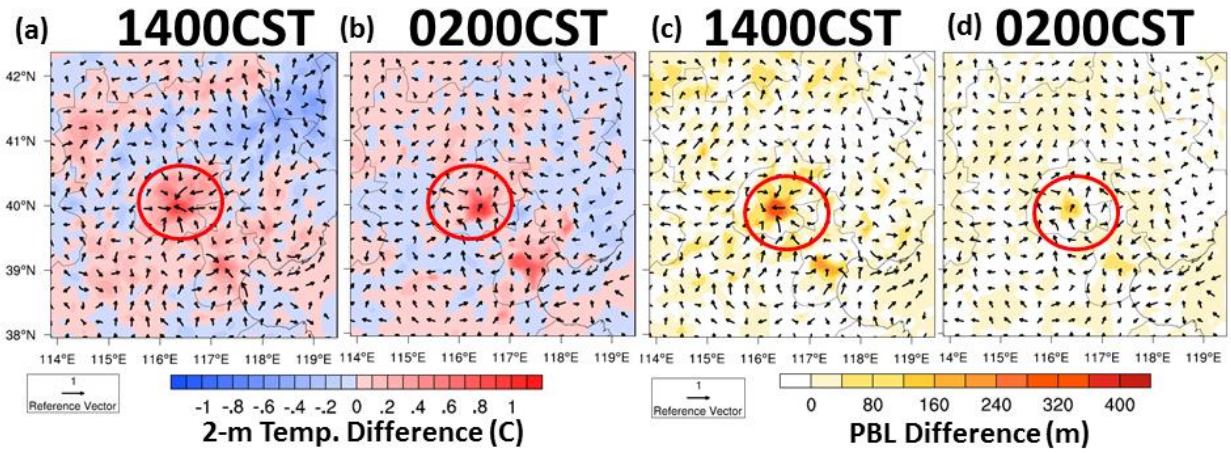

Figure 4.3Monthly-average spatial distribution for daytime and nighttime temperature differences (a-b) and PBL height differences (c-d) in Greater Beijing area. The differences in wind velocity and directions are also presented. The red circle indicates Beijing.

The Planetary Boundary Layer plays an important role in influencing surface pollution concentrations at the surface. Adding AH increases the PBL heights in the daytime and nighttime (Figure 4.3c-d). The maximum increase for daytime is as much as 320 m and 160 m for nighttime for Beijing area. The relative increase in PBL is bigger at night than for daytime due to the fact that the absolute values are lower in night than in day and temperature increases more during nighttime.

The changes in winds show that in populated areas AH causes an urban-breeze circulation with a stronger convergence wind pattern in the afternoon and a more divergent wind pattern in the nighttime (see the red circle). This phenomenon demonstrates a strengthened (by nearly 20%) urban-breeze circulation, which is consistent with Chen et al. (2009) and Ryu et al. (2013).

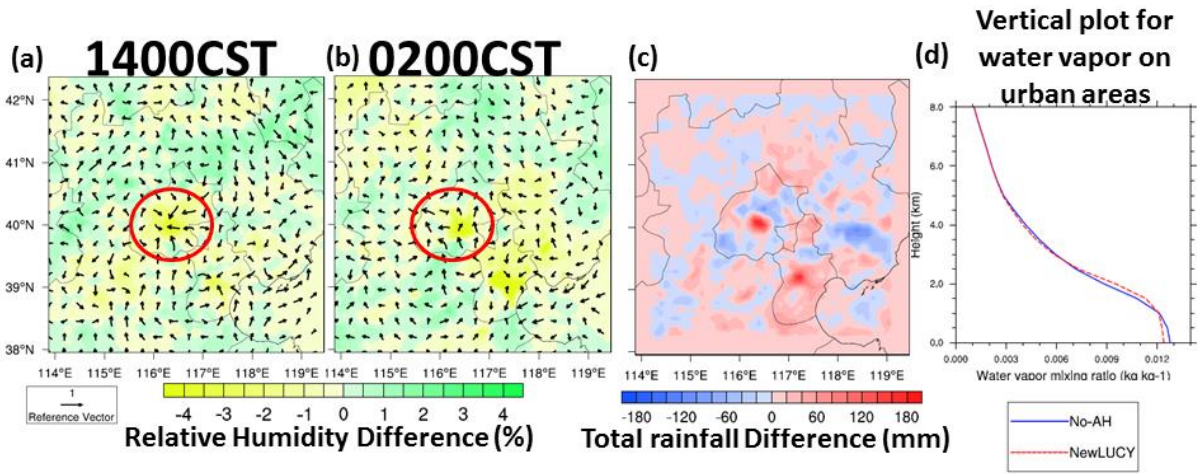

Figure 4.4 Monthly-average spatial distribution for daytime (a) and nighttime (b) RH differences in Greater Beijing area. The red circle indicates Beijing. c) Total rainfall difference. d) Vertical profile of water vapor for urban areas.

After adding the AH fluxes the energy balance between the surface and atmosphere is re-established by altering the sensible and latent heat fluxes, and the spatial and vertical distributions of moisture. Figure 4.4.a and 4.4.b show the spatial plots for

monthly-averaged surface relative humidity differences at 1400 and 0200 LT. Both daytime and nighttime differences show a negative center (-4%) over the AH centers, meaning the air near the surface became dryer. The vertical moisture distribution is modified as the AH is dissipated into the atmosphere and more rainfall is produced (+180 mm for August 2006 or 30%) in Figure4.4.c. Figure 4.4.d shows the vertical plot for water vapor over PKU. Consistent with Figure 4.4.a and b, it shows a dryer surface layer. Due to the strengthened urban-breeze circulation, more moisture is transported to the mid-troposphere (around 1.5~2 km), and also enhance rainfall inside urban areas (Figure 4.4.c).

4.5.1.2 Local Chemical Variables

Figure 4.5 shows the monthly-averaged concentration differences for chemical parameters due to AH at 1400 and 0200 LT. Carbon monoxide is reduced at all times, due largely to the increase in daytime PBL, and an even larger relative increase in nighttime. The maximum for nighttime CO decrease is more than 160 ppb, while daytime decrease is around 80 ppb for Beijing. NOX differences are similar to CO, with both daytime and nighttime decreases over urban areas. Ozone changes are more complicated as its concentration levels also depend on the chemical production and destruction processes which depend on temperature, relative humidity, sunlight and the concentrations of precursor species (e.g., NOX and CO). Temperature increases accelerate ozone production by raising reaction rates, and increases in PBL heights dilute the concentrations of NOx inside PBL, which in urban areas should increase ozone production efficiency during the day, and decrease the destruction by reaction with NO during the night. Overall, the net impact of adding AH is to increase ozone concentrations over urban areas in both daytime and nighttime. The maximum increase for the Beijing area is around 4 ppb for daytime and over 18 ppb for nighttime. For

suburban areas, where AH fluxes are smaller, the differences between the two runs are smaller.

Figure 4.5.c shows the spatial plot for PM2.5 difference. PM2.5 concentrations decrease in the urban area (by 12μg/m^3), due to a strengthened urban-breeze circulation and more wet removal from rainfall. Rural areas with increases (2~4 μg/m^3) in concentrations occur in regions with lower precipitation rates and less wet removal (Figure 4.5.c).

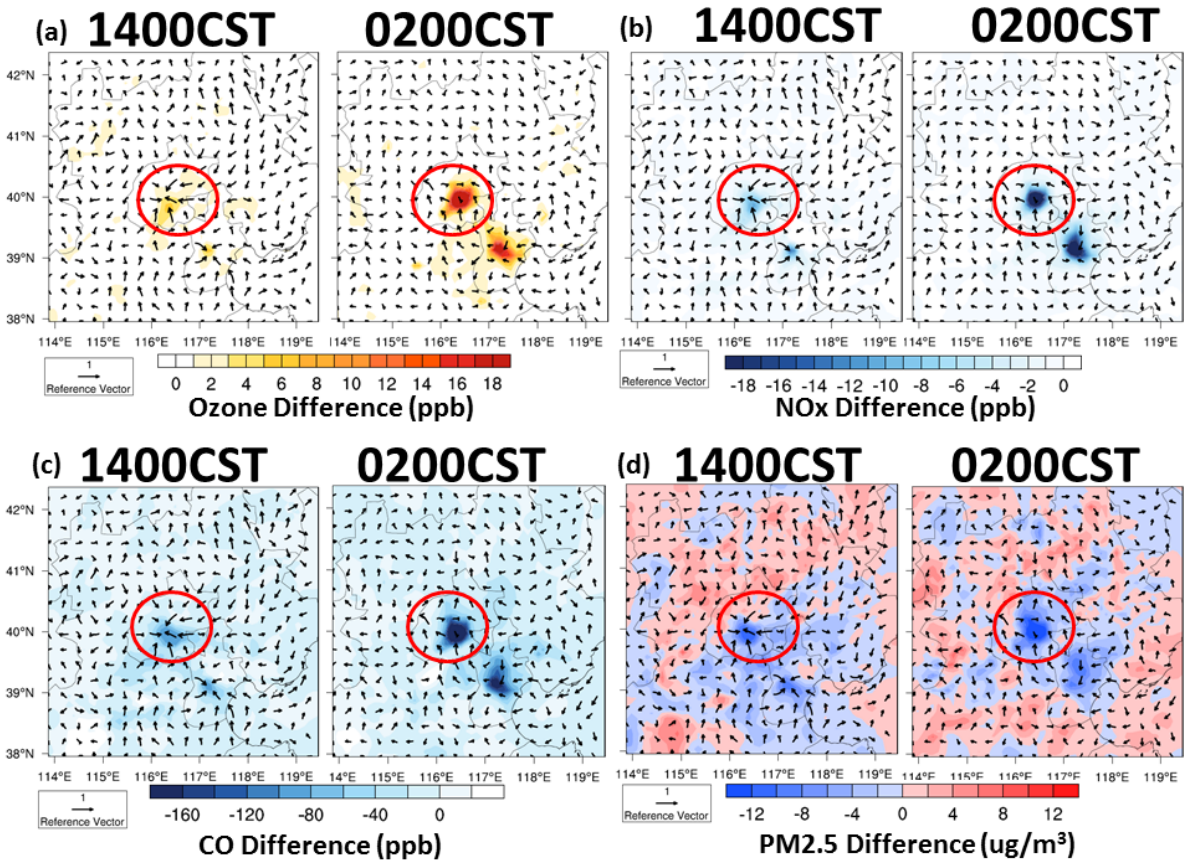

Figure 4.5 Monthly-average spatial distributions for daytime and nighttime pollutant differences in Greater Beijing area, a) ozone, b) NOX, c)CO and d) PM2.5. The red circle indicates Beijing.

4.5.2 Vertical Impacts from AH

The topography of Beijing plays an important role in pollutant transport. In summer Beijing area is under the influence of the East Asia Monsoon. The dominate direction for background wind is from the southeast. Figure 4.6 shows the terrain height in our simulated domain. It changes dramatically from 0 m to 1800 m within hundreds of kilometers, which generates a 3-d valley-breeze circulation. Superimposed on these two flow features is the urban-breeze circulation. Adding AH reinforces this urban circulation. To better understand how urbanization and AH change the vertical and spatial distribution of meteorology and chemical species, we show changes along a cross-section from (40.6 ° N, 115.6 ° E) to (39.6 ° N, 116.7 ° E) as shown by the black solid line in Figure 6a. Figure 6b shows the NewLUCY heat release along this cross-section line. Urban grids cover from grid 8 to grid 12. For daytime the maximum of heat release is~ 84.4 W/M2.

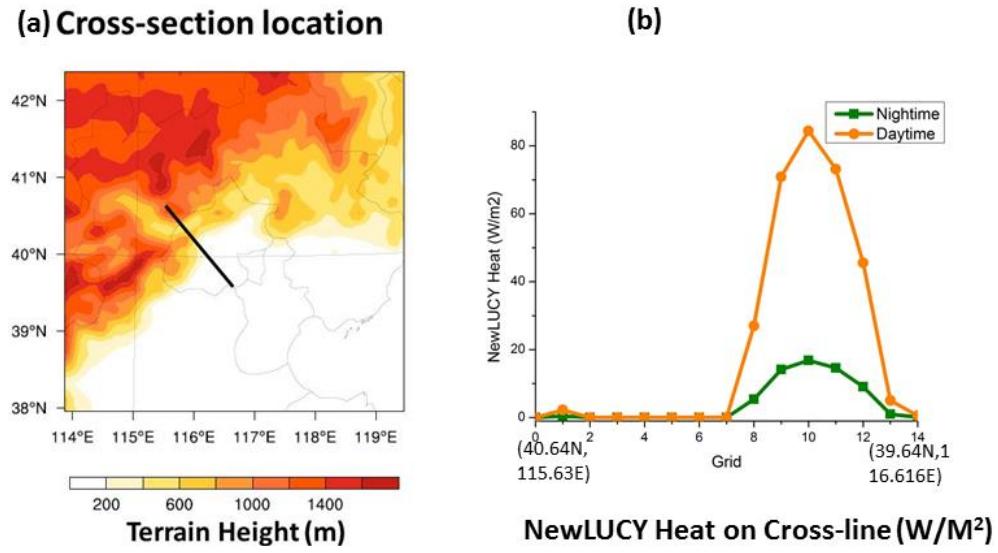

Figure 4.6 Terrain height plot in Greater Beijing area (a) and black line indicated the cross-section location and NewLUCY heat on this line. b) The New-LUCY heat release along this cross-section line.

Figure 4.7 shows the vertical differences (NewLucy case minus No-AH case) of temperature and water vapor along this cross-section. Arrows represent the wind velocity and direction differences. During daytime the near surface atmosphere is heated by the additional heat release from human activities and more heat is transferred upwards as the PBL increases. This is accompanied by an increase in vertical flow (shown in red box in Figure 4.7) over the urbanized grids with the strengthening of the urban-breeze circulation. The decrease in temperature at around 2 km above ground corresponds to a region of increase in water vapor. This results in more cloud-formation and a decrease in temperature. For nighttime, temperature increases are relatively smaller at the surface and limited to a lower portion of the atmosphere.

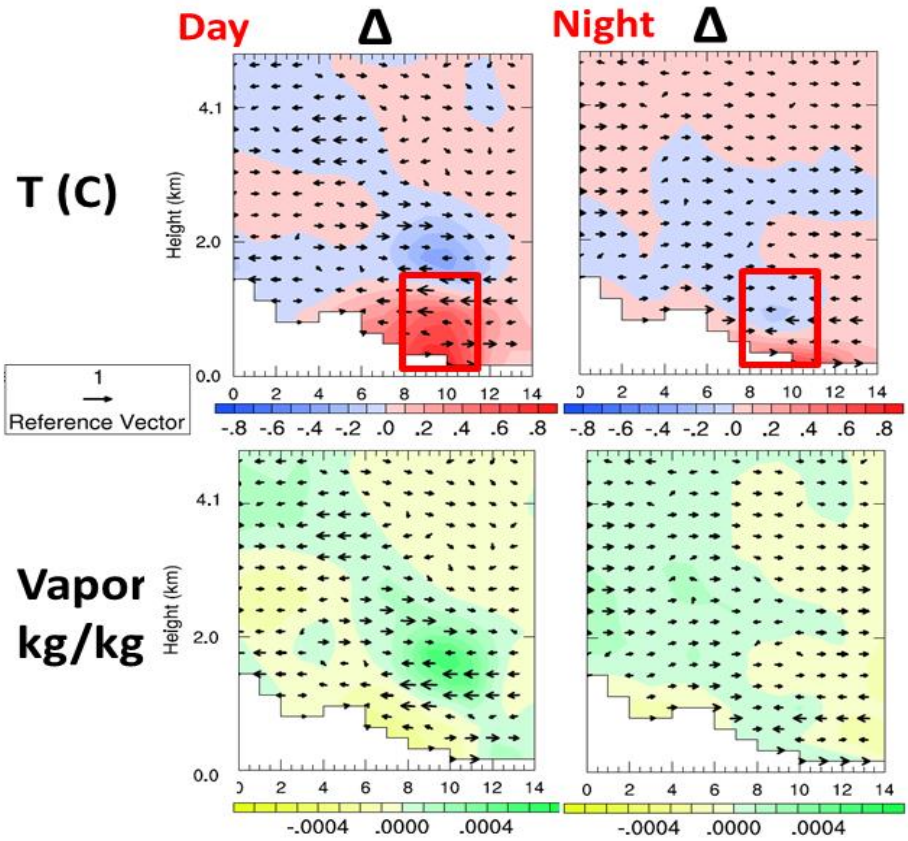

Figure 4.7 Daytime and nighttime vertical plots from point (40.6° N, 115.6° E) to (39.6° N, 116.7° E) (shown as the black line in Figure 6a)for temperature and water vapor

Figure 4.8 shows the vertical plots on the cross-sectional line for chemical species. The AH flux decreases surface CO concentrations near the surface in daytime and nighttime due to the increases in the PBL. There is also an increase in CO above the PBL and this is quite similar to the pattern for water vapor. This indicates that this is a reflection of the change in transport patterns in the region due to AH. NOX changes are analogous to carbon monoxide. Ozone levels over the urban areas and downwind regions show increases in near surface ozone for day and night periods of between 2-5 ppb. The maximum increase in ozone is found about 2 km over the urban area during the day, with values as large as 18 ppb. This is the result of both transport and the increase in ozone production as more NOX and other ozone precursors are transported into these upper levels. At night the higher levels of NOX above the boundary layer cause an increase in ozone depletion and a decrease in ozone. The differences in PM2.5 show a strong transport from surface to upper atmosphere (around 2 km from ground), leading to an accumulation center with enhancements as large as $18\ \mu g/m^3$. The asymmetric difference centers in Figure 8 can be well-explained by enhanced urban-breeze circulation interacting with local valley-breeze circulation (Ryu and Baek, 2013). The opposite direction of urban and valley breeze in northwest side of Greater Beijing area makes total wind decrease and limits pollutants transport, while in the southeast part, the same direction of urban and valley wind reinforces total wind and help diluting chemicals (Figure 4.8).

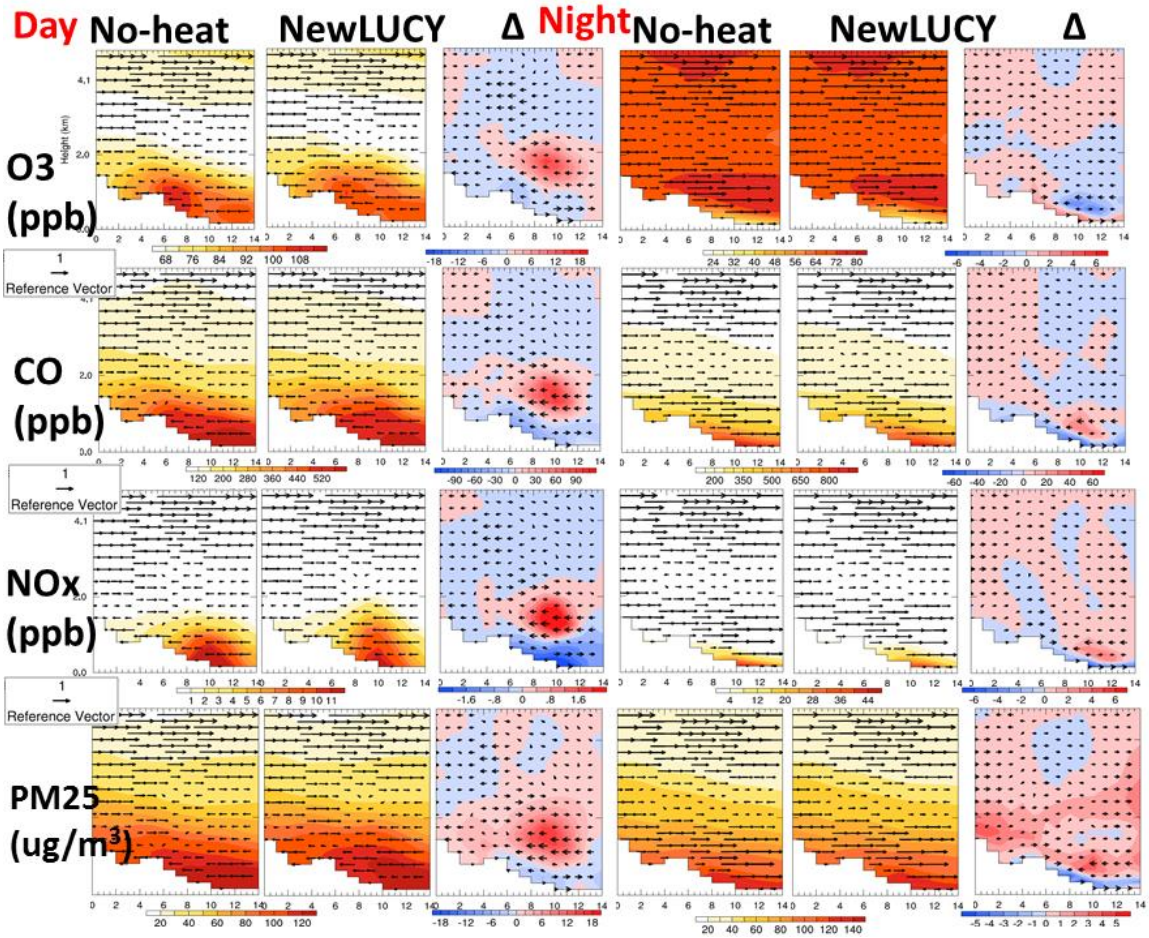

Figure 4.8 Daytime and nighttime vertical plots from point (40.6° N, 115.6° E) to (39.6° N, 116.7° E) (shown as the black line in Figure 6a)for ozone, CO,NOX and PM2.5

In order to better understand the vertical transport of the chemical species, two sets of horizontal distributions were made at different altitudes (Figure 4.9). For daytime, level of 1800 m was interpolated which is the corresponding height of the positive enhancements, and 570 m was chosen for nighttime. Horizontal winds diverge over cities at daytime and converge at nighttime, the opposite direction to surface wind, which reinforce the urban-breeze circulations. These wind changes also lead to the re-distribution of pollutants. For instance, more daytime CO and other chemicals (including both gas-phase and particles) are transported from the surface to this layer, causing an accumulation center. Nighttime winds converge over urban areas at high altitude,

bringing these transported and diffused chemicals back from the sub-urban areas. As a result, ozone destruction increase substantially and PM2.5 increase (Figure 4.9).

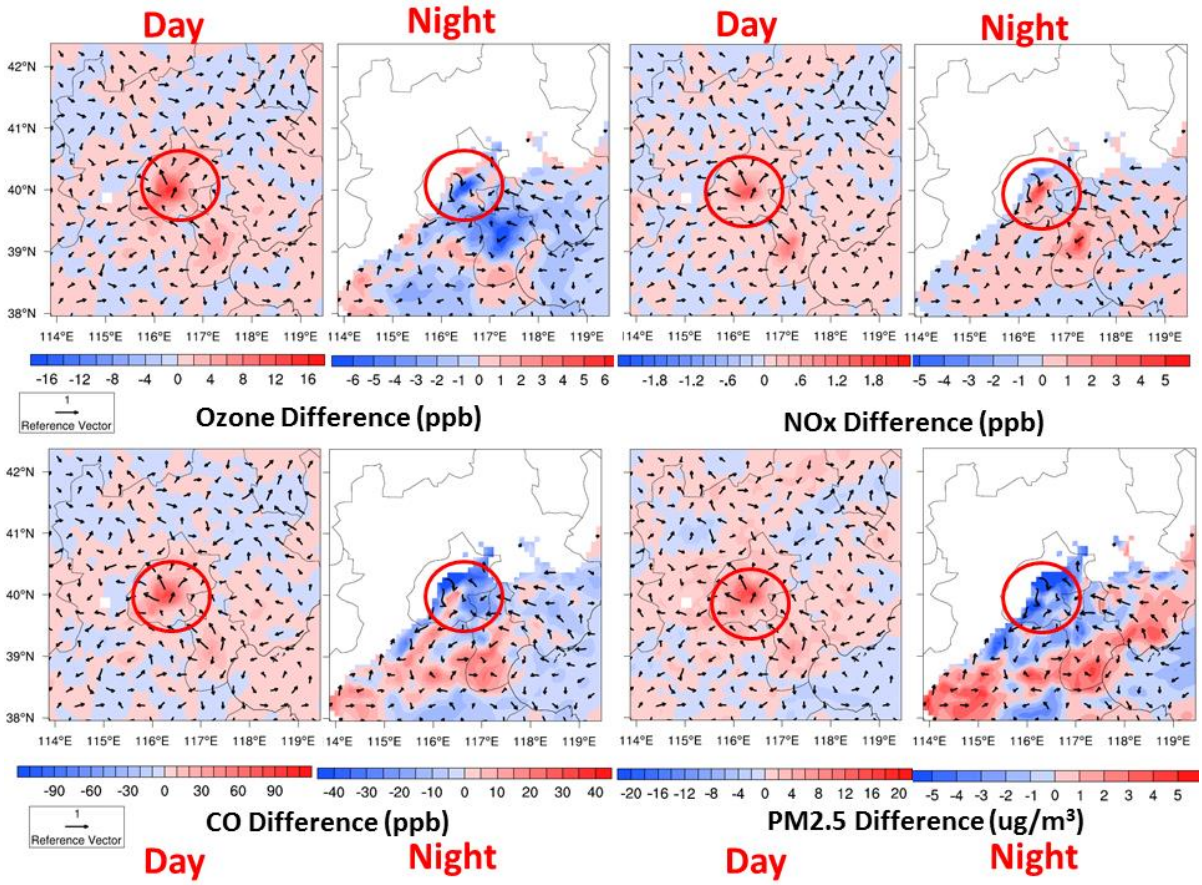

Figure 4.9 Spatial plots for Ozone, NOX, CO and PM2.5 for daytime at 1800m and nighttime at 570m

4.5.3 Comparison with Observations

Figure 4.10 shows a comparison between observations and simulation sat the PKU location. HFX is enhanced with the addition stream of the AH flux. The medium increase was as large as 70 W/m^2 (Figure 10d). The 2-m temperature predictions were improved as shown in Figures 4.10.a, b and c, and the Mean Error (ME) decreased from 1.55 ℃ (No-heat Case) to 0.61 ℃ (NewLUCY Case). However, the NewLUCY results

still underestimate 2-m temperatures by as much as 2 ℃ for high temperatures (>30℃) as shown in Figure 4.10.b. This could be an indication that under high temperature days the AH is underestimated and does not reflect the added energy needs associated with peak air condition loads. Nighttime temperatures are much better represented when including the AH in (Figure 4.10.b). For ozone simulations, adding AH improved the daytime predictions, especially for the most relevant concentration levels for air quality management (above about 60 ppb (Figure 4.10.h). For these high ozone periods (> 60 ppb) the ME for ozone was reduced from 4.34 ppb (No-heat) to 0.21 ppb (NewLUCY).

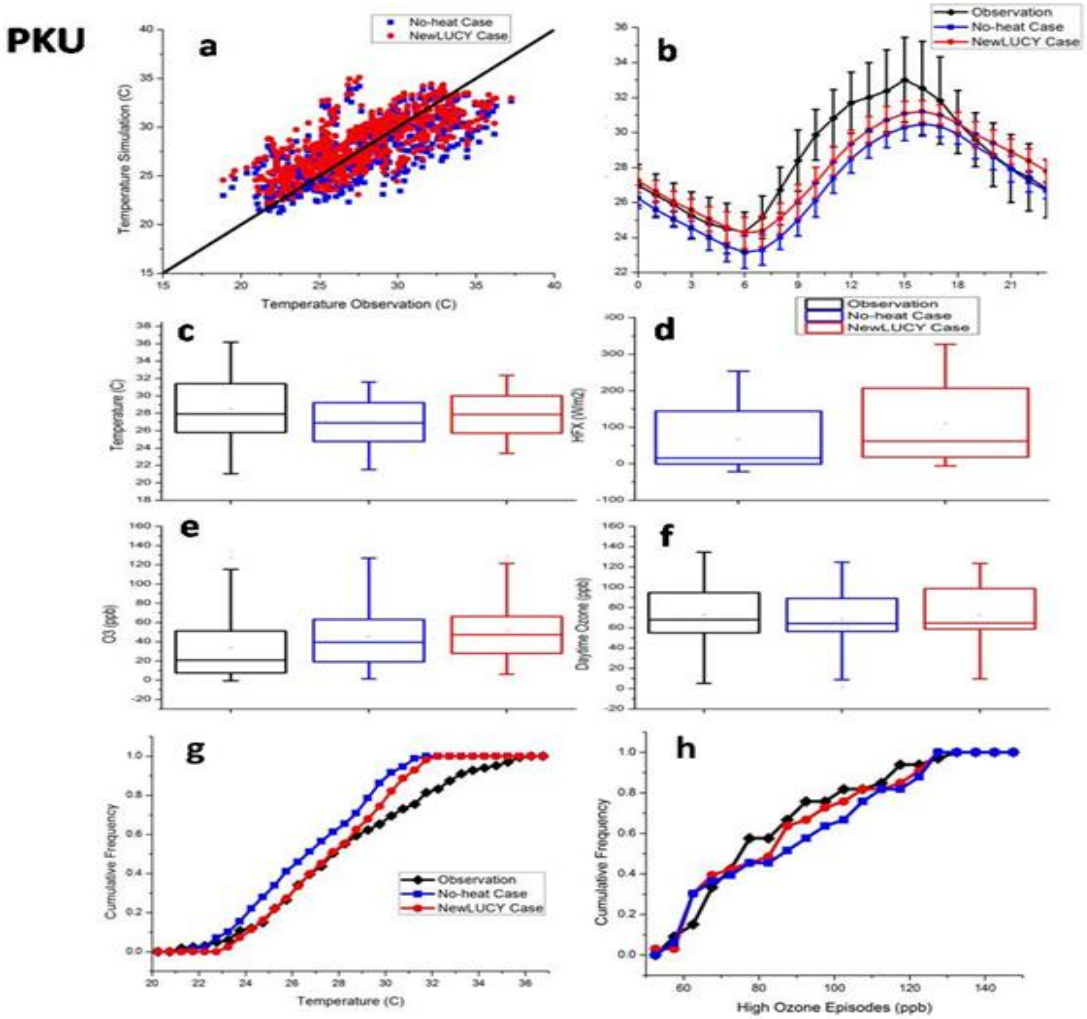

Figure 4.10 Statistical, box and cumulative frequency plots between observations and simulations at PKU site.

4.6 Conclusions

Urbanization impacts the atmospheric environment in many ways. In addition to the increases in pollution emissions from intensification of transport and economic activities, changes in surface albedo due to land use changes and the built environment can affect the meteorology and air pollution levels in the city. In greater Beijing area, we found that land use changes due to urban growth increased temperature (by 2.4 ℃) and surface ozone concentration (enhanced by 20 ppb) (Yu et al., 2012). In this paper we addressed the impact of anthropogenic heat (AH) release on the city environment. A new method for including AH emissions, NewLUCY, was developed based on two known methods (SLUCM and LUCY). The method estimates hour heat fluxes, with a diurnal variation with a single peak value and utilizes updated urban built-up land use data. Inclusion of the AH enhanced the urban heat island in Beijing, by increasing temperature by 0.8 ℃in daytime and 1.2 ℃at night. It also increased the PBL heights by 320 m and 160 m for daytime and nighttime, respectively. The urban-breeze circulation was strengthened when AH was included in the simulations. Pollutant spatial and vertical distributions were also impacted by the AH. Surface ozone concentrations increased in the urban areas (4 ppb daytime and 18 ppb nighttime). The impacts of AH were not limited to the urban centers, but extended regionally. For example, PM2.5 concentrations increase in rural areas, due to a decrease in rural precipitation rates when AH was included. In general inclusion of AH increased the accuracy of the predictions. Atthe PKU observation site, the ME (Mean Error) of the 2-m temperature prediction was reduced from 1.55 ℃to 0.61 ℃. The predictions of the high ozone levels were also improved. These results show that the air pollution predictions in and around large urban areas are highly sensitive to the land use changes and anthropogenic heat inputs. It is important that these factors be included when simulating air pollution in large urban areas such as Greater Beijing. Further improvements in city-scale air pollution predictions

require better information on land use and detailed urban structure of the cities and more studies of the anthropogenic heat release in these environments.

4.7 Collaborators and Funding Sources

This paper was supported in part by NSF grant CHE-1049140 and NASA grant NNX11AI52G.

The CAREBeijing 2006 campaign was supported by the Beijing Council of Science and Technology (HB200504-6, HB200504-2).

CHAPTER 5 ANTHROPOGENIC EMISSION IMPACT FROM URBANIZATION IN CHINA BY USING WRF-CHEM

5.1 Abstract

Rapid population growth and economy boost have driven a trend in energy consumption increase in China. Based on the current energy sources profile, the emissions of criteria air pollutants are expected to grow. This study focuses on emission impacts from urbanization on air quality modeling. WRF-Chem is employed to include two-way feedbacks between the meteorology model and the chemical transport model. In this paper, we study two different emission inventories, INTEX-B for the year 2006 and MICS for 2010. Great mitigations for emissions occurred around Beijing area due to success in government regulations before and after Beijing Olympics. In contrast, another city (Tangshan) becomes the major emission contributor in North China Plain. Comparing to observations, MICS produces a more reliable simulation of NOx and other pollutants. Also using MICS emissions tends to increase the possibility of precipitation in city area and decrease precipitation in suburban. Vertical profile investigation reveals a different distribution of PM2.5 for using different emission inventories. More PM2.5 (around 20 $\mu g/m^3$) near surface and less (around 10 $\mu g/m^3$) PM2.5 in upper troposphere are found in the MICS case.

5.2 Introduction

With rapid increase in population and industry, energy consumptions in Asia tends to contribute around 30% of the worldwide total by 2015 and 80% of it comes from fossil fuels (Shah et al., 2000). And this trend in Asia will continue to increase in the future (Akimoto et al., 2003). More anthropogenic emissions are expected from fossil fuel combustion. Between 1980 and 2003, the emission for SO2, NOx and NMVOC increased by 119%, 176 % and 108%, respectively (Ohara et al., 2007). Increased emissions in greenhouse gases and ozone precursors will bring in a more polluted ambient air scenario (Hogrefe et al., 2004).

Many previous studies have focused on rapid emission change in China. Ohara et al. (2007) revealed an extremely high growth for NOx in China after 2000. SO2 emissions were projected to have a slower growth and only reached 40-45 Th/yr by 2020 (Carmichael et al., 2002), due to emission controls and slow-down growth for China's economy. Zhang et al. (2006) calculated a 36%, 55%, 18% and 29% increase between 2001 and 2006 for SO2, NOx, CO and VOC, respectively. Tsinghua University in China developed a multi-resolution emission inventory. The Figure 5.1 (Wang et al., 2014) below is emission trends from 1990 to 2010. The growth for NOx and CO2 accelerates at an extreme rate since 2000 in all sectors. The total emission of SO_2 showed a decrease trend after 2005, with a major reduction in the power section, indicating a success in FGD (Flue-Gas Desulfurization) device implanted in power plants.

However, fewer of these studies evaluated the emission impact on air quality. And even fewer studies took the emission feedback into consideration. In this study, we investigate this emission increase as a third impact from urbanizations by using an "online" model, WRF-Chem.

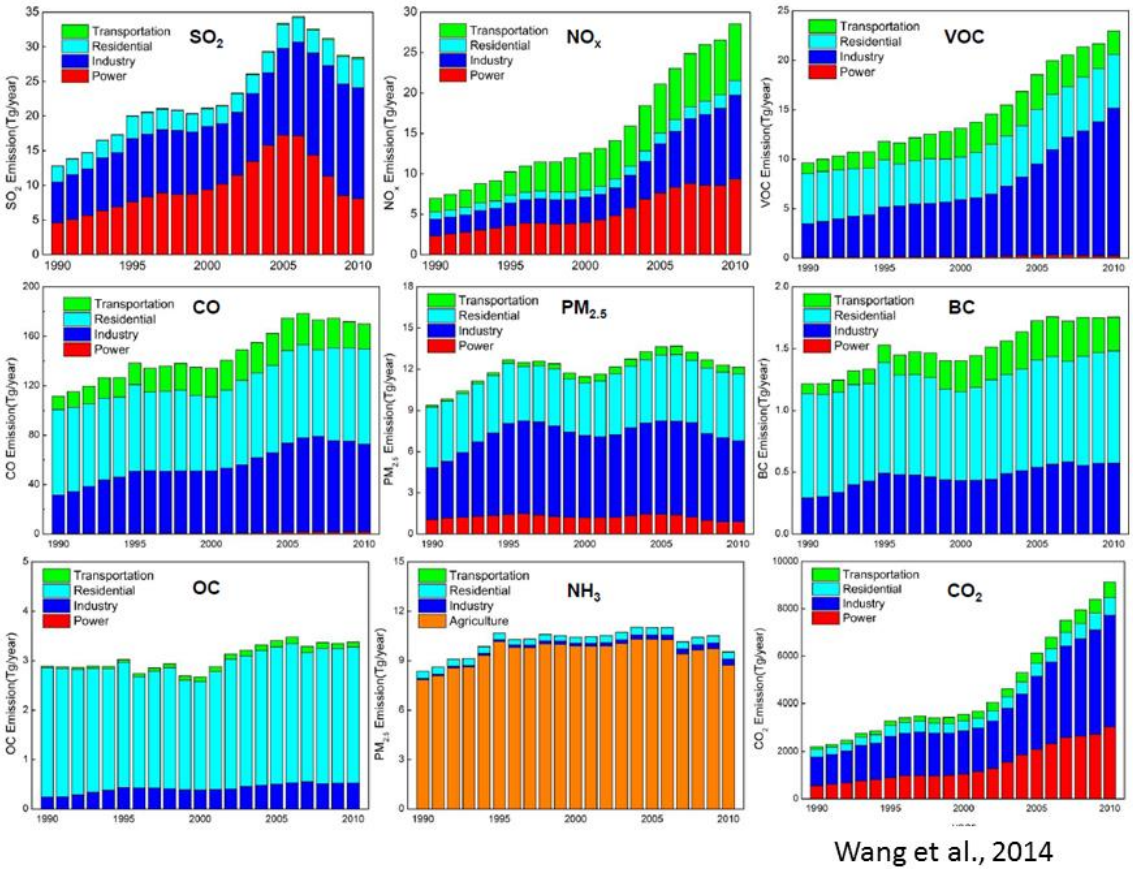

Figure 5.1 Emission trends in China from 1990 to 2010 for each species.

5.3 Description of Study Area, Tools and Data

WRF-Chem is new generation model, which couples meteorology model (WRF) with the chemical transport model step by step (Grell et al., 2005) and has been proved as a solid simulation tools (Yu et al., 2012) (Jiang et al., 2012) (Wang et al., 2012) (Tie et al., 2013). The major reason for employing WRF-Chem is that it enables model's ability to access emission impact on meteorology field.

Three-nested domains are employed to evaluate emission impact. The study area is same as Yu et al. (2014). For more detailed information, please refer to section 4.3 in this paper.

Two different emission scenarios are used in this study. Both of them are developed by Dr. Qiang Zhang from Tsinghua University, China. The first one is called

the Intercontinental Chemical Transport Experiment-Phase B (INTEX-B) funded by the National Aeronautics and Space Administration (NASA). The data is collected for the year 2006. INTEX-B now is available at CGRER website: http://cgrer.uiowa.edu/projects/emmison-data. The second emission data is from MEIC (Multi-resolution Emission Inventory for China. And it reflects anthropogenic emissions for the year 2010. Data is downloaded from ftp://166.111.42.46/.

5.4 Emission Change from 2006 to 2010 in China

Emission pre-processing in this study is conducted by the EPRESS code, developed by Dr. M. Lin and modified by Dr. Y. Cheng in CGRER at University of Iowa. Figure 5.2 shows the projected emission on the first domain for INTEX-B and MICS, respectively. Overall, emissions in China increase from 2006 to 2010, in both magnitude and spatial area. The regional pattern is extended from eastern coastline to west direction, corresponding to the direction of urbanization expansion in China. Besides China, South Korean is also going through a rapid growth in pollutant emissions, especially for isoprene and other NMVOC. Since the resolution of INTEX-B is 0.5-degree ×0.5-degree and MICS is 0.25-degree × 0.25-degree, more cities with large emissions in CO, NO2 and PM2.5 appear on the emission plot in 2010. The large dots in Figure 5.2 represent the large cities (like Kunming, Huerhaote, etc.) in China. In these two inventories, only four sectors (Industry, residential, Transportation and Power) of PM2.5 are included. Figure 5.3 is the spatial difference for projected emissions between 2006 and 2010 in domain 03. Within the smallest domain, due to emission regulations after the 2008 Olympics, the enhancement around Beijing area is relatively smaller than other cities, especially urban Beijing area. In contrast, the high center around (118.2 °E, 39.5 °N) corresponds to Tangshan, the biggest city in Hebei Province. Under Chinese government pressure and regulations in Beijing and Tianjin, steel and automobile manufacture companies tend to relocate in Heibei Province, mostly Tangshan. This and

other factors have driven a trend for extremely increase around Tangshan area. In the future, more emission strategies and regulations should be implemented and highly recommended in Tangshan.

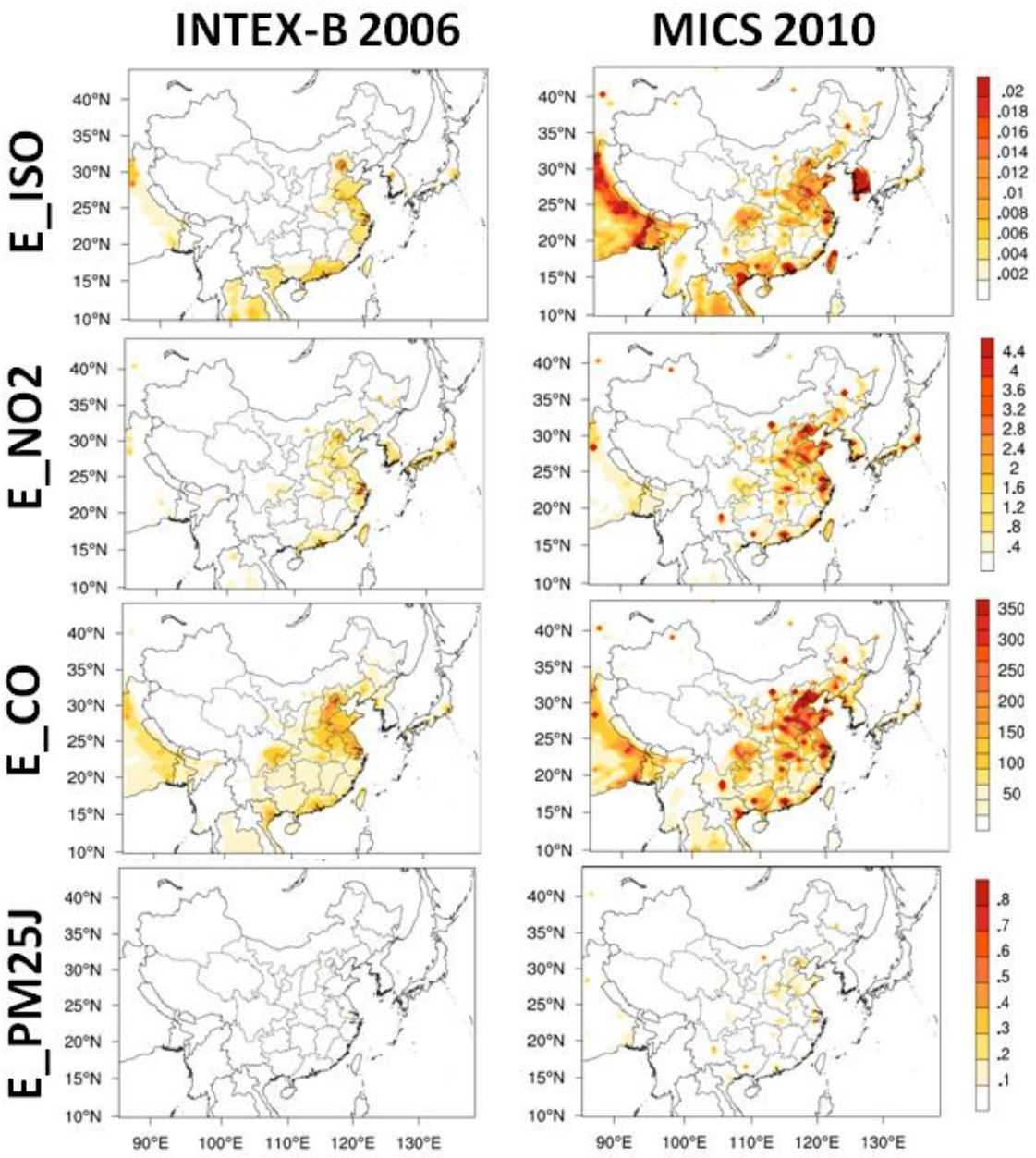

Figure 5.2 Projected emissions on Domain 01 for INTEX-B and MICS

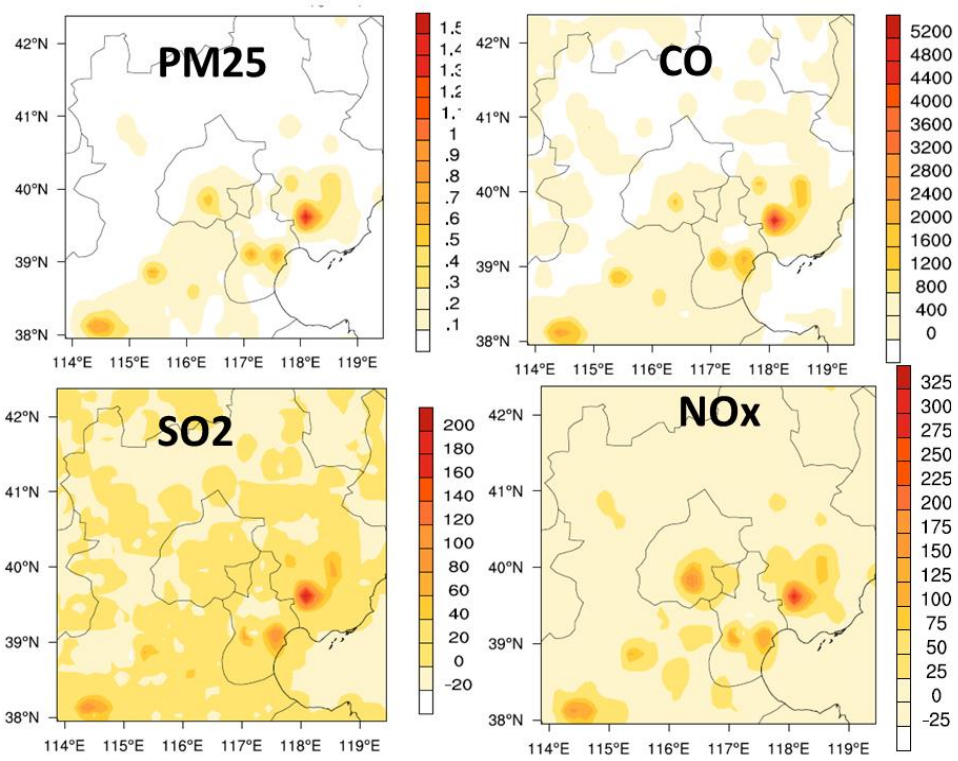

Figure 5.3 Regional differences in emissions from INTEX-B to MICS in third domain

5.5 Results and Discussions

Two identical runs, except for different anthropogenic emissions were performed from August 01 to August 31 2006. Results are shown in this chapter.

5.5.1Temporal Plots on Urban and Suburban Points

To compare with available observations from CAREBeijing 2006, we extract temporal simulations on two locations, PKU (116.31°E, 39.99°N) and Yufang (116.31°E, 39.51°N). In Figure 5.4, simulations using INTEX-B and MICS yield nearly identical meteorological results on urban point (PKU), while tends to overestimate 2-m temperature on suburban point (Yufang). Heat flux from surface also illustrates a slight decrease by using emission data from 2010. Case by MICS 2010 inventory is likely to predict a more polluted scenario for both urban and suburban points, with higher

concentrations in ozone, NOx, and PM2.5. The average enhancement in PM2.5 is about 55 $\mu g/m^3$.With regards to observations at PKU site, significant improvements in NOx simulation are achieved by using MICS inventory, by reducing mean error by 8.2 ppb. On Yufang site, MICS also helps reduce the false peak value for NOx on August 19 and August 22 2006.

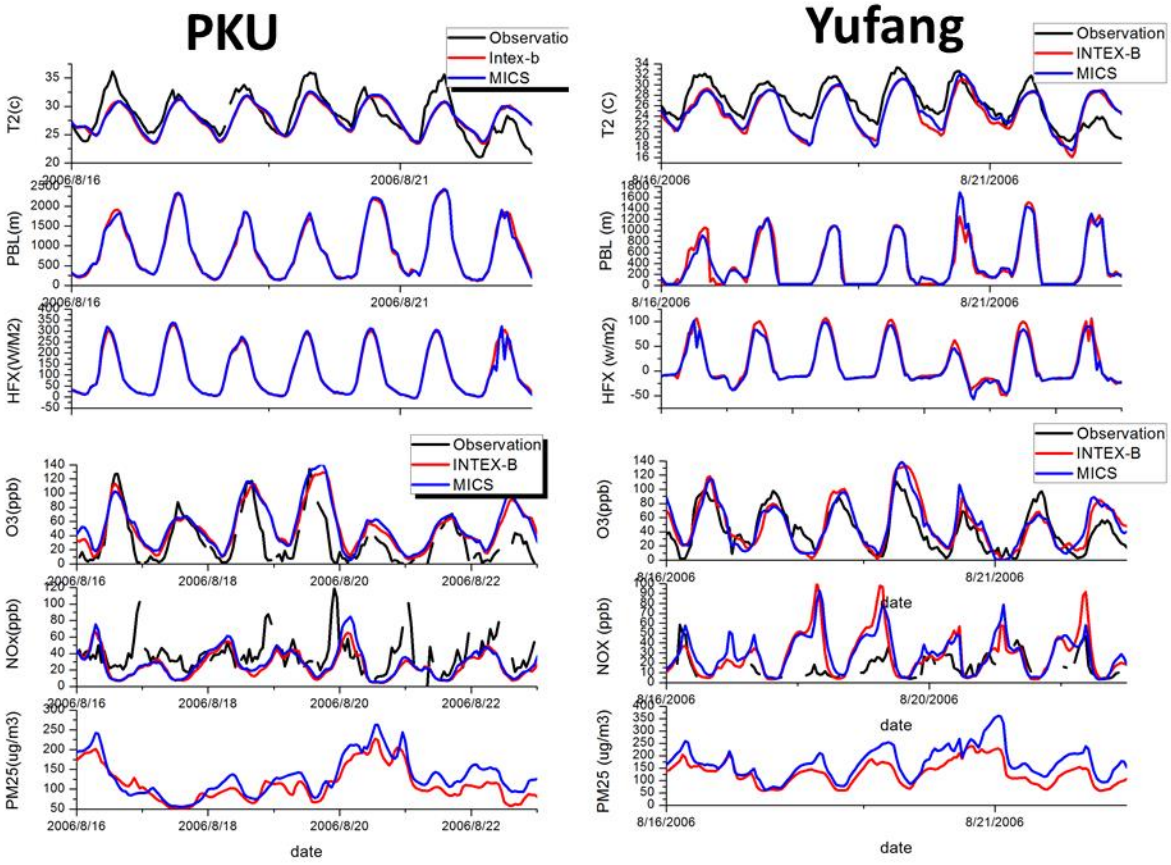

Figure 5.4 Temporal plots for observations and simulations using INTEX-B and MICS emissions.

5.5.2 Sensitivity on Precipitation and Vertical Profile

As we discussed before, MICS case produced higher particulate matter concentrations near the surface. Particulate matter plays important roles in cloud nucleation mechanism and precipitation fields. In summertime Beijing, the dominant

wind (Asian Monsoons) brings in moisture and vapor from the Pacific Ocean, making it a wet season (Sun et al., 2007). Figure 5.5 shows the accumulated rainfall in each run and their differences. For urban areas in both cases, higher concentration of particles enlarges the possibility in precipitations (Figure 5.5). 520 mm rainfalls are found in Beijing and Tijian. Comparing to INTEX-B, MICS increases the precipitation by 100 mm (~20%) in Beijing and its downwind area, while decreases precipitation in upwind area.

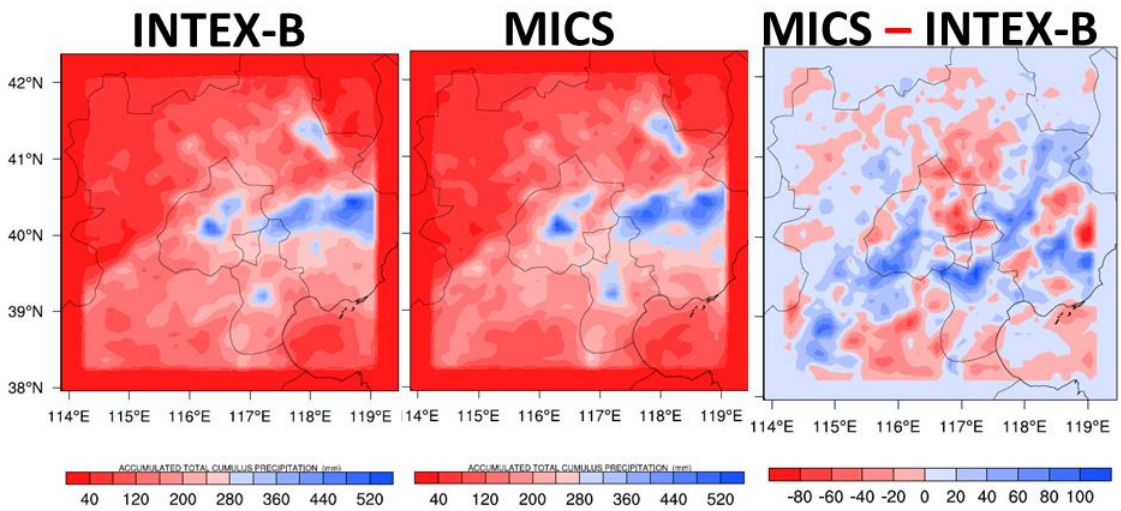

Figure 5.5 Regional plots for total rainfalls in each case and their differences.

To better understand the different results using INTEX-B and MICS emissions, another differences plot for PM2.5 on vertical layers are shown in Figure 5.6. Layer 1 represents the bottom atmosphere layer near the surface and Layer 14 is about 4.8 km above the surface. Higher particulate matter concentrations are discovered in MICS case on Beijing and southern Beijing areas. The maximum difference is about 20 $\mu g/m^3$. When altitude increases, the discrepancy tends to decrease. Around layer 9, about 1.6 km the difference is zero. Finally, in layer 14, INTEX-B results in a higher concentration (about 10 $\mu g/m^3$) for particles. This is consistent with vertical plots in Figure 5.7, where

a cross-section is studied. The black line in Figure 5.7 shows the cross-section location. MICS gives higher estimations in downwind direction and lower values in the upper atmosphere.

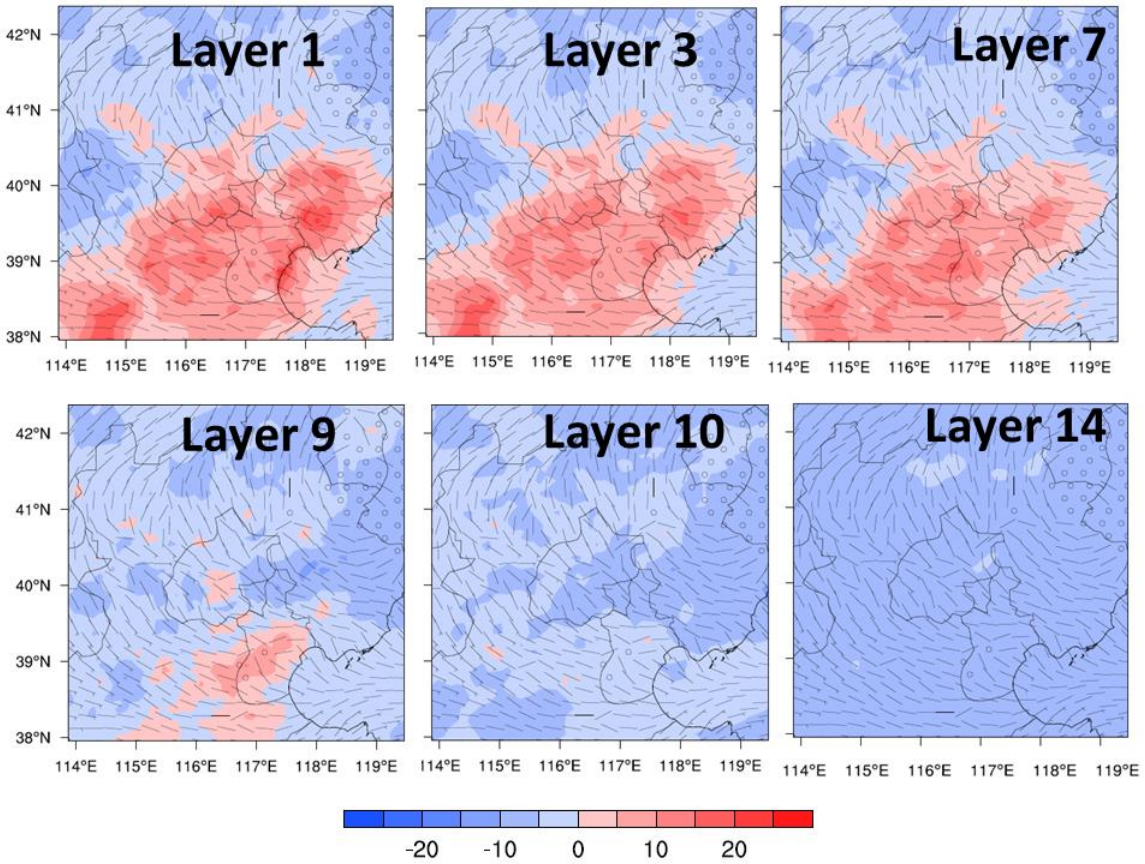

Figure 5.6 Spatial plots for PM2.5 difference on different vertical layers

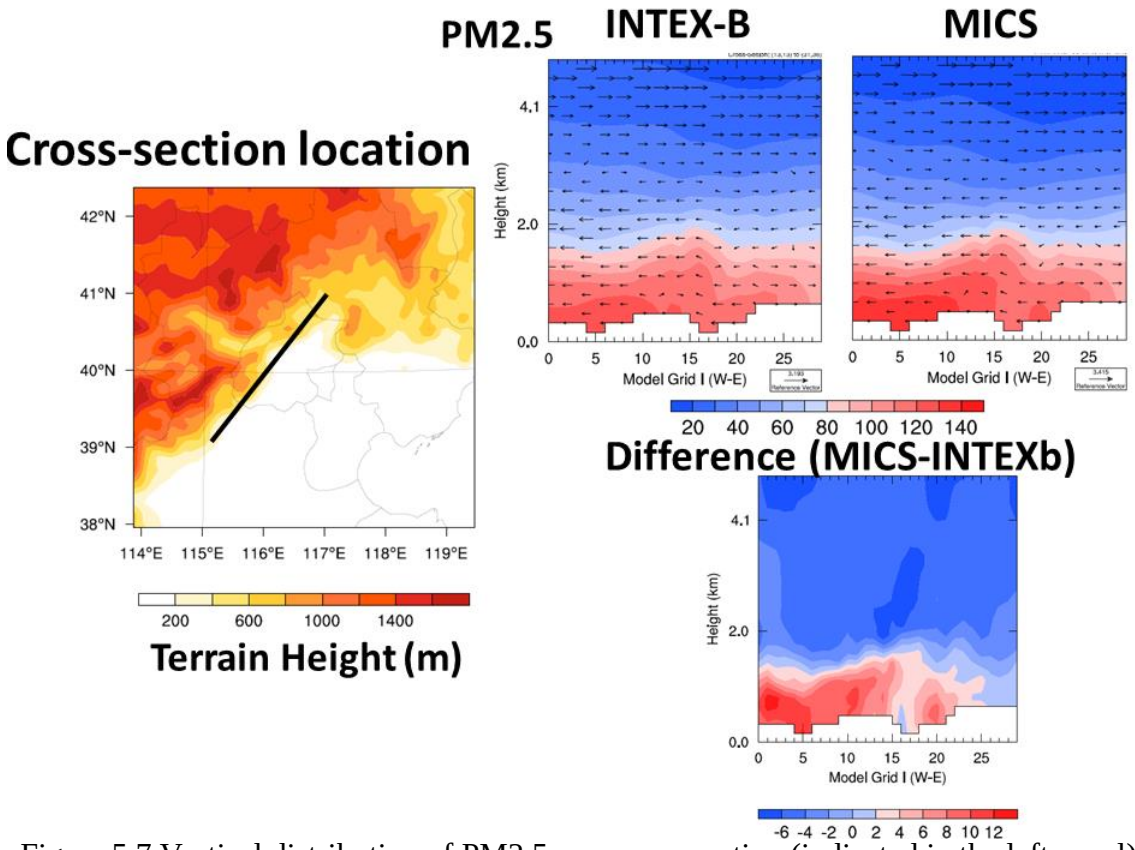

Figure 5.7 Vertical distribution of PM2.5 on a cross section (indicated in the left panel)

5.6 Conclusions

Anthropogenic emission is a key factor for air quality simulation and forecasts. With rapid urbanization rate in China, increasing release of these criteria pollutants tends to worsen air quality, especially for urban area. In this study, we use WRF-Chem to evaluate the emission impact.

Two different emission inventories were adopted in this study, INTEX-B and MICS. Both of them are developed by Dr. Qiang Zhang using the same methodology. INTEX-B reflects the emission scenario for the year 2006, while MICS is for 2010.

From preliminary results, the growth of emissions inside Beijing area is largely slow down by effective regulations. For urban points inside Beijing, the meteorology simulations manifest a high similarity between INTEX-B and MICS case. MICS case better captures the high NOx episode on both PKU and Yufang sites.

PM2.5 in MICS case tends to increase by 20 ppb on surface and decrease by 10 ppb in upper atmosphere, which corresponds to the vertical plots on cross-section study. The main cause is from wet deposition and vertical re-distributions.

CHAPTER 6 MODEL RESOLUTION IMPACT AND CONFIGURATION OPTIMIZATION IN GREATER BEIJING AREA

6.1 Abstract

Air quality modeling has become a reliable method for forecasting particle matter and other pollutants in China. Choosing the appropriate domain resolutions can be a trick question, with regards to both accuracy and efficiency. This paper is devoted to the development of a set of optimal resolutions in Beijing area. The sensitivity test for resolutions includes two aspects: horizontal and vertical. Four resolutions are employed to test spatial resolution impacts. Results show that higher resolution can better capture surface temperature trends and distributions of chemical species. 81 km resolution performs the worst, while 27 km, 9 km and 3 km (highly related) improve the predictions step by step. However the improvement from 9 km to 3 km case is very limited in this test run. For vertical resolution impact, three vertical meshes (9 layers, 27 layers and 54 layers) are studied. Mean bias for 2-m temperature decreased from 4 ℃ using 9 layers to 2 ℃ using 27 layers. Also surface ozone concentrations are better simulated in 27 layer case than 9 layers. Although 54 layer further improves simulations, it shows a highly correlation (R =0.9925) to case using 27 layers. Overall the optimal configuration is recommended with 9 km spatial resolutions and 27 vertical layers for future forecast campaign in Beijing.

6.2 Introduction

In the past several years, air pollution, mostly photochemical smog and widespread haze, have become severe in China, especially for northern China (Zhao et al., 2013 and Tao et al., 2014). The maximum hourly PM2.5 had exceeded 680 $\mu g/m^3$ in the Greater Beijing Area (Wang et al., 2014). For the 20 million people living within this city cluster (the sixth national census in China, 2010), efficiently forecasting daily

pollutant levels is important for pollutant exposures and preventing/mitigating human health damages.

Air quality in the lower atmosphere is difficult to predict and is sensitive to many factors, for instance monsoon, anthropogenic emissions, and boundary inflows (Lin et al, 2009). Model resolution (horizontal and vertical) also play a key role in the accuracy of the predictions. Choosing the appropriate resolution choice is a dilemma for air quality modeling. Limited resolution brings in systematic errors into model simulations (Esler et al., 2004), while finer resolution adds computational costs and may not practical for daily air pollution forecasts, as computing resources are often a limiting resource in operational forecasts. Moreover the required input data sets of land use and emissions may not be available to support fine resolutions.

In this paper we explore the role of model resolutions in predictions of air pollutants in eastern China. Several studies have focused on assessing resolution impact on air modeling. The transport from stratosphere to troposphere contributes about 40% in troposphere ozone concentrations (Roelofs et al. 1997). Kentarchos et al. (1999) found that a refinement in horizontal resolution led to a 12% increase for this transport from stratospheric to troposphere and improved ozone profile. According to Lin et al. (2009), 27 km resolution and 29 vertical layers (compared to 81 km and 23 vertical layers) are better choice for simulating ozone intensity in East Asia. Vivanco et al. (2011) did a sensitivity run in Spain and discovered that the maximum increase occurred between 0.5-degreeand 0.2-degree cases and gave similar predictions for ozone concentration for higher resolutions. Cohan et al. (2006) found out that 12-km grid-resolution was sufficient to reproduce ozone pollutions in Atlanta, US. For vertical resolutions, Menut et al. (2013) pointed out vertical mesh plays little impact over chemistry-transport model. However few studies are concerned with appropriate resolution in the forecast use. In this study, we plan to evaluate resolution impact from both spatial and vertical grids and

analyze pollutant sensitivities. With the recommended resolutions, model fidelity in future forecast can be improved.

Results of the sensitivity air quality predictions to changes in horizontal and vertical resolution are evaluated using on-line coupled WRF-Chem simulations. The paper is organized as follows. Section 2 is the descriptions of modeling tools and configurations. In section 3, we present the methodology used in evaluating horizontal and vertical sensitivity. For each aspect, some preliminary results are shown in section 4, including validation with observation, spatial impact and vertical impacts.

6.3 Description of Tools, Study Area and Data

In this study, WRF/CHEM V3.1.1 was used (Grell et al., 2005). It couples the Weather Research and Forecasting model (WRF) developed by NCAR with chemistry model, and has been proved as one of reliable models for air quality in China (Yu et al., 2014, Tie et al., 2013 and Jiang et al., 2012). For all runs studied in this paper, we used the Carbon Bond (CBMZ) chemical mechanism and MOSAIC with 4 sectional aerosol bins (Fast et al., 2006). We used the MICS-Asia 2010 (Multi-resolution Emission Inventory for China) developed by Q. Zhang and K.B. He at Tsinghua University for the anthropogenic emission inventory and MEGAN V2.04 (the Model of Emissions of Gases and Aerosols from Nature) (Guenther et al., 2006) for the biogenic emission. Land-cover data was retrieved from MODIS (MODerate resolution Imaging Spectro radiometer) (Yu et al., 2012). Anthropogenic heat emissions was also taken into considerations by using the NEWLucy method (Yu et al., 2014). The Model for Ozone and Related chemical Tracers, version 4 (MOZART-4) was used for the initial chemical state and the lateral boundary conditions for coarse domain (Emmons et al., 2010).

We focused on the greater Beijing area in this paper. It contains one of biggest city clusters in China, including Beijing, Tianjin, and part of Province Heibei.

Observation data at urban location (PKU, (116.31 °E, 39.99 °N)) from CAREBeijing field campaign for August 2006 was used in model evaluations.

6.4 Methodology

For each test run, simulations are conducted from 0000 UTC 01 August to 0000 UTC 31 August 2006.

6.4.1Model configuration for spatial resolution

To evaluate horizontal resolution impact, an experiment was designed using 4-nested domains, where the feedback option was turned off to perform one-way nested simulations. Figure 1.a shows the 4-nested domains. The resolutions for four domains are 81-km, 27-km, 9-km and 3-km, respectively. The coarsest domain covers eastern Asia, with 81 X 57 grid numbers. Second domain zooms in the northern part of China and has49 X 49 grids. The third domain located at the North China Plain (NCP) uses 55 X 55 grids and the finest domain centered at Beijing with 82X 58 grids. Figure 1.b is the terrain height plot in Domain 04 and PKU is located inside the city center symbol. In August, East Asian Monsoon (from northeast or southeast directions) is dominant for the whole North China Plain (Wu et al., 2010). Combined with Beijing's unique topography (altitude significantly arises in western counties in Figure 6.1.b), pollutants are likely to accumulate in Beijing and its western area (Wu et al, 2011).

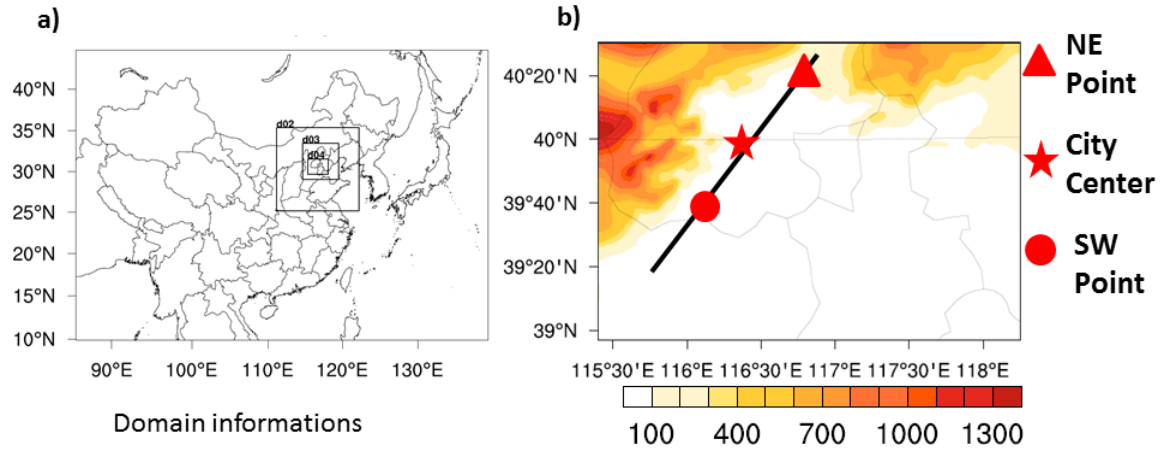

Figure 6.1 Domain plots for spatial resolution evaluation (a). The resolution for Domain 01 is 81-km, for Domain 02 is 27-km, for Domain 03 is 9-km and for Domain 04 is 3-km, respectively. b) Terrain heights plot inside domain 04. The black line is perpendicular to terrain height gradients. The symbol represents three different grids on this line: City center, NE point and SW point.

6.4.2 Model Configuration for Vertical Resolution

Three cases were performed to evaluate vertical resolution impacts, using 9 layers, 27 layers and 54 layers. All of these three cases used the same bottom and top staggers. The middle setting (27-layers) is the default vertical parameters for WRF model and called original case, while the 9 layers, called one-third case converged every three layers in the 27 layers into one, and the 54 layers divided every layer in the 27 configuration into two (called the double case).

6.5 Results and Discussion

6.5.1Sensitivity to Horizontal Resolutions

6.5.1.1 Data Validation with Observations

Figure 6.2 show the temporal plots for each meteorological and chemical species at PKU. Results are plotted for these locations from each of the 4 model domains, with results interpolated to the site locations. The 81 km resolution is typical of that used in many global chemical transport models, while 27 and 9 km grids are often used in

regional and urban applications, and 3 km resolution is often used in finer-scale urban applications that do not try to resolve urban corridor issues. At the urban site PKU, our simulations underestimate 2-m Temperature under all resolutions. However, with higher resolutions, the mean bias is reduced by 3.72 ℃ (85%) from 81 km to 27 km, 0.36 ℃ further to 9 km and eventually decreased to 0.11 ℃ in the finest domain (Table 6.1). This improvement is also represented in Figure 6.3.a. The greatest improvement is found between Domain 01 and Domain 02, while domain 02, 03 and 04 provide similar results for 2-m temperature.

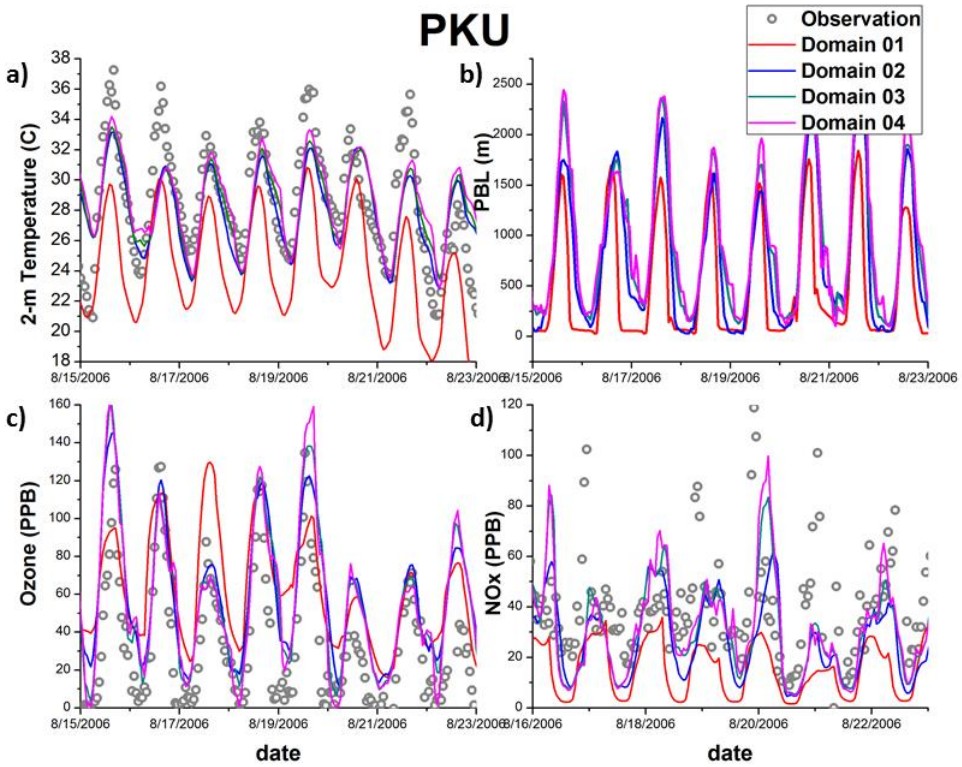

Figure 6.2 Figure 2 Temporary plots on PKU for 2-m Temperature, PBL heights, Ozone and NOx concentrations.

Table 6.1 Statistical table between observations and simulations by using 81-km, 27-km, 9-km and 3-km resolution on PKU.

		2-m Temp. (C)		Ozone Con. (ppb)		NOx Con. (ppb)	
		Mean Bias	Mean Error	Mean Bias	Mean Error	Mean Bias	Mean Error
PKU	Domain 01	-4.34787	4.35967	-1.54097	1.90073	-24.0411	24.0651
	Domain 02	-0.626425	2.01655	-1.14468	2.22041	-11.8818	17.7208
	Domain 03	-0.268284	2.01987	-1.55700	2.49357	-6.55838	17.6232
	Domain 04	0.112615	2.08333	-1.41716	2.41534	-5.34942	17.6182

Temporal ozone simulations are also represented in Figure 6.2. Cases with 27, 9 and 3 km resolutions give similar results at PKU. The 81 km case overestimates ozone values, especially at night. Ozone simulation is significant improved when resolution increases. The peak value for ozone enhances step by step from Domain 01 to Domain 04. The mean bias decreased by 6.3 ppb from the coarsest to the finest domains. Even bigger improvement is found during nocturnal periods for ozone simulations. In the real case, ozone destruction rates are highly strengthened by circulations (dominated by both valley-breeze and urban-breeze) (Yu et al. 2014) (Ryu et al. 2013) and by NOx (which serves as a precursor) emissions into the stable night time PBL in urban area. As a result observed ozone levels are very low (only around several ppb) in urban centers in the Greater Beijing area. However, in the 81-km resolution case ozone remains elevated at night as it underestimates the NOx build-up. Employing finer increases NOx; between 81 km and 3 km the increase is as large as 70 ppb (Figure6.2.d). Therefore nighttime ozone simulations decreases with higher resolutions. Some statistical analyses are also performed in this study, shown in Figure 6.3. From the scatter plot (Figure 6.2.a) between temperature observations and simulations, significant improvement was found between 81-km and 27-km resolutions. Figure 6.3.b and 6.3.c are the diurnal plots for temperature and ozone, respectively. The shade indicates the range for observations. The 81-km case does not capture the heterogeneity in the land-cover use, and smoothens the topography

around Beijing, resulting in a lower temperature simulation for the entire day. Using 27-km resolution is able to increase nighttime surface temperature by 5 ℃ and daytime by 3 ℃. For ozone simulation, nighttime concentration near surface decreased by 17 ppb from 81 km to 27 km, then 20 ppb further to 9 km and eventually 29 ppb to 3 km (Figure 6.3.c).

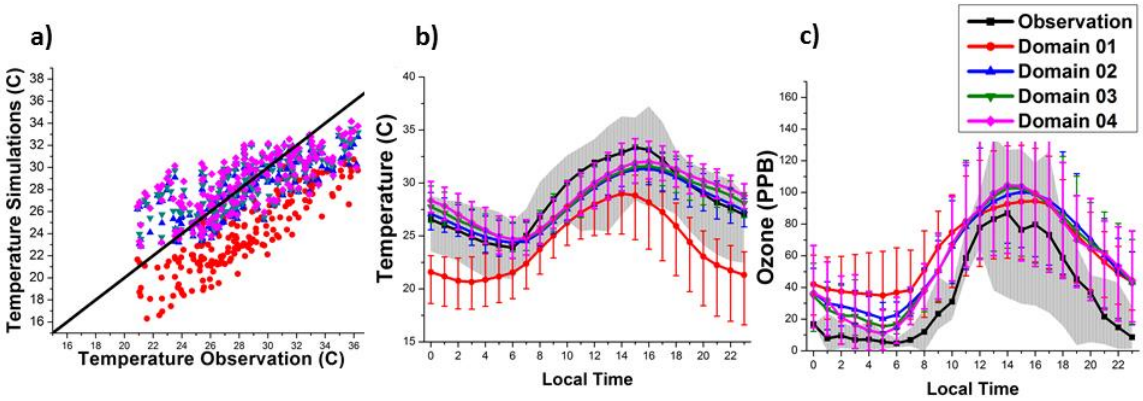

Figure 6.3 Some statistical plots for observations and simulations using 81-km, 27-km, 9-km and 3-km resolutions. The shade indicates observation range for temperature and ozone.

6.5.1.2 Spatial Resolution Impacts over Beijing Area

Figure 6.4 is the spatial plots over Beijing area from the different horizontal resolution cases (different domains, all plotted over the same spatial window) during nighttime. Resulting from UHI, there should be two hotspots in our domain for surface temperature. One is on Beijing and the other one is on Tianjin, another big city southeast of Beijing. However, domain 01 fails to capture any of these hotspots and under-estimates the maximum 2-m temperature by over 5 ℃. Beginning from the 27-km case, two high-value centers appears as expected. When comparing domain 02 with higher resolutions, surface temperature shows an under-prediction in both the magnitude and the spatial extent. Averaged performances for 3-km and 9-km cases are nearly identical

(99.15% correlation for city center) (Table 6.2), with similar maximum values and similar spatial patterns, except for a more detailed distribution in domain 04. PBL height distribution is also shown in Figure 6.4. Since no urban features are captured in 81-km resolution, the PBL estimates are relatively low over the Greater Beijing area, ranging from 40 meters to 60 meters. When moving to the next scale, two large hotspots, indicating city areas, appears in 27-km case. However the locations of two hotspots are shifted from city (south direction). In domain 03, the two hotspots appear at the correct locations and the maximum PBL heights during nighttime are over 300 meters. In domain 04, besides those two large spots, some small hotspots around Beijing and Tianjin arise.

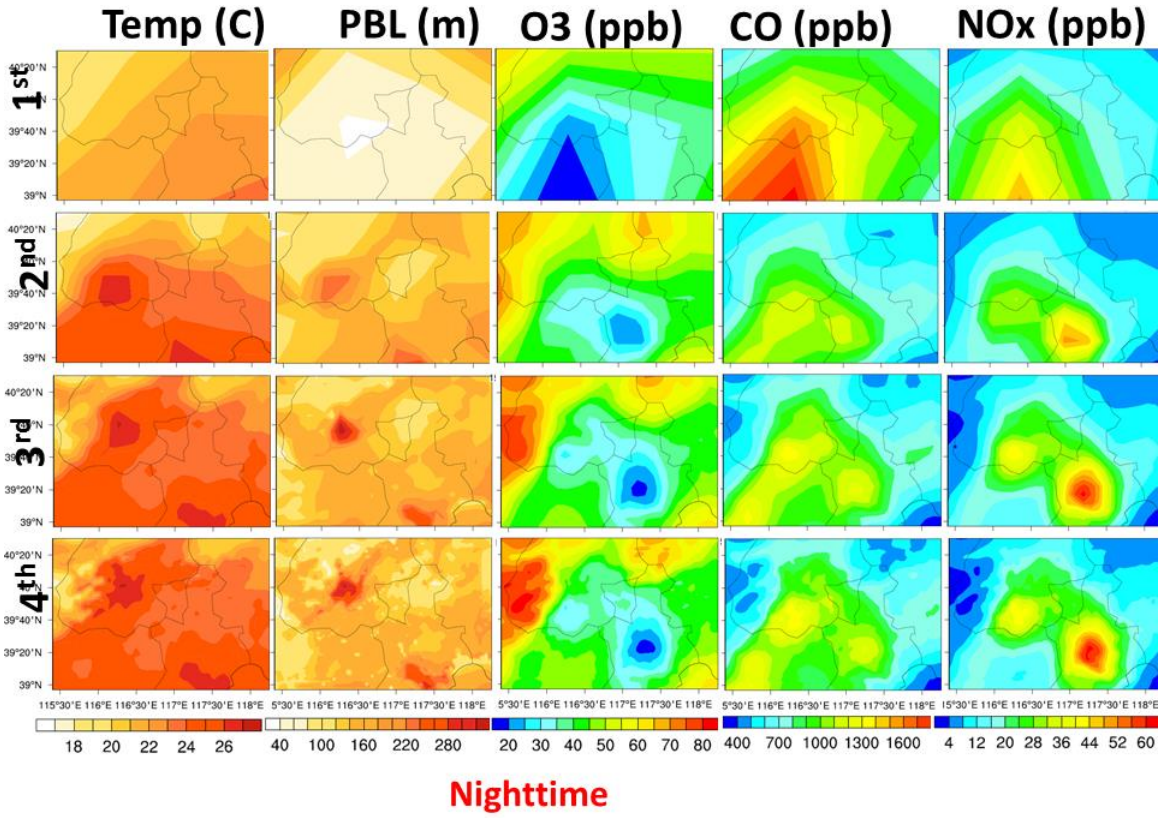

Figure 6.4 Spatial plots for monthly-averaged meteorological and chemical variables using 81-km, 27-km, 9-km and 3-km resolutions at nighttime..

Monthly-averaged nighttime concentration of ozone, CO, and NO_X is also shown in Figure 6.4. CO is used as an indicator for pollutant transport in our study area. Due to extremely low PBL profile around the Greater Beijing area in 81-km resolution, CO shows a high value center at Beijing and its southern counties, with maximum values exceed 1800 ppb. Using 27-km resolution improves the spatial distribution. Based on an elevated PBL, maximum of CO simulations decrease to around 1300 ppb and also two hotspots reflecting emissions from two cities emerge as a result. The 9-km and 3-km resolutions are able to further resolve CO gradients around Beijing city and southwest of it, which corresponds to the dominant down-wind direction during this period. The 9-km case is highly correlated to 3-km case in city center of Beijing, with R (area-averaged) equals to 0.9883. NOx distribution is similar to CO. There is no hotspots formed in 81-km resolution and gradually, two hotspots become to take shape using higher resolutions. From 9-km to 3-km resolutions, because of the enhanced PBL heights, the maximum value for city centers drops a little for NOx simulation. Ozone monthly-averaged concentration is also represented in Figure 6.4. The sharp edges of its gradient in 81-km case are mainly caused by interpolations on scarce points. With refiner resolutions from 27-km resolution, ozone destruction rates are largely enhanced by high NOx value within enhanced PBL. Therefore, very low-ozone scenarios are captured using 9-km and 3-km resolutions during nighttime.

Monthly-averaged daytime spatial distributions for temperature, PBL, O3, CO and NOx are shown in Figure 6.5. Similarly, 81-km resolution case is unable to capture the individual hotspot in Beijing and Tianjin and instead merges those two hotspots into one. Thus there are overestimates (around 2 ℃) for rural area temperatures. Consequently, higher PBL heights and lower CO concentration are expected. Using 27-km resolution is capable to distinguish the hotspots in surface temperature out of the one large one from 81-km resolution. From 27-km to 3-km resolutions, the high temperature center shrinks to the correct fully-developed city center, resulting in more pollutants

accumulates at city center. Daytime ozone formulations are highly dependent of its precursors, like NOx. In this case, 3-km resolution gives highest ozone estimates at city centers of Beijing and Tianjin (Figure 6.5).

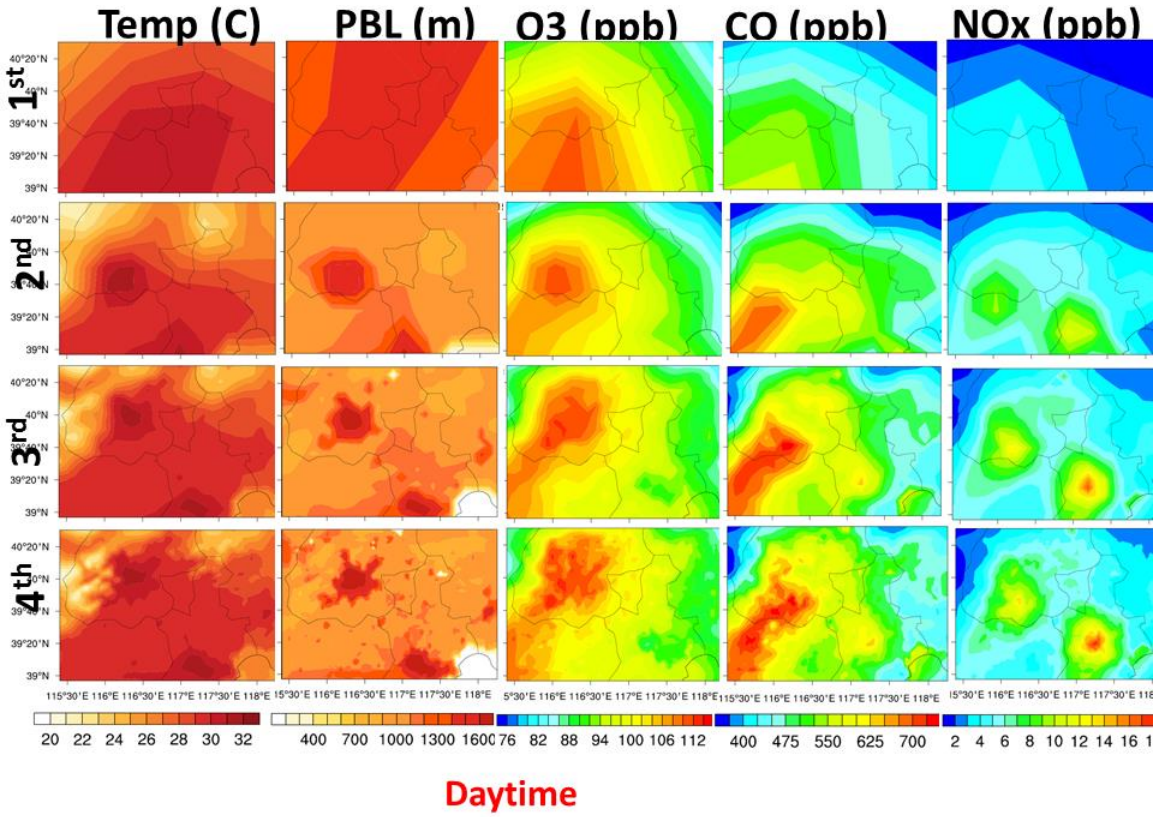

Figure 6.5 Spatial plots for monthly-averaged meteorological and chemical variables using 81-km, 27-km, 9-km and 3-km resolutions at daytime.

To understand how spatial resolution impacts pollutant transport and dispersion, a model called Flexpart is chosen in this study. Flexpart is a Lagrangian Particle Dispersion Model developed at the Norwegian Institute for Air Research in the Department of Atmospheric and Climate Research. Figure 6.6 shows particles dispersion patterns from each resolution case for the past 5 hours. Greatest differences are found between Domain 01 and Domain 02. Higher resolutions tend to increase the surface wind velocity and help particle matters and other pollutant transported further from the upwind direction.

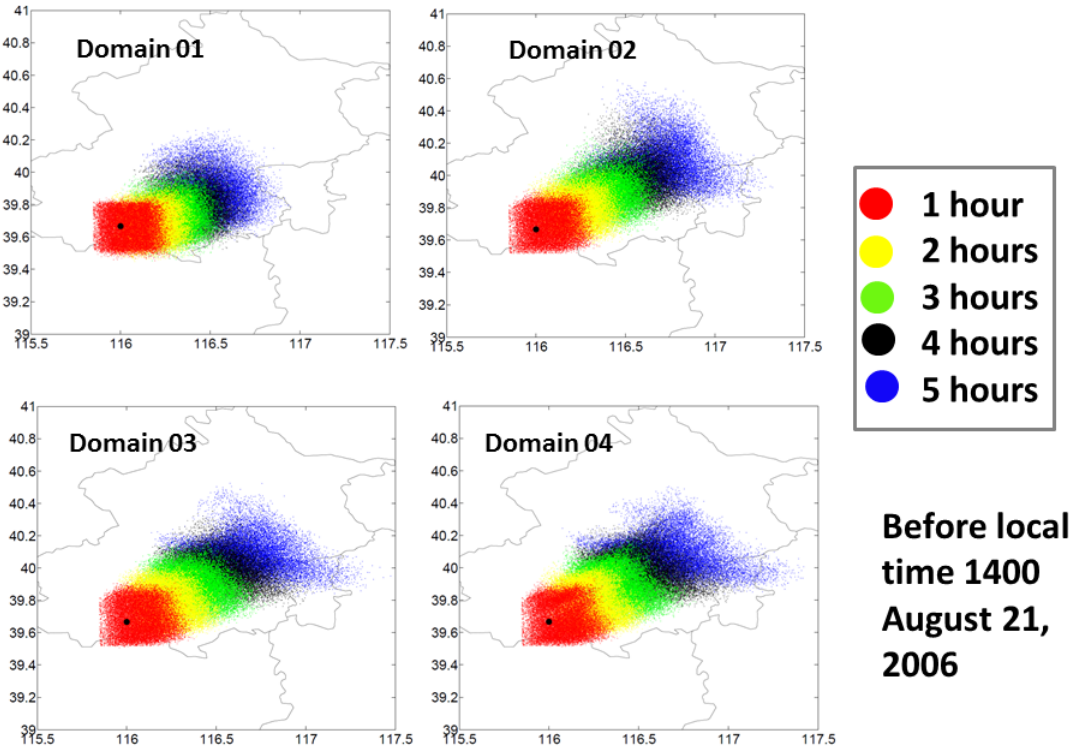

Figure 6.6 Particle matter dispersion results from 81-km, 27-km, 9-km and 3-km resolutions.

As we discussed before, the complex topography around Beijing area affect the flow conditions and resolving topography is a key factor for improving model performance. Three different grids are chosen on the black line in Figure 1.b., which is perpendicular to the terrain height gradient. We name it as, City Center, NE point (Northeast of City Center) and SW point (Southwest of City Center). For city center in Beijing, refining horizontal resolution increases surface temperature, and the maximum improvement is about 3.5 ℃ (Table 2).Temperature enhancement further alters the energy balance, resulting in a higher PBL height. In 81-km resolution simulation, the PBL is around 484 meters in the city center, while using 3-km resolution, it expands to 879 meters. Concentrations of carbon monoxide and NOx increase while ozone decreases

as resolution increases. Compared to the city center, meteorological differences on NE and SW grids are relatively smaller between each resolution case. The difference ranges for 2-m temperature is within 1 ℃ andwithin 60 meters for PBL simulations. When refining resolution from 81-km, carbon monoxide and NOx tend to increase on SW grids and decrease on NE grids. Meanwhile surface ozone decreases on SW grids and increase on NE grids. To better investigate diurnal trends on three points, another statistical result is shown in table 3. For City Center and SW point, ozone tends to increase during daytime and decrease during nighttime by using finer resolutions. NE point shows a different scenario, with lower ozone at daytime and higher at nighttime. Inside the North China Plain, the major emissions is from the southern part and using higher resolution is able to better resolve the spatial distributions. Some system errors might be brought into simulations if using insufficient resolution. Cumulative fraction of CO and ozone for these three grids is shown in Figure 6.7. For CO simulations on City Center and SW points, finer resolutions seem to enlarge peak time CO, while decrease peak time CO on NE points. Ozone cumulative fraction plots are consistent with our quantitative analysis in table 3. A large decrease for nighttime ozone is found on both city center and SW point and increase for daytime ozone simulations. The lower 25 % of ozone concentrations decreases from 30 ppb in 81-km resolution to less than 10 ppb in 3-km resolution case. At the meantime, the upper 5% of ozone increases from 100 ppb in 81-km to around 130 in 3-km at city center. Correlation between each resolution case is shown in the right column in Table 2. The R between 81-km and 27-km resolutions is around 0.75 for temperature and less than 0.60 for other chemical species. The lowest correlation is for carbon monoxide on upwind grids, which is only 0.43. The other three cases are highly correlated to each other for all variables, especially for 9-km and 3-km cases. The overall R between 9-km and 3-km is as large as 0.98.

Table 6.2 Statistical results on three different grids around Beijing area by using 81-km, 27-km, 9-km and 3-km resolutions.

City Center	Average				Correlation		
	81-km	27-km	9-km	3-km	81-km vs. 27-km	27-km vs. 9-km	9-km vs.3-km
2-m Temp.	24.4790	27.8339	27.9980	28.1554	0.747996	0.986524	0.986407
PBL heights	484.219	729.229	844.957	879.308	0.837234	0.985208	0.988881
NOx	17.8189	32.7224	48.2212	47.9474	0.693752	0.931099	0.963104
O_3	57.0567	55.4485	50.5962	50.4159	0.838372	0.979708	0.991012
CO	664.093	669.182	773.097	757.826	0.582573	0.949753	0.974086

NE Point	Average				Correlation		
	81-km	27-km	9-km	3-km	81-km vs. 27-km	27-km vs. 9-km	9-km vs.3-km
2-m Temp.	24.7514	24.9034	25.0248	24.8263	0.798351	0.974858	0.996434
PBL heights	481.068	416.863	392.032	410.029	0.929801	0.978550	0.992910
NOx	20.3429	14.5643	9.55915	8.45685	0.580076	0.942447	0.974903
O_3	58.1784	56.7269	60.8980	61.3783	0.782267	0.955119	0.988238
CO	669.401	520.971	442.538	418.825	0.427566	0.936171	0.986500

SW Point	Average				Correlation		
	81-km	27-km	9-km	3-km	81-km vs. 27-km	27-km vs. 9-km	9-km vs.3-km
2-m Temp.	24.6897	25.8073	25.5534	25.5608	0.789713	0.981903	0.994442
PBL heights	483.713	403.867	417.329	414.699	0.930376	0.979662	0.988038
NOx	21.2275	23.8146	35.2251	38.5917	0.626676	0.902991	0.961656
O_3	54.1292	59.4920	54.7586	52.2819	0.844352	0.973871	0.985956
CO	745.205	702.594	838.988	872.2623	0.526463	0.907535	0.969038

Table 6.3 Diurnal trends on City center, NE (Northeast point) and SW (Southwest point) for each species.

City Center	Daytime	Average				Nighttime	Average			
		81-km	27-km	9-km	3-km		81-km	27-km	9-km	3-km
	2-m Temp.	28.8934	30.7906	30.6778	30.7684	2-m Temp.	21.2252	25.8333	26.1143	26.5586
	PBL heights	1448.04	1634.33	1757.20	1810.09	PBL heights	64.5568	157.429	227.119	258.452
	Nox	2.35512	9.7184	13.8396	15.4819	Nox	30.0355	51.0899	81.9630	79.4820
	O3	89.2426	99.0552	99.4294	99.0008	O3	30.0527	19.9628	8.85124	8.87869
	CO	332.319	414.185	459.081	476.278	CO	949.799	902.218	1094.07	1039.72

NE Point	Daytime	Average				Nighttime	Average			
		81-km	27-km	9-km	3-km		81-km	27-km	9-km	3-km
	2-m Temp.	29.50344729	28.44045	27.97557	27.78609	2-m Temp.	21.20333	22.18143	23.03379	22.87855
	PBL heights	1482.797197	1151.721	1079.165	1145.536	PBL heights	62.70869	114.6925	112.4447	110.3936
	Nox	2.998532428	3.781484	2.763076	2.360837	Nox	34.17977	19.31351	11.93935	10.93562
	O3	92.3720886	82.99423	79.08635	77.63658	O3	28.42286	38.45078	48.347	49.9949
	CO	341.6035913	332.3253	320.4987	306.3791	CO	948.6786	653.2019	506.8698	484.171

SW Point	Daytime	Average				Nighttime	Average			
		81-km	27-km	9-km	3-km		81-km	27-km	9-km	3-km
	2-m Temp.	29.06765413	29.21905	29.37694	29.31414	2-m Temp.	21.35593	23.4997	22.63267	22.55975
	PBL heights	1456.410948	1111.473	1139.553	1106.197	PBL heights	47.32175	83.44871	81.99494	86.76869
	Nox	2.735687003	5.971036	8.226307	8.758784	Nox	35.96646	30.99176	42.64208	47.4106
	O3	91.9048152	99.41429	98.81002	97.71733	O3	21.86871	33.45753	23.07049	19.37802
	CO	350.618279	447.3295	478.0718	494.9495	CO	1086.935	817.1372	989.6612	1045.227

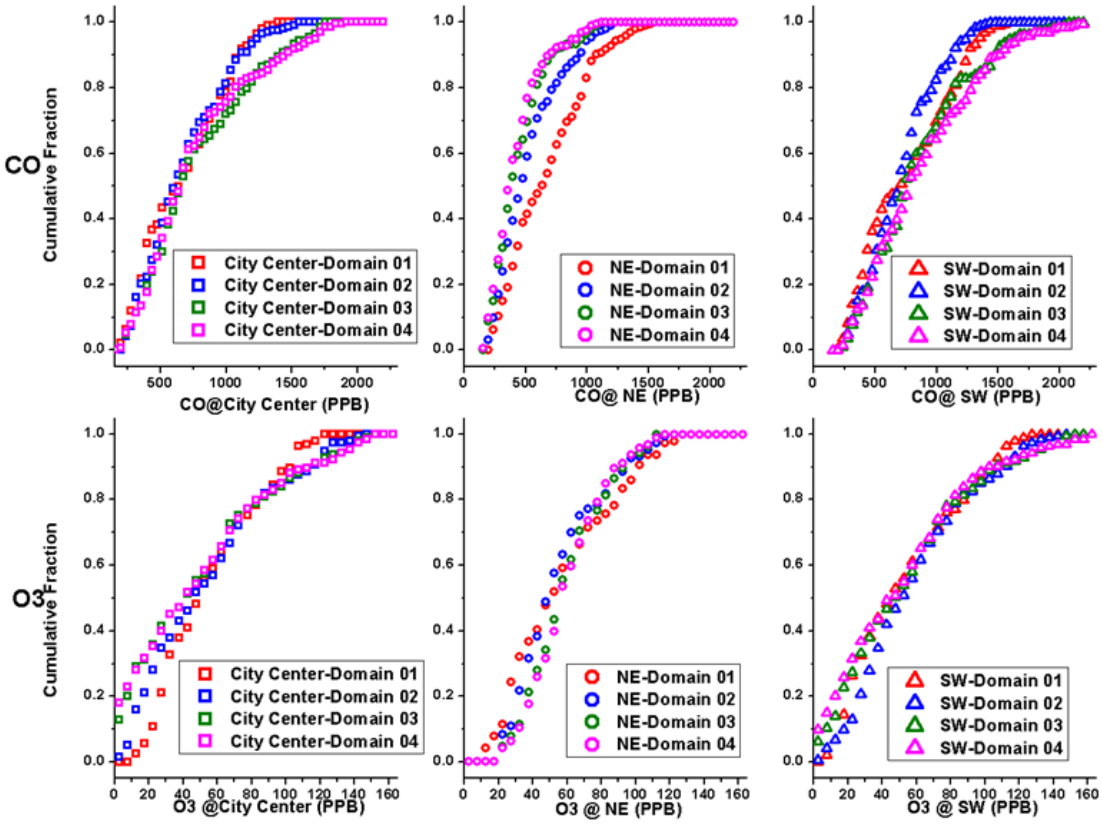

Figure 6.7 Cumulative fraction plots on City Center, NE and SW points for CO and Ozone.

Overall, smaller resolution can better resolve the distribution of both chemical and meteorological variables, especially for city and urban scale. Some systematic error may be brought in due to lack of detailed resolutions. However, only very limited improvements are found between 9-km and 3-km cases. Therefore with regards to current available data and computing resources, 9-km resolution seems to be the best option for future adequate and efficient forecast in Beijing.

6.5.2 Sensitivity to Vertical Impact

Three different vertical meshes are used in these sensitivity studies. First one using the default WRF/Chem vertical settings is called as original case. Second one (double case) is double the original layers, using 54 layers. The last one is one-third case,

containing only 9 vertical meshes. Results are extracted from innerest domain using three different vertical meshes.

6.5.2.1 Validation with Observations

Figure 6.8 shows the temporal plots and comparisons at PKU for 2-m temperature, PBL height, ozone and NOx concentrations. All of these three cases under-predict 2-m temperature for PKU. One-third case gives the lowest estimates, with a mean bias of over 4 ℃ for peak value. Original case are highly correlated to double case (99.25% correlation), and reduces the mean bias to 2 ℃. Using coarse vertical resolution might not be able to reproduce the whole structure of PBL. According to Figure 8, the PBL height simulations from the one-third case is around 30% lower than that from the other two cases at noon. Bigger effects of vertical resolution are found for ozone. During high ozone episode in August 2006, one-third case performances worst. For instance, it underestimates surface peak ozone by 40 ppb on August 15 2006 and overestimates by over 30 ppb on August 17 2006. Meanwhile, it predicts a nocturnal situation with high ozone (40 ppb), while the realistic case is a low profile. With refining vertical meshes, results demonstrate a considerable and gradually improvement (for both daytime and nighttime) in original and double cases. Mean bias for ozone simulations decreases by 3.2 ppb between one-third and original case and further decreased by 3.3 ppb when using 54 vertical layers.

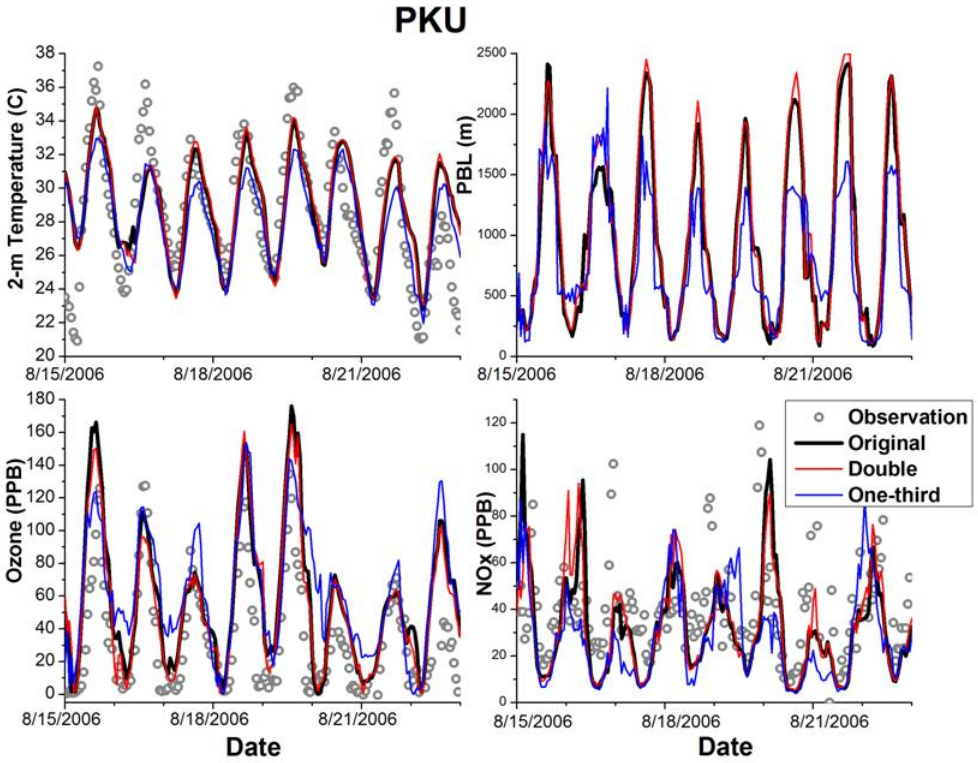

Figure 6.8 Temporal plots on PKU for observations and simulations from one-third (9 layers) case, original case (27 layers) and double case (54 layers).

6.5.2.2 Vertical Profile Differences from Vertical Resolution

Figure 6.9 is the monthly-averaged vertical profile for each meteorological and chemical species at the PKU site. The black solid line represents the original case (27 layers), the blue dotted line is the one-third case (9 layers) and the red dashed line represents double case (54 layers). For some variables, like temperature and pressure, the three cases give the similar predictions from surface level to the top of troposphere for the entire day. With regards to water vapor fields, original and double cases tend to predict similar profiles, while one-third case suggests a dryer lower atmosphere and more moisture situation in higher atmosphere which corresponds to cloud formation locations (Figure 9). Another discrepancy is found out at z-direction wind, a key factor for

pollutants vertical transport and dilutions. With more layers (original and double cases), model produces an upward flow from surface for both daytime and nighttime. One-third case, on the other hand, exhibits a depressed center with downward flow over PKU site. Ozone, NOx, CO and PM2.5 comparisons are also shown in Figure 6.9. Overall, compared to original and double case, one-third case underestimates pollutants concentration on surface and overestimates it in upper levels. The difference near surface is as large as 30 μg/m^3 for PM2.5 (around10 μg/m^3 (35.7%) enhancement from nitrate concentrations and 20 μg/m^3 (25%) increase from other inorganic matters) between one-third case and double case.

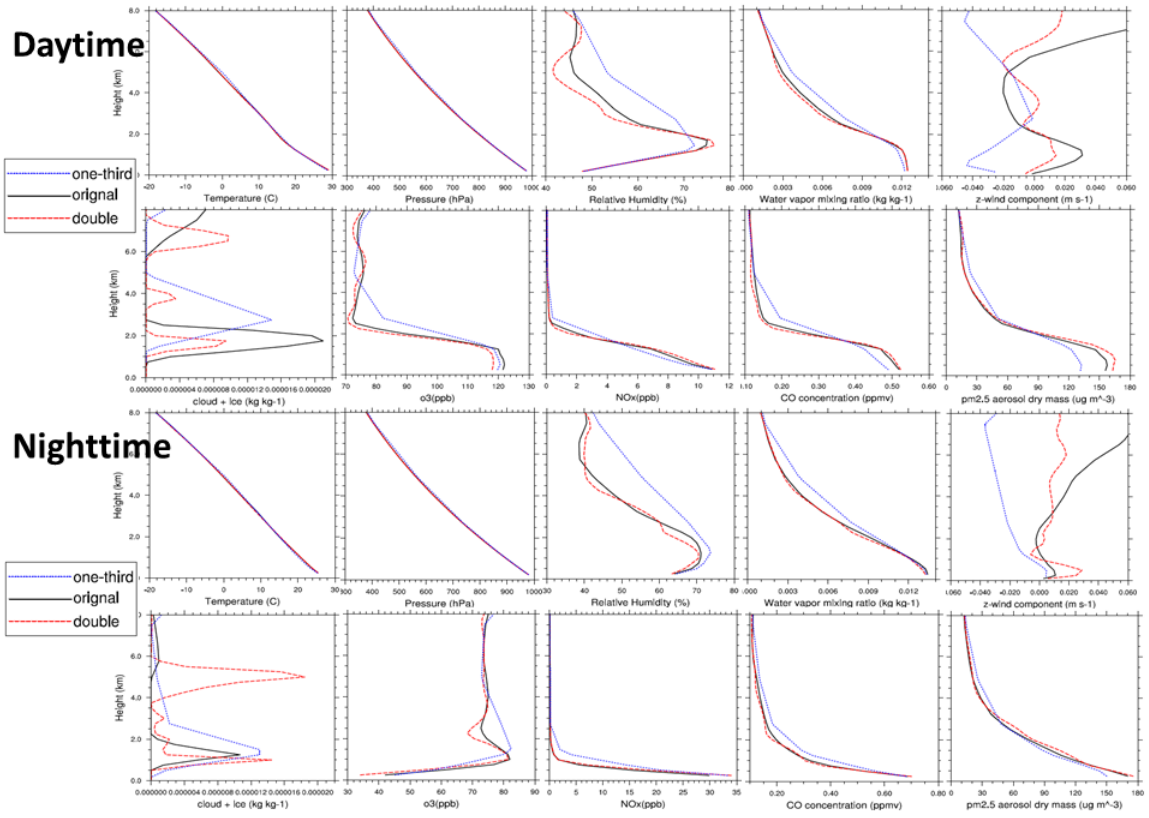

Figure 6.9 Vertical profile plots for Temperature, Pressure, RH, Water mixing ratio, Z-wind, Cloud and ice, Ozone, NOx, CO and PM2.5 in daytime and nighttime on PKU.

Figure 6.10 is the height versus time plots of PKU for carbon monoxide, ozone, NOx and PM2.5. The x-axis represents the date of the simulated month, which is August 2006. The left panel is the difference between original and one-third case. The middle panel is the original vertical profile plots at PKU and the right one is the difference between double and original case. With the same emission distribution from MICS 2010, one-third case predicts the lowest carbon monoxide concentrations near surface area, by underestimating both magnitude and length for polluted episodes, like August 24 2006. When it comes to the upper atmosphere, it tends to overestimate carbon monoxide. This could be caused by the different vertical wind profile in each case. For ozone concentrations, more downward intrusion from troposphere is found in one-third case and with more vertical layers, it is likely to have a higher ozone concentration in the lower atmosphere. Also more ozone intrusion from stratosphere to troposphere is simulated in original and double case, resulting in a higher value at upper atmosphere. PM2.5 concentration is also shown in Figure 6.10. More vertical meshes alter the formulation rates of secondary aerosols which in turn bring in more particle matter around Beijing area. The difference between original and one-third case is as large as 150 ug/m3 at surface and can influence up to 2 km above ground. Figure 6.11 is another Flexpart plot for particulate matter transport. From the comparison, finer vertical meshes tend to decrease surface horizontal wind and introduce a un-favorable condition for pollutants dispersions. With increasing accumulation in city areas, original and double cases are likely to reproduce a more polluted scenario within PBL (Figure 6.10.d).

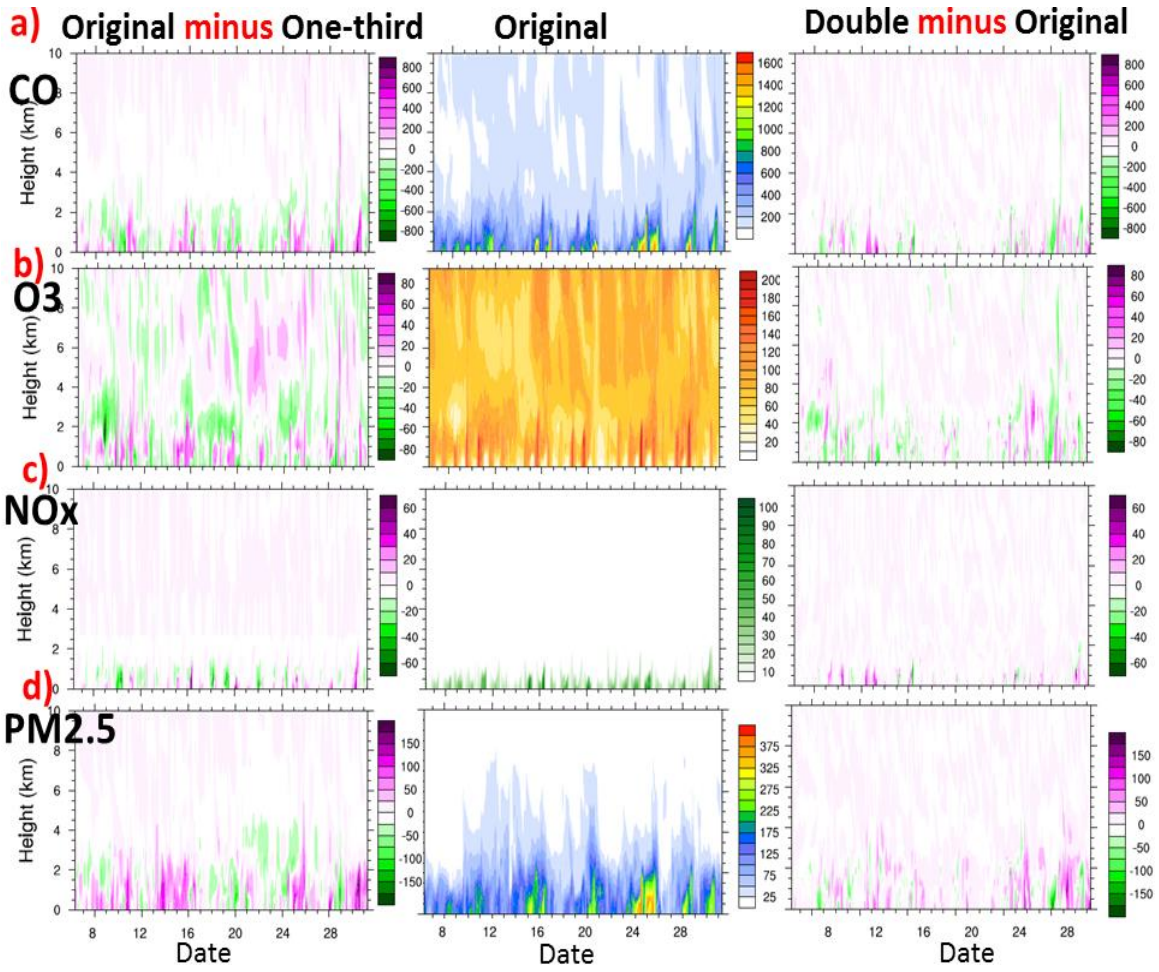

Figure 6.10 Height versus time plot on PKU for CO, O3, NOx, and PM2.5 for the entire simulated month.

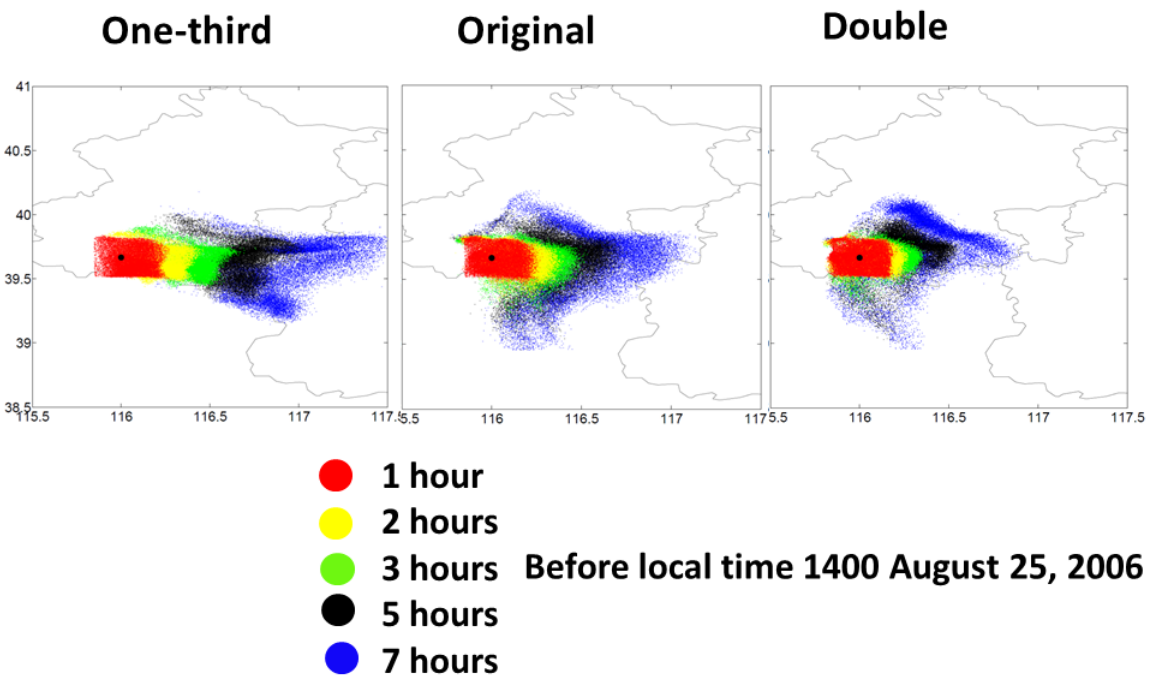

Figure 6.11 Particle matter dispersion results from one-third, original, and double cases.

6.5.2.3 Spatial Differences from Vertical Resolutions

Choice for vertical meshes is crucial for not only vertical profile but also spatial re-distribution. The monthly-averaged spatial difference is shown in Figure 12. The left panel is the differences between original case and one-third case and right is between double and original case. Involving from 9 layers to 27 layers enhances surface concentrations for carbon monoxide over Beijing and its downwind area. The maximum enhancement is around 160 ppb. Further involving form 27 layers to 54 layers results in a very limited increase (within 10 ppb) in carbon monoxide concentrations around Beijing area. NOx and PM2.5 share the same spatial pattern with carbon monoxide. Pollutant levels are better captured using original and double cases, especially for particle matters. A difference of over 44 $\mu g/m^3$ is shown between 9 layers and 27 layers. Menut et al. (2013) found that vertical resolution is not the most sensitive factor for air quality

modeling in Paris, while in Beijing, insufficient vertical resolution will under-estimate PM2.5 by nearly 20 ppb.

Vertical profile is easily affected under different choice of vertical resolutions. For urban area in Beijing, finer vertical resolutions tend towards a better and more realistic scenario. Great improvements are discovered using 27 and 54 layers. One-third case, using 9 vertical layers, is likely to underestimate peak values for surface ozone. Although some finite improvement can be achieved by using double case instead of original case, it is highly recommended to use 27 layers for a more efficient forecast process.

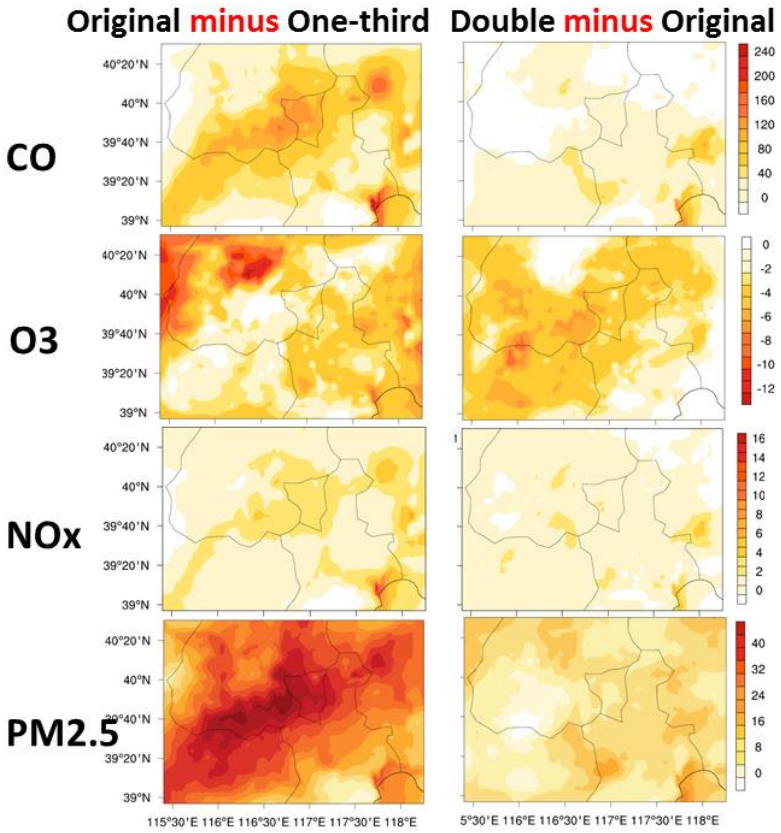

Figure 6.12 Spatial plots for monthly-averaged CO, O3, NOx, and PM2.5. Left panel: difference between 27 layers and 9 layers. Right panel: difference between 54 layers and 27 layers.

6.6 Conclusions

Widespread haze episode has become very frequently in northern China recently. An efficient and accurate forecast is needed for public health. In this paper, we focus on resolution impacts on air quality modeling in China and try to provide an optimal domain setting for future study.

Four different domains were designed to evaluate spatial resolution impact. The resolutions are 81-km, 27-km, 9-km and 3-km. For urban grid, higher resolution improves simulations. Mean bias for 2-m temperature deduced from -4.4 ℃ in 81-km case to only 0.11 ℃ in 3-km case. Ozone simulations are also improved by a higher daytime peak and a lower nighttime concentration with finer spatial grids. Biggest improvement are found out between 81-km and 27-km and the performances for 9-km and 3-km resolutions are nearly identical (R~0.98).

In this paper, vertical resolution impact is accessed by three vertical meshes, 9 layers, 27 layers and 54 layers. The results from 27 layers are highly related to 54 layers, while the case using 9 layers develops an opposite scenario for vertical wind and moisture distributions. It (9 layers) also fail to capture the peak value for 2-m temperature and ozone overestimate nocturnal ozone by 20~30 ppb. Vertical settings affect surface simulations as well. The maximum difference for PM2.5 in Beijing downwind direction is as large as 44 $\mu g/m^3$.

For future forecast in Beijing, we recommend a domain of 9-km spatial resolution and 27 vertical layers. However, if other precise data is available, for instance emission inventory or land-cover data, more improvements are expected from 3-km and 54 vertical layers. This setting might not be sufficient for forecasting. Future work will focus on using high-resolution emission and further evaluate model performances.

6.7 Collaborators and Funding Sources

This paper was supported in part by NSF grant CHE-1049140 and NASA grant NNX11AI52G.

The CAREBeijing 2006 campaign was supported by the Beijing Council of Science and Technology (HB200504-6, HB200504-2).

CHAPTER 7CHEMICAL AND METEOROLOGICAL FORECASTING DURING CAREBEIJING-NCP2013 FIELD CAMPAIGN

7.1 Abstract

Campaigns of Air Pollution Research in Megacity Beijing and North China Plain (CAREBeijing-NCP) 2013 were initialed by Peking University in summer 2013. To better served the field campaigns, CGRER (the Center for Regional and Environmental Research) participated in the forecasting project. Everyday a forecast report was sent out by midnight including four types of products. Some preliminary results revealed that CGRER was able to capture the main trend of meteorology, including severe convection weather in Beijing area. For future forecast runs, a more detailed emission inventory, especially for particulate matters is highly recommended.

7.2 Introduction

Urbanization and rapid economic progress in China, especially in Beijing, put a lot of pressure on air quality. Recent research and studies revealed the poor quality due to massive emissions and unfavorable metrological conditions (Zhao et al., 2013 and Tao et al., 2014). However the current understanding of haze formulation and mechanisms are far from complete in China. To address these uncertainties, CAREBeijing-NCP (Campaigns of Air Pollution Researchin Megacity Beijing and North China Plain) was planned in the summer of 2013, as a follow up of CAREBEIJING2006, 2007, and 2008. It was initialed by Peking University, China and executed from June 1st 2006 to July 15th 2006.

The major objectives for CAREBeijing-NCP 2013 field campaign fall into 4 aspects. Better understanding for 1) mechanisms for the producing, cycling, and sinks of HO_x radicals; 2) mechanisms of ozone, new particle, and secondary aerosol particles formation; 3 oxidative capacities and the multiphase reaction on the surface of fine

particles; 4) optical and hygroscopic properties of aerosol and their implication in climate impacts.

Dozens of teams participated in the CAREBEIJING-NCP 2013 field campaign in Beijing, including China, Korea, Japan, USA, Germany and other countries. Figure 7.1 is the campaign photos from Group Princeton, USA and Group Shangdong, China. Also a data policy was made on October 2013 for data sharing.

Figure 7.1 Campaign photos from Group Princeton and Group Shangdong

To support CAREBeijing-NCP field campaign, daily forecast reports were made during campaign periods. Two groups participated in forecast: Institute of Atmospheric

Physics (IAP) from Chinese Academy of Sciences and Center for Regional and Environmental Research (CGRER) from University of Iowa. IAP used MM5 (the fifth-generation NCAR/Penn State Mesoscale Model) as metrological model and NAQPMS (the Nested Air Quality Prediction Modeling System) as chemical transport model. CGRER employed WRF-Chem V3.5 as forecasting tools. Everyday two reports were sent out to campaign members by mid-night.

As we discussed before, CareBeijing-NCP is a follow up campaign from summer 2006 and expanded to the entire North China Plain. More sites outside Beijing as well as mobile measurement were designed for this 2013 campaign. Figure 7.2 below is the sites and routes map. In this field campaign, five major observation sites were chosen: 1)PKU site, at the campus of Peking University; 2) Xianghe Site, locating in Xianghe County between Beijing and Tianjin; 3) Gucheng Site, 100km south of Beijing;4) Quzhou, in southern part of Hebei Province; 5) Yucheng, northwest part of Shangdong Province. The lines in Figure 7.2 represented the designed route path for mobile platform.

Figure 7.2 Five major sites and route for mobile platforms in CAREBeijing-NCP 2013

7.3 Method

CGRER from University of Iowa used WRF-Chem (Grell et al. 2005), the online chemical transport model, in CAREBeijing-NCP 2013 campaign forecast. Three nested domains were performed everyday with three day forecast. The resolution for the largest domain is 81 km and the smallest is 9 km. Vertical meshes are 27 layers recommended from Section 6. Anthropogenic emissions were reassigned from the Intercontinental Chemical Transport Experiment Phase B (Zhang et al., 2009) for 2006. And the Model of Emissions of Gases and Aerosols from Nature (MEGAN) was used as biogenic emissions (Guenther et al., 2006). Land cover data was MODIS, with 20 classifications. Boundary and initial conditions were from MACC developed by Institute for Climate and Energy Research in Forschungszentrum Jülich, Germany. We downloaded from http://join.iek.fz-juelich.de/macc/access/. To better capture gaseous pollutants concentrations, we used The Carbon Bond (CBMZ) chemical mechanism and MOSAIC using 4 sectional aerosol bins

(Fast et al, 2006) in this study. Real time fire emissions were based on the Fire Inventory from NCAR (FINN), downloaded from http://bai.acd.ucar.edu/Data/fire/. Lin et al. scheme is chosen as microphysics (Lin, Farley and Orville, 1983). We used RRTM as long wave radiation (Mlawer et al., 1997) and Goddard (Chou and Suzrez, 1994) as shortwave radiation.

7.4 Preliminary Results

The whole forecast lasts from Jun 1st to July 1st 2013, and then extended to July 15th 2013.

7.4.1 Pre-campaign Analysis

Some test runs were designed before the field campaign period. To better capture pollutant levels in summer 2013, a parallel run for summer 2010 was performed in North China Plain. The simulated period was from 0000 UTC 01 June to 0000 UTC 30June 2010 using exact domain settings in section 7.3.

7.4.1.1 Basic Analysis

Figure 7.3 below is the terrain height plot (left) and urban fraction plot (right) in 3rd domain. The dots represent the five stationery observation sites at that time and lines are the analytic cross-section location, which is consistent with the dominant wind direction. The unique topography for Beijing makes it unfavorable conditions for pollutant dilutions. During summer monsoon seasons, both urban breeze and valley breeze circulations are of great importance for predicting air quality in North China Plain (Yu et al., 2014).

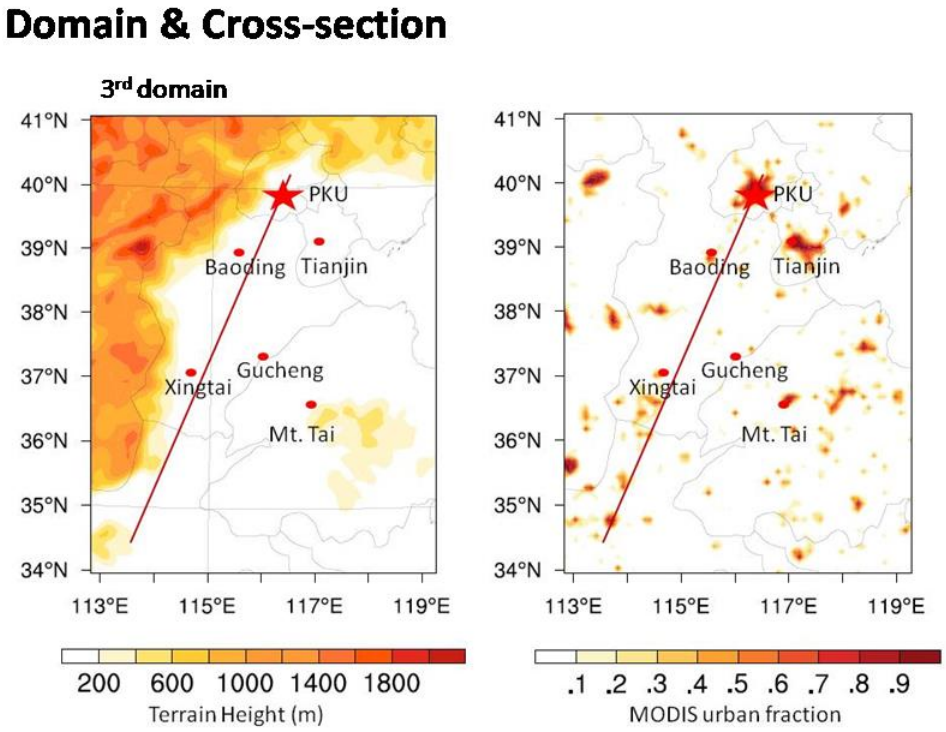

Figure 7.3 Terrain height (left) and urban fraction (right) plots in 3rd domain for CAREBeijing-NCP field campaign.

Figure 7.4 shows the spatial distributions for monthly-averaged 2-m temperature, 2-m dew point, PBL height and Aerosol Optical Depth (AOD) at 600 nm for daytime and nighttime in 3rd domain. The maximum of 2-m temperature is 32 ℃and 24 ℃ for daytime and nighttime respectively. Daytime PBL height expands to over 1800 meters for Beijing and its downwind area. High AOD area in Figure 7.4 is highly correlated to urban fraction plot in Figure 7.3. Spatial distributions of chemical species are also investigated in this study (Figure 7.5). Beijing and Tianjin serves as two major sources for carbon monoxide. Due to the elevated topography in the northwest part and background monsoon wind, high concentrations of pollutants accumulated from southwest to northeast in North China Plain. The maximum carbon monoxide value is over 500 ppb. High values for other criteria pollutants; like NO_X and Ozone are also found in Beijing, while sulphates mass is not. This indicates the regulation on cleaner energy resources has

taken into effect in Beijing. City of Shijiazhuang corresponds to the high center around (38 °N, 114.5 °E). It is a traditional industry city with high capacity power plant and steel industry.

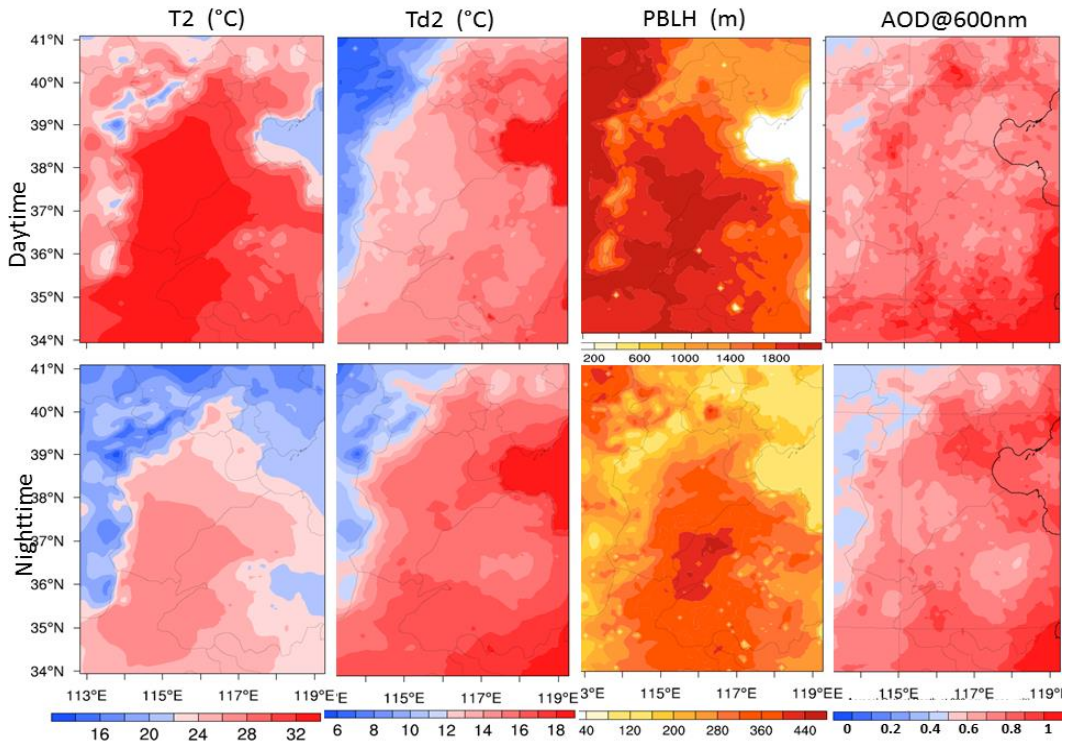

Figure 7.4 Monthly-averaged spatial plots in 3rd domain for 2-m Temperature, 2-m Dew points, PBL height and AOD at 600 nm.

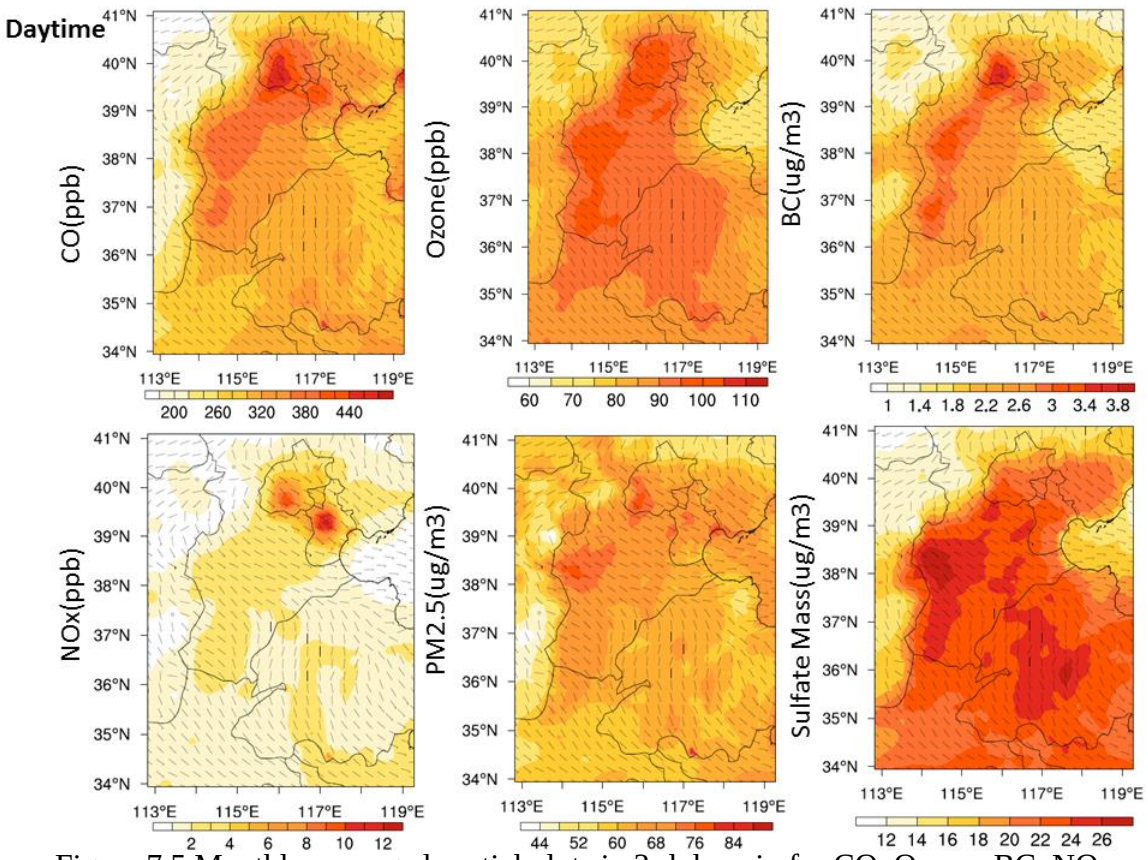

Figure 7.5 Monthly-averaged spatial plots in 3rd domain for CO, Ozone, BC, NOx, PM2.5 and Sulfate Mass.

Figure 7.6 shows the vertical profile for a cross-section line in Figure 7.3. We analyze a high episode that occurred on Jun 15th 2010. Two snapshots are taken: 2 PM Jun 15th 2010 and 2 AM Jun 16th 2010 (12 hours later). For the first snapshot, a strong upward flow is found for the Beijing area. Turbulence brings polluted air to an altitude of 4 km above ground. Ozone shows the similar vertical distribution. Because of the unfavorable dilution conditions, after 12 hours in the second snapshot, high ozone air mass shows at 2 km height along the cross-section line. A new plume of PM2.5 arises from Beijing area on 2 PM Jun 15th and after 12 hours it maintains the same high level at Beijing, with slightly expansion upward and to southwest part. Due to this plume, the averaged background PM2.5 in the downwind direction increases by 30 $\mu g/m^3$.

To better understand this high episode, height-versus-time plots are made on PKU site and Gucheng. In Figure 7.7, PKU represents the urban scenario for Beijing, while Gucheng is one of the downwind cities around Beijing. PKU has a peak PM2.5 on Jun 15th with maximum exceeding 130 $\mu g/m^3$, while Gucheng shows a later high episode for the next following day. When compared Gucheng with PKU, for all species there is a shift (approximately half day) in time. Therefore to control the air quality within North China Plain, Beijing is the key factor for its downwind cities.

7.4.1.2 Aerosol Feedbacks

It is crucial to include aerosol feedbacks (direct and indirect) in air quality. In this section, sensitivity runs were conducted with and without aerosol feedbacks for North China Plain.

Figure 7.8 is the spatial difference for short wave, long wave radiation, surface temperature and AOD at 600 nm. The total effect from aerosol is "cooling", with a surface temperature decrease (around -0.6 C) at Beijing area. And the maximum decrease in Beijing for shortwave radiation is about -160 W/m^2. AOD is expected to increase when considering feedbacks. At Beijing, the enhancement exceeds 2. We also extract temporal plots on PKU (Figure 7.9). Without feedbacks, simulations tend to yield higher surface temperature during daytime, which results from more short wave radiation reaches surface when feedback option is turned off. Higher surface temperature always comes with higher PBL height. More chemical components are transported into upper atmosphere. Thus the ambient air in Beijing is turned out to be cleaner on Jun 10th 2010, for instance.

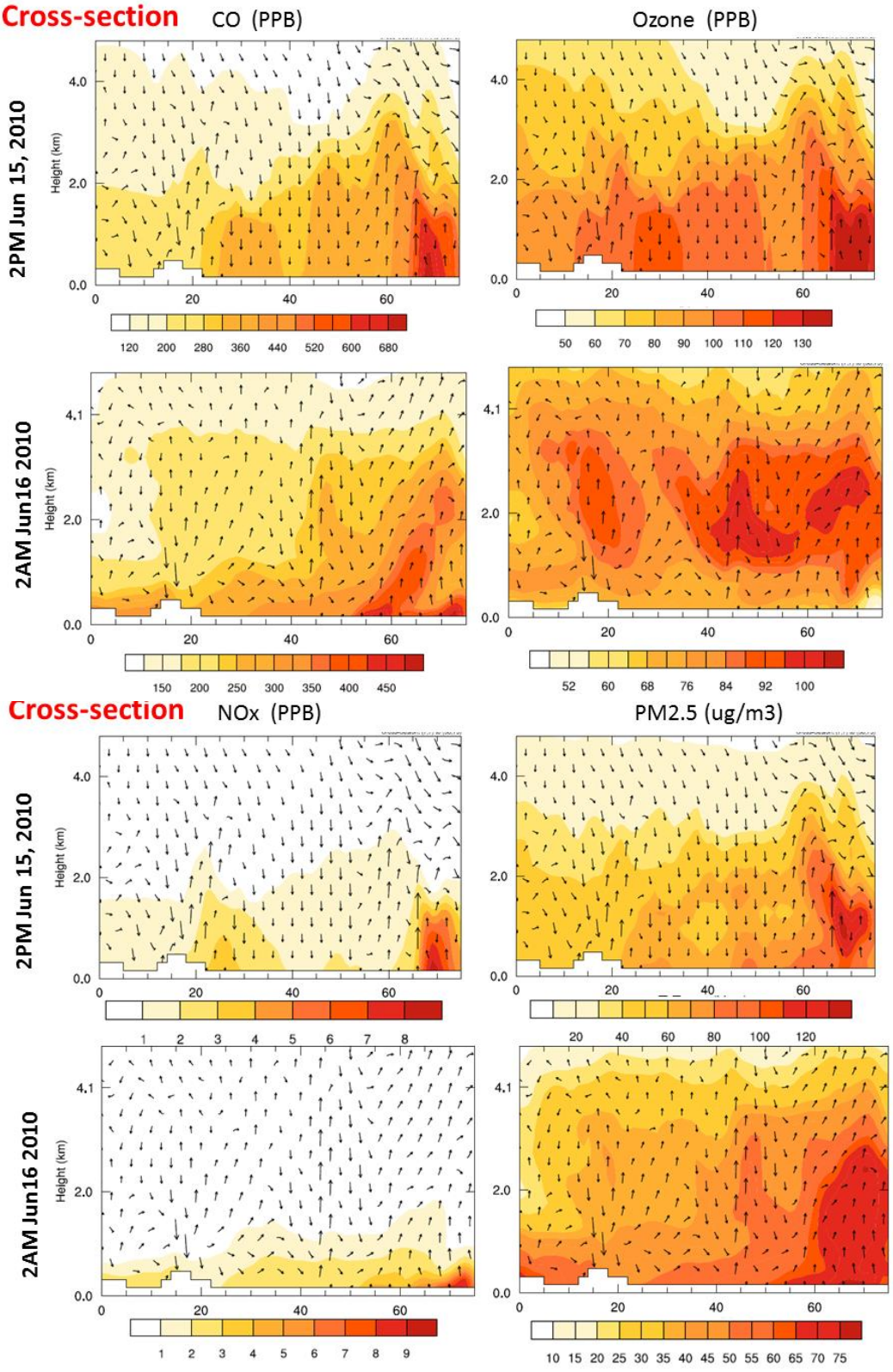

Figure 7.6 Cross-section plots for CO, Ozone, NOx and PM2.5 in a heavily polluted episode.

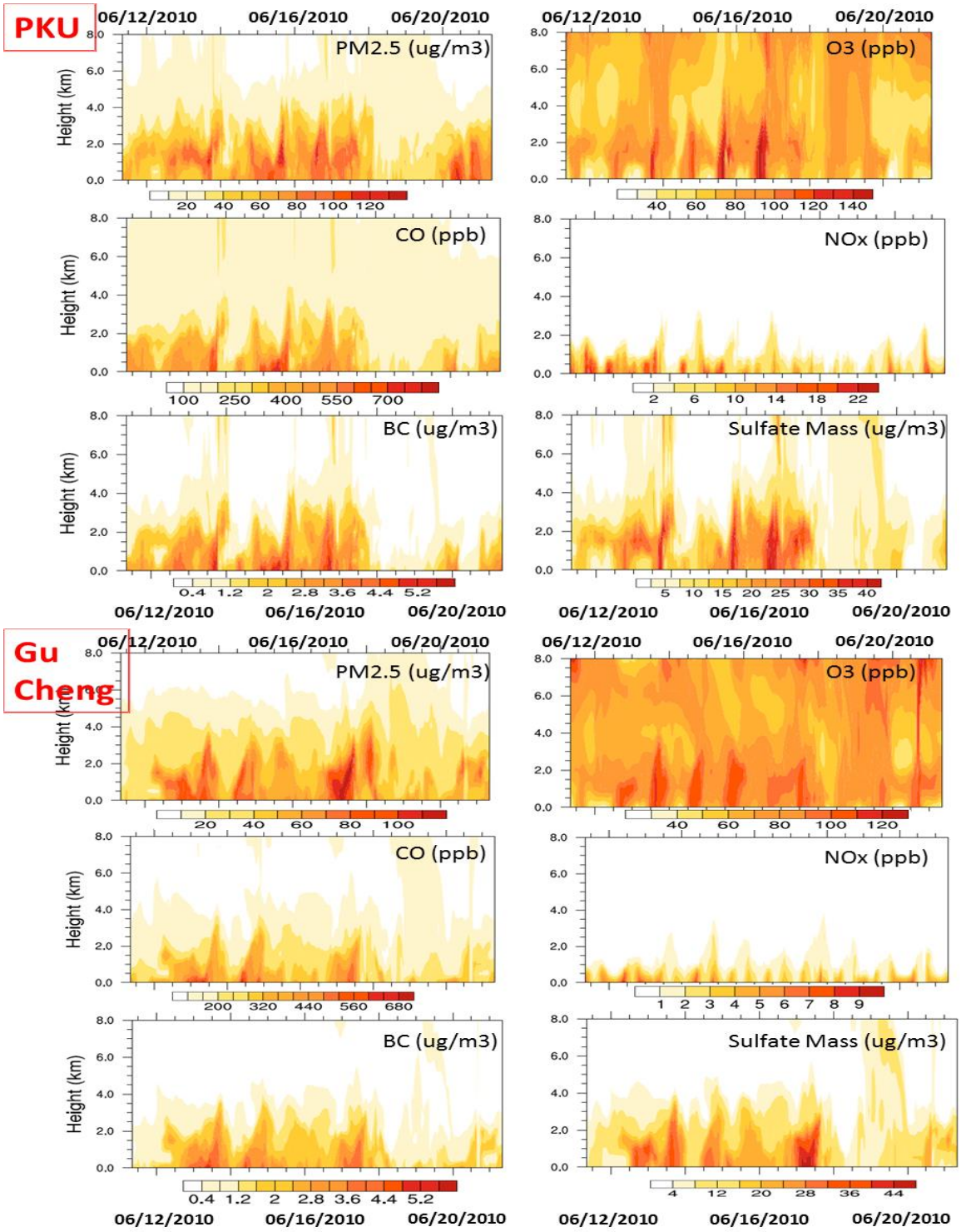

Figure 7.7 Height versus Date plots on PKU and Gucheng for PM2.5, ozone, CO, NOx, BC and sulfate mass.

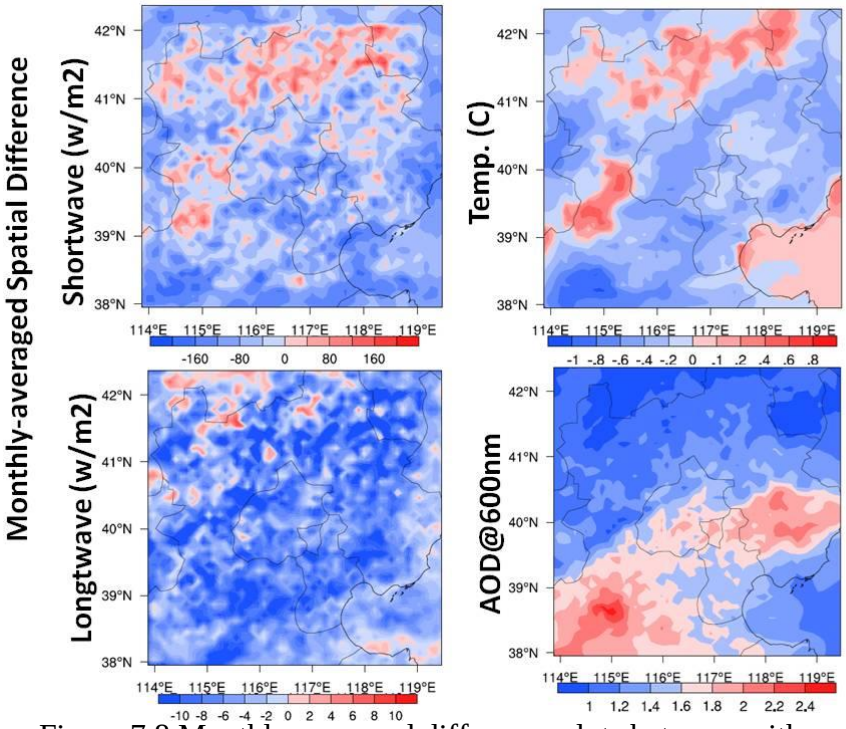

Figure 7.8 Monthly-averaged difference plots between with and without aerosol feedbacks for Short wave, long wave, 2-m Temperature and AOD @ 600nm.

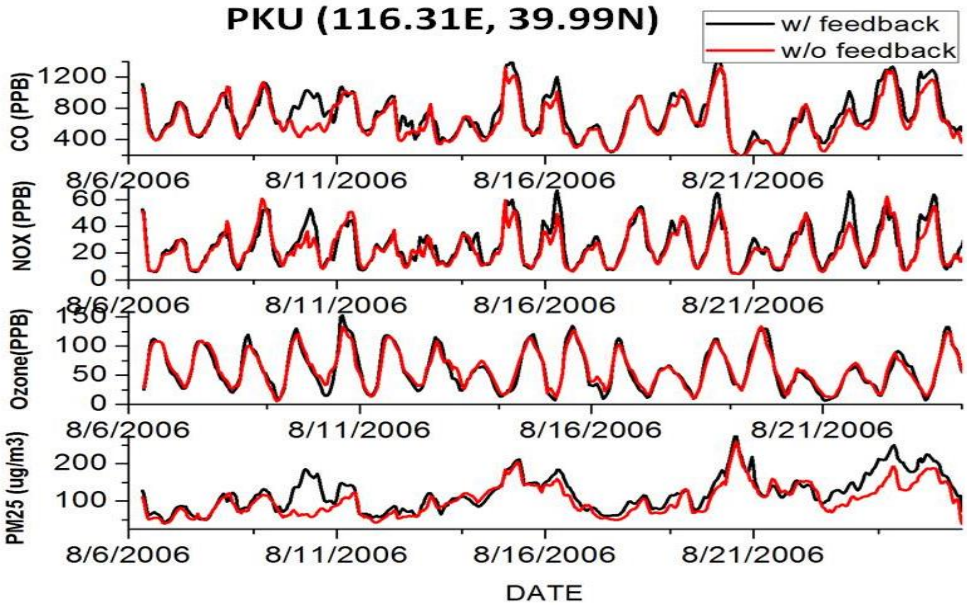

Figure 7.9 Temporal plots on site PKU for CO, NOx, ozone, and PM2.5 for case with and without feedbacks.

Figure 7.10 shows the vertical profile on PKU with regards to time. The case without feedback is likely to reproduce a stronger vertical mixing for Beijing area. In Figure 7.10, more carbon monoxide, NOx, ozone and PM2.5 are transported to upper atmosphere from surface. In without aerosol feedback case, surface pollutant levels tend to reduce by 12%. Besides this, more ozone intrusions (from stratosphere to troposphere) are also found out around 6 km above ground in without feedback case. The average increase for ozone is around 30~40 ppb at 6km height.

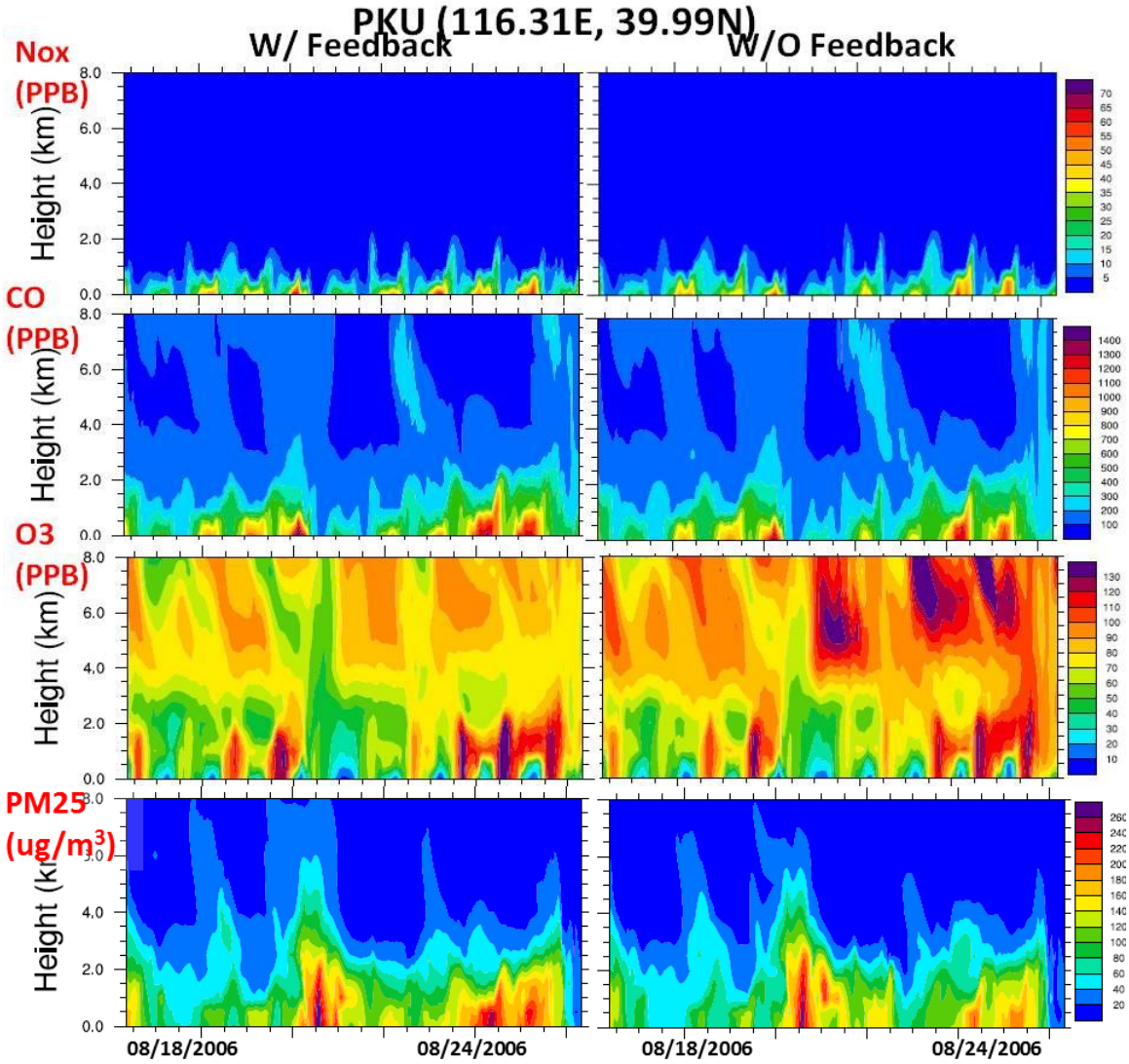

Figure 7.10 Height versus Date plots on PKU for NOx, CO, ozone and PM2.5 between with and without feedback cases

7.4.2 Real Campaign Forecast

For each day from Jun 1st to July 15th 2013, a forecast with latest fire emissions, and boundary conditions was started six hours before mid-night. Within three to four hours, helium (the computing cluster from University of Iowa) will finish the forecast for the next three days. A summary report was sent out and other correlated files were synced on the ftp server (https://www.cgrer.uiowa.edu/ACESS/shared/data_share/).

7.4.2.1 Daily Product

Group CGRER provided 4 different types of forecast products every day. The first is time serial plots on five major field sites, including PKU, Xianghe, Gucheng, Quzhou and Yucheng (Figure 7.2). The second product is the spatial plots for precipitation and chemical pollutants. The snapshots were extracted every 6 hours. The third was a cross-section plot (114.9414 °E, 36.9564 °N) to (116.2597 °E, 40.2860 °N) for chemical distributions. And the last one is height versus date plots on Xianghe site. Figure 7.11 below is one example from our daily forecast products.

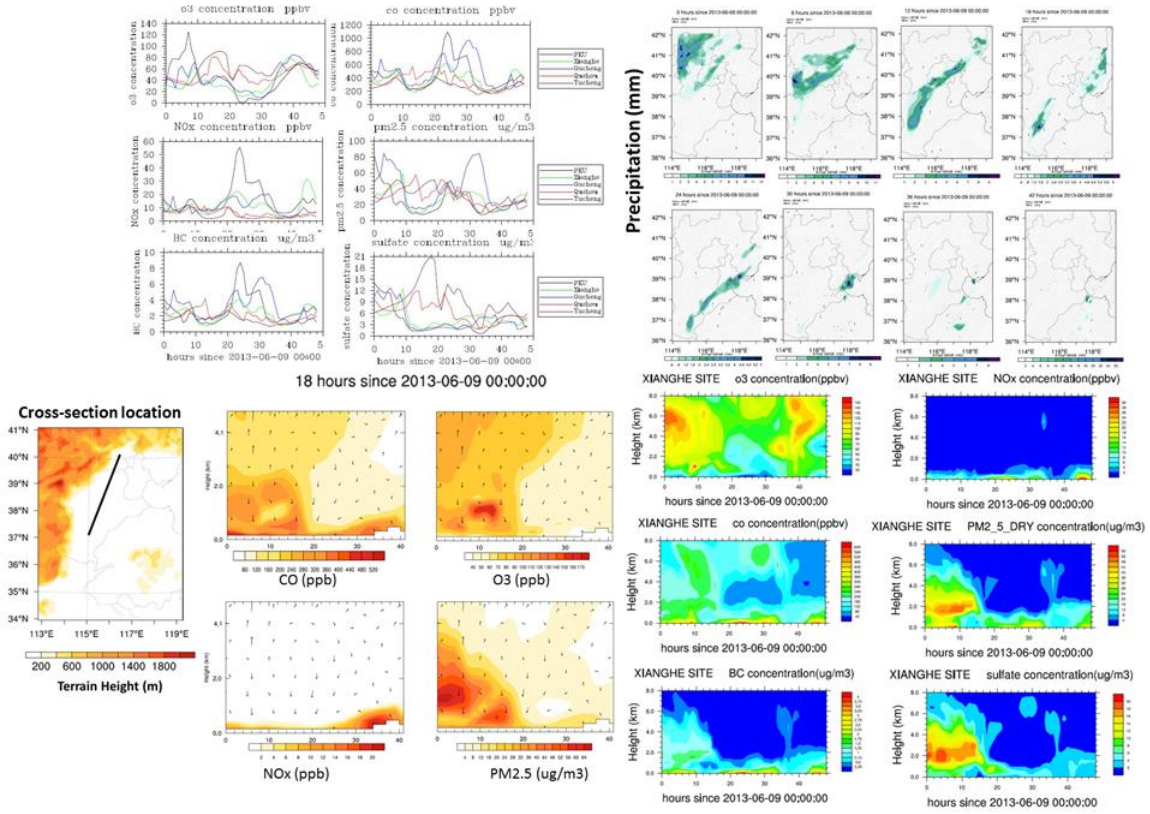

Figure 7.11 One example for CGRER daily forecast products

7.4.2.2 A Precipitation Process on June 4 2013

According to field campaign on Jun 4th 2013, a heavy precipitation occurred in northern part of Beijing. Due to this large amount of rainfall inside Beijing area, pollutant levels dropped in the afternoon of Jun 4th 2013. From the forecast product in Jun 3rd 2013(Figure 7.12), a heavy precipitation appeared in the northern part of Beijing from 12:00 to 18:00 Jun 4th 2013. And the accumulated precipitation was as large as 22 mm. After 18:00 Jun 4th 2013, the center moved northeast into Province Hebei. With regards to the real scenario, our simulation tended to underestimate the intensity of this precipitation process and also produced a shift spatial in the pattern.

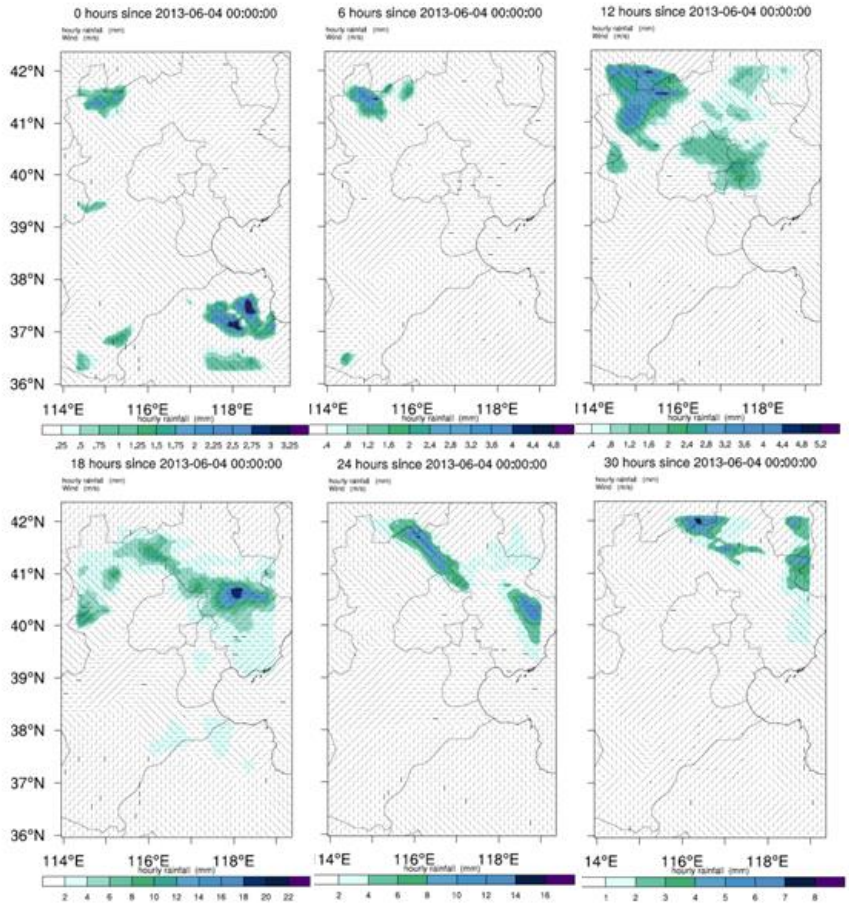

Figure 7.12 Forecast for precipitation on Jun 4th 2013 over North China Plain

Some preliminary comparisons were included in Figure 7.13 for observations and model outputs from both CGRER and IAP group. On PKU site, PM2.5 reached a peak value during morning rush hour. The maximum PM2.5 was above 200 $\mu g/m^3$. After precipitation in the afternoon, both PM2.5 and PM 10 decreased by wet deposition. IAP group was not able to predict this strong convection weather and overestimated particulate matters. For NO_2 simulations, both groups underestimated it by over 40 ppb, indicating an uncertainty in current anthropogenic emissions. On Xianghe site, CGRER's results showed a highly correlation with observation, especially for SO_2 and NO_2. However neither group captured the high particulate episode in the morning of Jun 4th. According to Wu et al. (2011), the local PM emissions contributed about 75% of total

surface PM2.5 in Beijing. For future runs, we recommend including more detailed dust emissions, like road dust and construction dust to decrease these discrepancies.

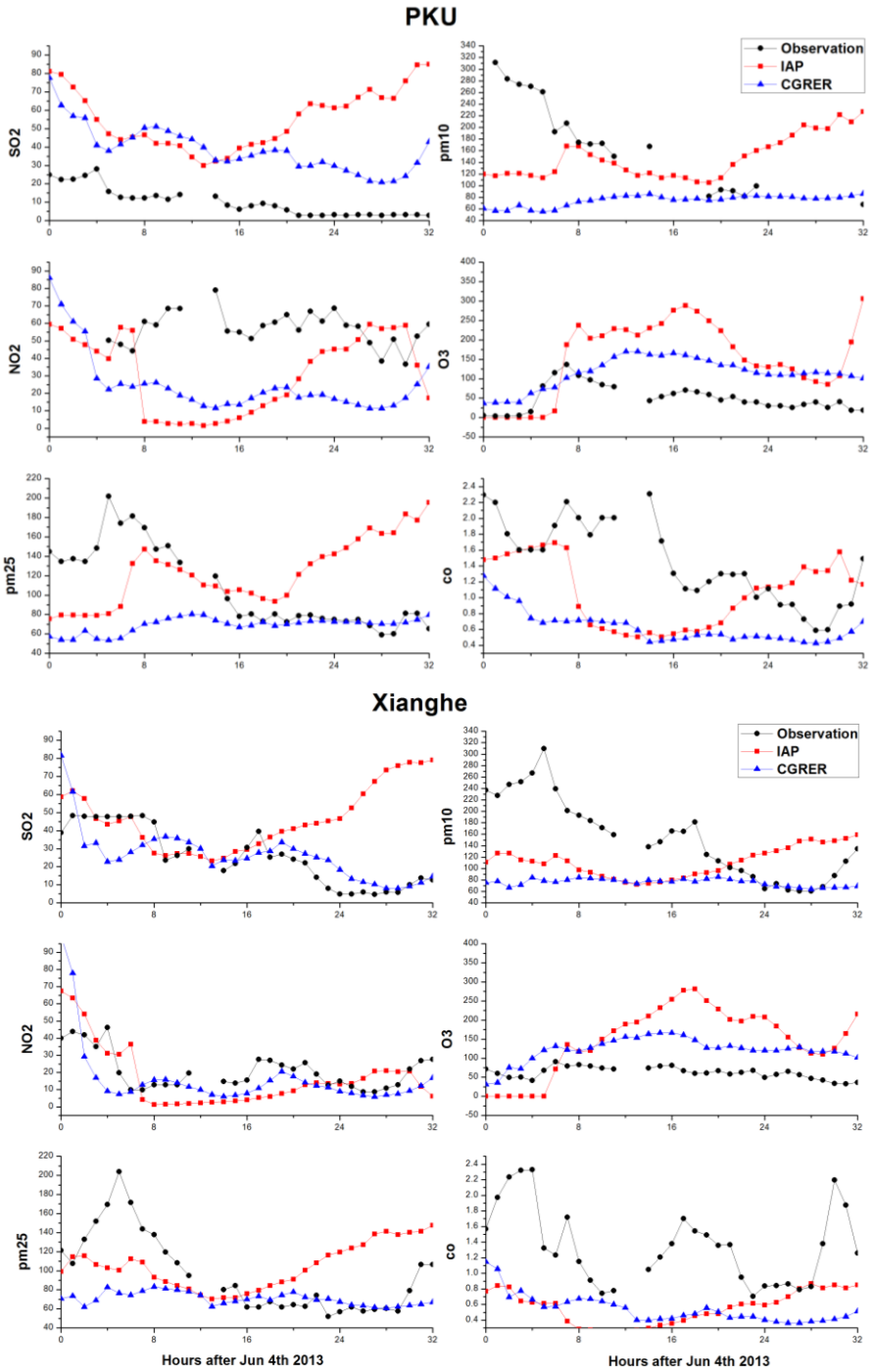

Figure 7.13 Comparison between observations and forecasts on PKU and Xianghe sites

7.5 Conclusion

Haze and other associated air pollutions in Beijing has become a heated topic all over the world. To better investigate it, CAREBeijing-NCP field campaign was conducted from Jun 1st to July 15th 2013. To assist those groups in the campaign, CGRER from University of Iowa used WRF-Chem to predict both meteorology and chemical distributions. Four types of products were produced every day from CGRER, including temporal plots on five major sites, spatial plots for every 6 hours, cross-section vertical plots and height-versus-date plots on Xianghe site. Major meteorology features were welly simulated by our model, including severe precipitation. However due to lack of comprehensive emission inventories, there remains large uncertainty for particulate matter simulations. Impletion of other dust emissions into model might help to improve model fidelity in the future.

CHAPTER 8 CONCLUSION AND FUTURE WORK

Through different sensitivity runs in this thesis, one mutual objective is shared within chapters, to advance the simulations of air quality in China by using WRF-Chem. This goal is achieved by finding the appropriate chemical mechanism and its other physical parameters, replacing the current out-dated land-cover data, developing and implanting a new anthropogenic heat emission into model, remapping the updated emission data and seeking the best domain and vertical resolutions.

8.1 Conclusions

In Chapter 2, we described the method on how to introduce MODIS land-cover into WRF-Chem. Based on this sensitivity run, a warm/dry scenario was found out in Beijing after urbanization process. The average temperature increase exceeded 3 ℃ in Beijing. Ozone was enhanced by over 10 ppb for the entire day and PM2.5 increased due to less precipitations. Simulations containing land cover impact from urbanization demonstrated a significant improvement in many aspects.

Chapter 3 was a follow-up study from Chapter 2. The purpose was trying to find the maximum impacts from land-cover change. Two sensitivity runs were conducted using pre-industrialization and current land-cover data. Results revealed a potential increase of 2 ℃ in Beijing area. Besides temperature increase, a dryer condition on surface was also expected. Compared to Chapter 2, the maximum increase from land-cover was determined to be 20 ppb from the sensitivity runs.

We discussed the current status for inputting anthropogenic heat into WRF-Chem in Chapter 4. A new methodology (NEWLucy) was invented to better describe emission scenarios in China. After coupling NEWLucy with WRF-Chem model, sensitivity runs revealed an increase in temperature and PBL height. We managed to improve model fidelity in high-ozone episodes.

Chapter 5 focused on the emission impacts. Urbanization process typically increases emission release to accommodate increasing population. In this chapter, we utilized two emission inventories (2006 and 2010). We analyze the total emission trends, as well as spatial distribution change in North China Plain. Results showed a considerable increase in NOx and other pollutants since 2006. Surface ozone and PM2.5 were largely enhanced. Since there are only 4 sectors included in these two inventories, a more detailed emission inventory is highly recommended for future forecasts.

Model resolution is another crucial setting for air quality modeling. In Chapter 7, we designed two sensitivity runs on spatial and vertical resolutions. Based on the current available emission and land-cover data, the optimal resolution settings were found to be 9-km (spatial) and 27 layers (vertical). This result guarantees the future forecasts with both accuracy and efficiency. However large uncertainties still remain in emission inventory and urban canopy model. If provided with precise data, the optima settings might change accordingly.

Finally, by using all the experience in previous study, a forecast to serve CAREBeijing-NCP field campaign was conducted in summer 2013. Four kinds of different forecast products were sent to each member by mid-night every day. Major meteorology features were well-simulated in North China Plain, including precipitation processes. However concerning chemical distributions, our results showed the insufficiency in emission inventory (INTEX-B 2006). Future study should focus on improving emissions, especially for particulate matters.

To sum up, another table regarding all the sensitivity study in this paper is shown in table 8.1. The results were extracted from city center of Beijing. Land cover and additional heat release had the bigger impacts on temperature and its associated variables. For the city center of Beijing, the potential surface temperature increase from land-cover change was 1.8 ºC (daytime) and 2.4 ºC (nighttime), respectively. PBL was expected to expand by 400 m at daytime and 80 m at nighttime. Anthropogenic heat had the similar

sensitivity impacts, with higher surface temperature simulations and higher PBL heights. However, the influence on ozone concentrations showed opposite directions for land-cover change and anthropogenic heat. Changing into paved surface tended to increase surface ozone levels, while anthropogenic heat was likely to decrease due to expanded PBL heights. In the greater Beijing Area, aerosol tends to have a "cooling" effect. The "cooling" surface produced a condensed PBL, with 40 ppb (daytime) and 200 ppb (nighttime) more CO in the low atmosphere. PM2.5 was also enhanced over 40 ug/m^3 during nighttime. The choice of resolution (horizontal and vertical) is another key factor for urban air quality modeling in the Greater Beijing Area. At city center of Beijing, the difference between 81-km and 27-km were 1.9 ºC and 4.5 ºC for daytime and nighttime respectively. Regarding to vertical resolutions, using insufficient vertical meshes might bring in some systematic errors. The difference for PM2.5 between 27 layers (the default settings in WRF) and 9 layers was as large as 40 ug/m^3 for Beijing area.

Table 8.1 Conclusion table for all sensitivity runs in city center of Beijing

	Δ 2-m Temp. (C)		Δ PBL heights (m)		Δ CO (ppb)		Δ Nox (ppb)		Δ O3 (ppb)		Δ PM 2.5 (ug/m3)	
	Day	Night	Day	Night	Day	Night	Day	Night	Day	Night	Day	Night
Δ land-cover (2004-1992)	1.8	2.4	400	80	20	-40	-4	-10	16	6	16	5
Δ anthropogenic heat (NewLucy-no heat)	0.8	1.2	300	100	-60	-160	-6	-18	3	18	-8	-12
Δ pollution emission (2010-2006)	0.3	0.24	50	20	40	200	7	30	8	-16	15	40
Δ aerosol feedbacks (with – without)	-0.8	-0.6	-240	-80	100	160	0.8	7	7	-10	22	25
Δ horizontal resolutions (27km -81km)	1.9	4.5	190	90	80	-50	7.3	21	10	-10	-10	-37
Δ horizontal resolutions (9km -27km)	-0.1	0.3	120	70	55	-45	4	30	0.5	-11	3	23
Δ horizontal resolutions (3km -9km)	0.1	0.4	50	30	16	-55	1.6	-2	-0.4	-0.02	0.1	-6
Δ vertical resolutions (27layers -9layers)	1.6	1.2	350	-40	75	300	4	40	6	-30	44	40
Δ vertical resolutions (54layers -27layers)	0.3	0.2	100	-20	10	100	2	30	-2	-8	10	20
base value	30.8	26.6	1810	258	476	1040	15.5	79.5	99	8.87	153	202

8.2 Future Study

In this thesis, all the sensitivity runs were conducted from a regional scale. Based on this condition, many important processes (vertical and horizontal) are ignored or not well simulated. The future study should focus on city-scale, like convective cells, if high resolution land-cover data is available. Uncertainty in urban model requires numerous sensitivity tests for the optimal configurations in China, like building height, density and canopy options. Also detailed information on land-cover will enable the ability to further classify urban cells into three different types, low-intensity residential, high-intensity residential and industrial commercials.

Additional improvement can be achieved by fine resolution emission inventories. In this thesis, most of the sensitivity runs are conducted with either INTEX-B or MICS. The resolutions for these two inventories are $0.5^o \times 0.5^o$ and $0.25^o \times 0.25^o$, respectively. Recently a new global anthropogenic emission was published online, called HTAP (the Task Force on Hemispheric Transport of Air Pollution). It's equipped with high-resolution ($0.1^o \times 0.1^o$) for the year 2010. More studies should focus on this new source and comparisons with the current MICS emissions.

In Chapter 4, we developed a new methodology for simulating anthropogenic heat emissions. This NEWLucy model is calculated based on several assumptions. For instance, we assumed average speed of vehicles to be 48 km/h and 80% of total vehicles on road in the Greater Beijing area. These assumptions might be accurate when considering both large cities and small cities inside North China Plain. More sensitivity runs are needed to access these uncertainties. Also, the differences between weekdays and weekends are not well predicted in this thesis. Future study could utilize more than one global heat emissions to improve model fidelity.

Besides these, another possible study should be developing more comprehensive emissions for particulate matters. According to recent studies, it is likely to underestimate PM2.5 concentrations (also shown in this thesis). Many factors could contribute to it, like

limited emission inventory and chemical mechanism options. In this thesis, we used CBMZ with MOSAIC. This combination is proved to be good in simulating ozone, but its mechanism for Secondary Organic Aerosol (SOA) is far from complete. How to improve and test it in Beijing area could be the key issue in future studies.

REFERENCES

AKIMOTO, H. AND NARITA, H. 1994. Distribution of So2, Nox and Co2 Emissions from Fuel Combustion and Industrial Activities in Asia with 1-Degrees-X1-Degrees Resolution. Atmospheric Environment 28, 213-225.

ALAN STRAHLER, DOUG MUCHONEY, JORDAN BORAK, MARK FRIEDL, SUCHARITA GOPAL, 'ERIC LAMBIN AND AARON MOODY. 1999. MODIS Land Cover Product Algorithm Theoretical Basis Document (ATBD) Version 5.0. http://modis.gsfc.nasa.gov/data/atbd/atbd_mod12.pdf.

BASCOM, R., BROMBERG, P., COSTA, D., DEVLIN, R., DOCKERY, D., FRAMPTON, M., LAMBERT, W., SAMET, J., SPEIZER, F. AND UTELL, M. 1996. Health effects of outdoor air pollution. American Journal of Respiratory and Critical Care Medicine 153, 3-50.

BELL, M., MCDERMOTT, A., ZEGER, S., SAMET, J. AND DOMINICI, F. 2004. Ozone and short-term mortality in 95 US urban communities, 1987-2000. Jama-Journal of the American Medical Association 292, 2372-2378.

BRUNEKREEF, B. AND HOLGATE, S. 2002. Air pollution and health. Lancet 360, 1233-1242.

BUKA, I., KORANTENG, S. AND OSORNIO-VARGAS, A.R. 2006. The effects of air pollution on the health of children. Paediatrics & child health 11, 513-516.

CARMICHAEL, G., STREETS, D., CALORI, G., AMANN, M., JACOBSON, M., HANSEN, J. AND UEDA, H. 2002. Changing trends in sulfur emissions in Asia: Implications for acid deposition, air pollution, and climate. Environmental science & technology 36, 4707-4713.

CHEN, F. AND DUDHIA, J. 2001. Coupling an advanced land surface-hydrology model with the Penn State-NCAR MM5 modeling system. Part I: Model implementation and sensitivity. Monthly Weather Review 129, 569-585.

CHEN, F., KUSAKA, H., BORNSTEIN, R., CHING, J., GRIMMOND, C.S.B., GROSSMAN-CLARKE, S., LORIDAN, T., MANNING, K.W., MARTILLI, A., MIAO, S., SAILOR, D., SALAMANCA, F.P., TAHA, H., TEWARI, M., WANG, X., WYSZOGRODZKI, A.A. AND ZHANG, C. 2011. The integrated WRF/urban modelling system: development, evaluation, and applications to urban environmental problems. International Journal of Climatology 31, 273-288.

CHEN, J. 2007. Rapid urbanization in China: A real challenge to soil protection and food security. Catena 69, 1-15.

CRAWFORD, T., STENSRUD, D., MORA, F., MERCHANT, J. AND WETZEL, P. 2001. Value of incorporating satellite-derived land cover data in MM5/PLACE for simulating surface temperatures. Journal of Hydrometeorology 2, 453-468.

EMMONS, L.K., WALTERS, S., HESS, P.G., LAMARQUE, J.-., PFISTER, G.G., FILLMORE, D., GRANIER, C., GUENTHER, A., KINNISON, D., LAEPPLE, T., ORLANDO, J., TIE, X., TYNDALL, G., WIEDINMYER, C., BAUGHCUM, S.L. AND KLOSTER, S.

2010. Description and evaluation of the Model for Ozone and Related chemical Tracers, version 4 (MOZART-4). Geoscientific Model Development 3, 43-67.

FAST, J.D., GUSTAFSON, W.I., JR., EASTER, R.C., ZAVERI, R.A., BARNARD, J.C., CHAPMAN, E.G., GRELL, G.A. AND PECKHAM, S.E. 2006. Evolution of ozone, particulates, and aerosol direct radiative forcing in the vicinity of Houston using a fully coupled meteorology-chemistry-aerosol model. Journal of Geophysical Research-Atmospheres 111, D21305.

FRIEDL, M., MCIVER, D., HODGES, J., ZHANG, X., MUCHONEY, D., STRAHLER, A., WOODCOCK, C., GOPAL, S., SCHNEIDER, A., COOPER, A., BACCINI, A., GAO, F. AND SCHAAF, C. 2002. Global land cover mapping from MODIS: algorithms and early results RID E-3208-2010 RID F-3944-2010. Remote Sensing of Environment 83, 287-302.

GRELL, G., PECKHAM, S., SCHMITZ, R., MCKEEN, S., FROST, G., SKAMAROCK, W. AND EDER, B. 2005. Fully coupled "online" chemistry within the WRF model. Atmospheric Environment 39, 6957-6975.

GU, C., HU, L., ZHANG, X., WANG, X. AND GUO, J. 2011. Climate change and urbanization in the Yangtze River Delta. Habitat International 35, 544-552.

GUENTHER, A., KARL, T., HARLEY, P., WIEDINMYER, C., PALMER, P.I. AND GERON, C. 2006. Estimates of global terrestrial isoprene emissions using MEGAN (Model of Emissions of Gases and Aerosols from Nature) RID B-1617-2008 RID D-1891-2009 RID F-7008-2010. Atmospheric Chemistry and Physics 6, 3181-3210.

HIDALGO, J., MASSON, V. AND PIGEON, C. 2008. Urban-breeze circulation during the CAPITOUL experiment: numerical simulations. Meteorology and Atmospheric Physics 102, 243-262.

HIDALGO, J., PIGEON, G. AND MASSON, V. 2008. Urban-breeze circulation during the CAPITOUL experiment: observational data analysis approach. Meteorology and Atmospheric Physics 102, 223-241.

HOGREFE, C., LYNN, B., CIVEROLO, K., KU, J., ROSENTHAL, J., ROSENZWEIG, C., GOLDBERG, R., GAFFIN, S., KNOWLTON, K. AND KINNEY, P. 2004. Simulating changes in regional air pollution over the eastern United States due to changes in global and regional climate and emissions. Journal of Geophysical Research-Atmospheres 109, D22301.

HONG, S., NOH, Y. AND DUDHIA, J. 2006. A new vertical diffusion package with an explicit treatment of entrainment processes. Monthly Weather Review 134, 2318-2341.

HU, X., NIELSEN-GAMMON, J.W. AND ZHANG, F. 2010. Evaluation of Three Planetary Boundary Layer Schemes in the WRF Model. Journal of Applied Meteorology and Climatology 49, 1831-1844.

JIANG, F., WANG, T., WANG, T., XIE, M. AND ZHAO, H. 2008. Numerical modeling of a continuous photochemical pollution episode in Hong Kong using WRF-chem. Atmospheric Environment 42, 8717-8727.

JIANG, F., ZHOU, P., LIU, Q., WANG, T., ZHUANG, B. AND WANG, X. 2012. Modeling tropospheric ozone formation over East China in springtime. Journal of Atmospheric Chemistry 69, 303-319.

JIANG, F., ZHOU, P., LIU, Q., WANG, T., ZHUANG, B. AND WANG, X. 2012. Modeling tropospheric ozone formation over East China in springtime. Journal of Atmospheric Chemistry 69, 303-319.

JUSTICE, C., TOWNSHEND, J., VERMOTE, E., MASUOKA, E., WOLFE, R., SALEOUS, N., ROY, D. AND MORISETTE, J. 2002. An overview of MODIS Land data processing and product status. Remote Sensing of Environment 83, 3-15.

KIM, H. AND WANG, B. 2011. Sensitivity of the WRF Model Simulation of the East Asian Summer Monsoon in 1993 to Shortwave Radiation Schemes and Ozone Absorption. Asia-Pacific Journal of Atmospheric Sciences 47, 167-180.

LI, Y., LI, Y., ZHOU, Y., SHI, Y. AND ZHU, X. 2012. Investigation of a coupling model of coordination between urbanization and the environment. Journal of environmental management 98, 127-133.

LI, Y., AN, J., MIN, M., ZHANG, W., WANG, F. AND XIE, P. 2011. Impacts of HONO sources on the air quality in Beijing, Tianjin and Hebei Province of China. Atmospheric Environment 45, 4735-4744.

LIN, C., CHEN, W., CHANG, P. AND SHENG, Y. 2011. Impact of the Urban Heat Island Effect on Precipitation over a Complex Geographic Environment in Northern Taiwan. Journal of Applied Meteorology and Climatology 50, 339-353.

LIN, Y., FARLEY, R. AND ORVILLE, H. 1983. Bulk Parameterization of the Snow Field in a Cloud Model. Journal of Climate and Applied Meteorology 22, 1065-1092.

LOVELAND, T., REED, B., BROWN, J., OHLEN, D., ZHU, Z., YANG, L. AND MERCHANT, J. 2000. Development of a global land cover characteristics database and IGBP DISCover from 1 km AVHRR data RID C-9888-2010. International Journal of Remote Sensing 21, 1303-1330.

MAKAR, P.A., ZHANG, J., GONG, W., STROUD, C., SILLS, D., HAYDEN, K.L., BROOK, J., LEVY, I., MIHELE, C., MORAN, M.D., TARASICK, D.W., HE, H. AND PLUMMER, D. 2010. Mass tracking for chemical analysis: the causes of ozone formation in southern Ontario during BAQS-Met 2007. Atmospheric Chemistry and Physics 10, 11151-11173.

MENUT, L., BESSAGNET, B., COLETTE, A. AND KHVOROSTIYANOV, D. 2013. On the impact of the vertical resolution on chemistry-transport modelling. Atmospheric Environment 67, 370-384.

MLAWER, E.J., TAUBMAN, S.J., BROWN, P.D., IACONO, M.J. AND CLOUGH, S.A. 1997. Radiative transfer for inhomogeneous atmospheres: RRTM, a validated correlated-k model for the longwave. Journal of Geophysical Research-Atmospheres 102, 16663-16682.

MLAWER, E.J., TAUBMAN, S.J., BROWN, P.D., IACONO, M.J. AND CLOUGH, S.A. 1997. Radiative transfer for inhomogeneous atmospheres: RRTM, a validated correlated-k

model for the longwave. Journal of Geophysical Research-Atmospheres 102, 16663-16682.

MU, F.Y., ZHANG Z.X., CHI, Y.B., ZHOU Q.B., WANG, C.Y. AND TAN, W.B. 2007. Dynamic monitoring of built-ip area in Beijing during 1973-2005 based on multi-origianl remote sensed images. Journal of Remote Sensing 11 (2), 257-268 (in Chinese).

OHARA, T., AKIMOTO, H., KUROKAWA, J., HORII, N., YAMAJI, K., YAN, X. AND HAYASAKA, T. 2007. An Asian emission inventory of anthropogenic emission sources for the period 1980-2020. Atmospheric Chemistry and Physics 7, 4419-4444.

RYU, Y., BAIK, J. AND HAN, J. 2013. Daytime urban breeze circulation and its interaction with convective cells. Quarterly Journal of the Royal Meteorological Society 139, 401-413.

SHAH, J., NAGPAL, T., JOHNSON, T., AMANN, M., CARMICHAEL, G., FOELL, W., GREEN, C., HETTELINGH, L.P., HORDIJK, L., LI, J., PENG, C., PU, Y.F., RAMANKUTTY, R. AND STREETS, D. 2000. Integrated analysis for acid rain in Asia: Policy implications and results of RAINS-ASIA model. Annual Review of Energy and the Environment 25, 339-375.

SHI, J. AND CUI, L. 2012. Characteristics of high impact weather and meteorological disaster in Shanghai, China. Natural Hazards 60, 951-969.

SKAMAROCK WILLIAM C., KLEMP JOSEPH B., DUDHIA JIMY, GILL DAVID O., BARKER DALE M., DUDA MICHAEL G., HUANG XIANG-YU, WANG WEI AND POWERS JORDAN G. A Description of the Advanced Research WRF Version 3. http://www.mmm.ucar.edu/wrf/users/docs/arw_v3.pdf.

SUN, Z.H., FENG, S.Y., YANG, Z.S. AND WU, H.S. 2007. Primary analysis of the precipitation characteristics for Beijing during the period from 1950 to 2005. Journal of Irrigation and Drainage 26(2), 12-16(in Chinese).

TAO, M., CHEN, L., WANG, Z., MA, P., TAO, J. AND JIA, S. 2014. A study of urban pollution and haze clouds over northern China during the dusty season based on satellite and surface observations. Atmospheric Environment 82, 183-192.

TIE, X., GENG, F., GUENTHER, A., CAO, J., GREENBERG, J., ZHANG, R., APEL, E., LI, G., WEINHEIMER, A., CHEN, J. AND CAI, C. 2013. Megacity impacts on regional ozone formation: observations and WRF-Chem modeling for the MIRAGE-Shanghai field campaign. Atmospheric Chemistry and Physics 13, 5655-5669.

TIE, X., GENG, F., GUENTHER, A., CAO, J., GREENBERG, J., ZHANG, R., APEL, E., LI, G., WEINHEIMER, A., CHEN, J. AND CAI, C. 2013. Megacity impacts on regional ozone formation: observations and WRF-Chem modeling for the MIRAGE-Shanghai field campaign. Atmospheric Chemistry and Physics 13, 5655-5669.

TIE, X., MADRONICH, S., LI, G., YING, Z., ZHANG, R., GARCIA, A.R., LEE-TAYLOR, J. AND LIU, Y. 2007. Characterizations of chemical oxidants in Mexico City: A regional chemical dynamical model (WRF-Chem) study RID A-2942-2011 RID B-7409-2008. Atmospheric Environment 41, 1989-2008.

UNITED NATIONS. 2004. World Urbanization Prospects (the 2003 revision). Population Division, Department of Economic and Social Affairs, United Nations, New York .

VAN DE POEL, E., O'DONNELL, O. AND VAN DOORSLAER, E. 2012. Is there a health penalty of China's rapid urbanization? Health Economics 21, 367-385.

WANG XUEMEI, CHEN FEI, WU ZHIYONG, ZHANG MEIGEN, TEWARI, M., GUENTHER, A. AND WIEDINMYER, C. 2009. Impacts of Weather Conditions Modified by Urban Expansion on Surface Ozone: Comparison between the Pearl River Delta and Yangtze River Delta Regions. Advances in Atmospheric Sciences 26, 962-972.

WANG YUESI, YAO LI, WANG LILI, LIU ZIRUI, JI DONGSHENG, TANG GUIQIAN, ZHANG JUNKE, SUN YANG, HU BO AND XIN JINYUAN. 2014. Mechanism for the formation of the January 2013 heavy haze pollution episode over central and eastern China. Science China-Earth Sciences 57, 14-25.

WANG, T., JIANG, F., DENG, J., SHEN, Y., FU, Q., WANG, Q., FU, Y., XU, J. AND ZHANG, D. 2012. Urban air quality and regional haze weather forecast for Yangtze River Delta region. Atmospheric Environment 58, 70-83.

WANG, X., LIANG, X., JIANG, W., TAO, Z., WANG, J.X.L., LIU, H., HAN, Z., LIU, S., ZHANG, Y., GRELL, G.A. AND PECKHAM, S.E. 2010. WRF-Chem simulation of East Asian air quality: Sensitivity to temporal and vertical emissions distributions. Atmospheric Environment 44, 660-669.

WU, Q.Z., WANG, Z.F., GBAGUIDI, A., GAO, C., LI, L.N. AND WANG, W. 2011. A numerical study of contributions to air pollution in Beijing during CAREBeijing-2006. Atmospheric Chemistry and Physics 11, 5997-6011.

XU, D., LU, H., WU, N. AND LIU, Z. 2010. 30 000-Year vegetation and climate change around the East China Sea shelf inferred from a high-resolution pollen record. Quaternary International 227, 53-60.

YAN, P., WANG, Z., WANG, X., FU, Q. AND WANG, Q. 2011. Impact of Pollutant Transport on the Air Quality of Shanghai in 2007 RID B-5799-2011. Sola 7, 85-88.

YU, M., CARMICHAEL, G.R., ZHU, T. AND CHENG, Y. 2012. Sensitivity of predicted pollutant levels to urbanization in China. Atmospheric Environment 60, 544-554. .

YU, M., CARMICHAEL, G.R., ZHU, T. AND CHENG, Y. 2014. Sensitivity of predicted pollutant levels to anthropogenic heat emissions in Beijing. Atmospheric Environment 89, 169-178. .

YUCEL, I. 2006. Effects of implementing MODIS land cover and albedo in MM5 at two contrasting US regions. Journal of Hydrometeorology 7, 1043-1060.

ZHANG, Q., STREETS, D.G., CARMICHAEL, G.R., HE, K.B., HUO, H., KANNARI, A., KLIMONT, Z., PARK, I.S., REDDY, S., FU, J.S., CHEN, D., DUAN, L., LEI, Y., WANG, L.T. AND YAO, Z.L. 2009. Asian emissions in 2006 for the NASA INTEX-B mission. Atmospheric Chemistry and Physics 9, 5131-5153.

ZHAO, X.J., ZHAO, P.S., XU, J., MENG, W., PU, W.W., DONG, F., HE, D. AND SHI, Q.F. 2013. Analysis of a winter regional haze event and its formation mechanism in the North China Plain. Atmospheric Chemistry and Physics 13, 5685-5696.